Heterogeneous Organic Reactions on Gallium-Rich Gallium Arsenide, Gallium Phosphide, and Gallium Nitride Surfaces

by

Sabrina Louise Peczonczyk

A dissertation submitted in partial fulfillment
of the requirements for the degree of
Doctor of Philosophy
(Chemistry)
in the University of Michigan
2014

Doctoral Committee:
Assistant Professor Stephen Maldonado, Chair
Professor Mark M. Banaszak Holl
Associate Professor Pei-Cheng Ku
Professor Michael D. Morris

Dedication

For my mother, as promised.

Acknowledgments

I have been very fortunate during my graduate career to have had the pleasure of working with and getting to know some very special people. Your support, friendship and mentorship have been invaluable to me during this journey. The content on the following pages was very much made possible because I had you.

First and foremost I would like to thank my advisor, Professor Stephen Maldonado. Thank you for giving me a place in your lab five years ago, and for trusting me with what is most likely the most expensive instrument we have. In retrospect, that could not have been an easy thing to do. To say that I learned a lot from you would be an understatement. I have grown not only as a scientist, but also as a person under your direction. I want to thank you for taking the time to work one-on-one to help prepare me for several milestones (seminar, candidacy, conference, and job talks) over the last five years. You didn't have to. Thank you.

To my committee, Professor Morris, Professor Banaszak Holl, and Professor Ku, I would like to thank you for all of your feedback and support over the years. I can honestly say that I have walked away from every committee meeting with either the drive to become a better scientist or with excitement to try new experiments or ideas that you proposed. Thank you for continually motivating me.

To the first iteration of the Maldonado lab: Dr. Jhindan Mukherjee, Michelle Chitamber, Jeremy Feldblyum, Sean Collins, Azhar Carim, Justin Foley, Wen Wen, Junsi Gu, and Kevin Hagedorn, there has never been, nor will there ever be, a group quite like ours. I fondly look back at the time we shared as it definitely shaped my views and approach toward graduate school and life. I have watched many of you move on to 'bigger and better' endeavors and I could not be happier or more proud of you. I am also truly thankful that many of you have remained a prominent presence in my life even

though we are now literally spread across the country and world! I could not have asked for a better group of people to start my Ph.D. with.

I have been very fortunate I have had the opportunity to work closely with several individuals. I want to thank Dr. Jhindan Mukherjee for not only being my first friend in the lab, but for taking me under your wings and showing me the ropes. I really enjoyed our long conversations and your seemingly endless supply of dark chocolate. I would like to acknowledge Betsy Brown. It was a pleasure to work with you. Your smile always brightened up my day. Last, but not least, I would like to thank Shawn Eady. I very much enjoyed our time working together. Our conversations and your excitement in our project brought me back from a very dark place, and reignited my passion for this work. I can't thank you enough.

I would like to sincerely thank Steve Donajkowski from the instrument shop. Your support, whether is be through helping me fix a grumpy instrument, or by just having someone to talk to, has been invaluable to me throughout the years.

I would like to thank Casey Kilpatrick for being an unwavering source of support, even though we live very far away from one another. Your daily text messages never fail to brighten up my day. I am so happy that I still have you in my life. I would like to thank Jessica Zynda for sticking with me for the long haul. I really appreciate the history of our friendship.

During my time at Michigan I have made some truly exceptional friendships. I would like to thank Jessica Donehue for having my back, no matter what. I would like to thank Fangting Yu for always believing in me. I would like to thank Rachel Barnard and Beth Haas for our almost-weekly lunches over the last five years. Additionally, I would like to thank Laura Thoma, Anna Wagner, Tanya Breault, Noah Wolfson, Felicia Gray, and Masha Savelieff for your friendship and support.

I would like to thank my family, Voiko, Chacha Tami, Chacha Rosey and Hnat for being my 'reset' button over the last five years. I would like to thank my California family, Aunt Kathie, Aunt Donna, Martina, and Mo, for adopting me. I would like to thank Uncle John Salas, your Salas-isms never fail to make me giggle.

Most of all I would like to thank my mother, you helped me become the woman I am today. Words will never be able to express how much I miss and love you.

Table of Contents

List of Figures

List of Tables

Abstract

This dissertation details a wet chemical reaction strategy that has been developed to impart chemical and electronic stability, as well as chemical functionality to Ga-rich gallium arsenide (GaAs(111)A), gallium nitride (GaN(0001)), and gallium phosphide (GaP(111)A) surfaces. These materials have a broad range of applications in the fields of sensing, electronics, and photoelectrochemistry. However, the native unprotected surfaces of these materials are highly susceptible to oxidation and chemical attack, which cause deleterious surface states that facilitate charge recombination. Currently, the number of wet chemical routes available for surface passivation is limited. I have demonstrated that the addition of organic groups onto Ga-rich surfaces of GaAs(111)A, GaP(111)A, and GaN(0001) *via* a two-step chlorination/Grignard reaction sequence effects a surface that is chemically resistant to oxidation in ambient and aqueous environments and has a lower density of electronic defects relative to the native oxide. The Grignard reaction sequence was further used to covalently bind allyl and pentenyl groups, with terminal reactive olefins, to GaP(111)A surfaces. In addition to imparting resistance to oxidation that is comparable with alkyl-terminated GaP(111)A surfaces, covalently bound alkenyl groups allow for further modification of the GaP(111)A surface *via* secondary reactions. For proof of principle, allyl-terminated GaP(111)A surfaces were secondarily functionalized through Heck cross-coupling metathesis, hydrosilylation and electrophilic addition of bromine reactions. The resultant surfaces were characterized using X-ray photoelectron spectroscopy and grazing-angle attenuated total reflectance Fourier transform infrared spectroscopy. Finally, pentenyl-terminated GaP(111)A surfaces were sequentially modified first through electrophilic addition of bromine and then nucleophilic substitution with sodium azide. The azide-terminated GaP(111)A

surface was then functionalized through a Huisgen 1,3 dipolar ‘Click’ reaction with an alkyne derivatized Fe-based molecular catalyst. This wet chemical reaction strategy provides a method to create robust Ga-C surface bonds that impart stability on Ga-rich III-V semiconductor surfaces while also affording chemical functionality that can be leveraged to attach technologically relevant organic molecules to the surface.

Chapter 1

Introduction

I. Motivation and Technological Importance

Gallium (Ga)-based III-V semiconductors, namely gallium arsenide (GaAs), gallium nitride (GaN), and gallium phosphide (GaP) have been and are predicted to continue to be key components in current and emerging optoelectronic technologies. Since the 1950's GaAs has received much attention as a contender that was thought to supplant silicon (Si) as the material of choice for many electronics applications.[1] GaAs has a direct band gap (1.41 eV)[2] that is well suited for photoelectrochemical solar conversion and light emitting diode devices. The width of the band gap also makes GaAs markedly insensitive to heat and exhibits less noise than Si electronic components, which has precipitated the use of GaAs in weak-signal amplification systems. These characteristics, coupled with an electron mobility that is six times higher than that of Si, and a saturation velocity that is twice as high,[3] have led to the description of GaAs as "the material of the future…".

GaN has an extremely high heat capacity[4] and thermal conductivity.[5] Coupled with high breakdown voltages[6] and high electron mobilities, it has become a niche material for high-power, high-frequency devices, such as power amplifiers at microwave frequencies. GaN also has a wide direct band gap (3.4 eV),[2] which has made GaN ideal for high-performance blue light emitting diodes and violet laser diodes. Lastly, GaN has exhibited strong stability against ionizing radiation, which has precipitated its use in satellite solar cell arrays.

GaP has a mid-sized indirect optoelectronic band gap (2.26 eV) that makes this material well-suited for solar-powered water electrolysis because GaP can simultaneously support large photovoltages and absorb a significant portion of the solar spectrum.[7,8] Also, the conduction band edge of GaP is well-positioned for the reduction of protons into H_2, a useful chemical fuel.[9] Couple this with large carrier mobilities (300 cm^2 V^{-1} s^{-1} for electrons and 500 cm^2 V^{-1} s^{-1} for holes) GaP is a promising material for photoelectrochemical systems.[7] Currently, GaP is mostly used in the commercial production of red, orange, and green light emitting diodes.[10]

II. Materials Challenges

While Ga-based III-V semiconductors have a multitude of intrinsic bulk properties that are highly desirable for many optoelectronic applications, the full capacity of these properties has not been fully realized. Ga-based III-V semiconductors have been limited in their development as metal-insulator-semiconductor devices and incorporation into photoelectrochemical systems because the native surface is highly susceptible to chemical attack and rapid surface oxidation in ambient or aqueous conditions. The native oxide that forms under these environments is not structurally or electronically uniform or pure, in contrast to the Si/SiO_2 interface. For example, the native oxide of GaAs has an incredibly high density of surface states (> 10^{13} cm^{-2}).[11] Also, the growth of a thermal oxide with good electronic properties is not possible on GaAs, GaN, and GaP. When there are two types of elements present at the surface, the surface atoms will oxidize at different rates. The atom with the smaller heat of formation will be oxidized slower and will be buried within the oxide layer, resulting in an oxide that is non-homogeneous. For example, several types of oxides are known to form at the GaAs surface. Ga surface atoms will form Ga_2O and Ga_2O_3 oxides. As surface atoms will form As_2O_3 and As_2O_5 oxides; there can also be the formation of mixed oxides such as $GaAsO_4$.[12] Thus, the resulting oxide layer is non-homogeneous with a high density of surface states.[13] Surface states that have mid-band gap energies can act as deleterious sites for charge recombination which reduces device performance.[14] Given the propensity for detrimental surface oxide formation on Ga-based III-V semiconductor surfaces much effort has been

devoted to the fundamental understanding and subsequent control of chemical reactions that can occur at the surfaces of these materials.

III. Understanding Surface Bonding

In order to improve the quality of the surface an understanding of the nature of the chemical bonding that occurs at the surface is required. A surface atom simultaneously experiences two distinctly different chemical bonding environments. From the bulk, there is a repeating ordered bonding environment such that the bonding and antibonding orbitals make up the conduction and valence bands in a semiconductor. The surface atom also has an electron-rich or electron-deficient orbital ("dangling bond") that is not involved in bulk chemical bonding and does not overlap with neighboring atoms. This orbital can appear as a discrete energy level in the mid-band gap region (Figure 1.1).[15] Mid-band gap energy levels, generated through either dangling bonds or defects/impurities present at the surface, can act as intrinsic surface states that facilitate charge recombination. By filling this energy level, through bonding to the surface, the antibonding and bonding orbitals can be shifted out of the mid-band gap region into the conduction and valence bands, respectively. Orbitals that make up the conduction and valence bands do not participate in charge recombination.

GaAs and GaP both possess the Zincblende crystal structure, which is a cubic crystal structure similar to the diamond crystal structure exhibited by silicon but with alternating Ga and As (or P) atoms. If we consider the (111) plane, a surface atom has three completely satisfied orbitals in the bulk with one unsatisfied unoccupied orbital (Figure 1.2). The (111) plane can either be Ga-rich (111)A or group V (P or As)-rich (111)B. GaN has the Wurtzite crystal structure, which is the hexagonal analogue of the zincblende crystal structure (Figure 1.1). Similarly, the (0001) plane of GaN can be either Ga- or N-polar. Ga-rich surface atoms are expected to have electron-poor dangling bonds, and thus would be more receptive to nucleophilic attack. On the other hand, group V surface atoms are expected to have electron-rich dangling bonds, and hence have electrophilic nature.

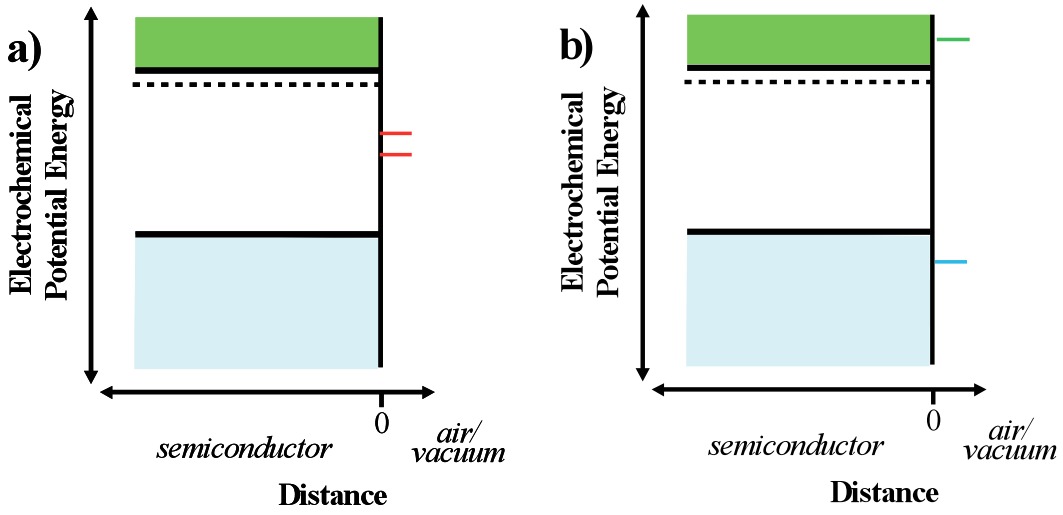

Figure 1.1. Idealized band structure of an n-type semiconductor. (a) Red lines represent energy levels of chemically unsatisfied surface atoms in the mid-band gap region. (b) Green and blue lines represent filled orbitals after chemical bonding to the surface.

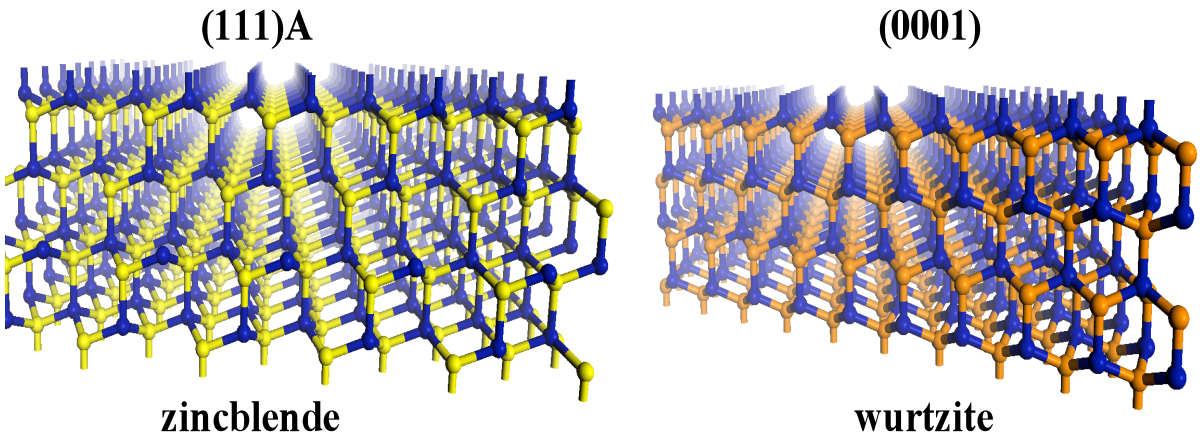

Figure 1.2. Graphical representation of (left) Zincblende GaAs and (right) Wurtzite GaN crystal slabs. The (111)A and (0001) faces are at the top of each slab, respectively, and feature atop Ga atom with one bonding orbital not participating in lattice bonding. Ga atoms are depicted in blue. As or P atoms are shown in yellow, and N atoms are depicted in orange.

IV. Wet Chemical Passivation Strategies for GaAs, GaN, and GaP

The first step toward wet chemical passivation of Ga-based III-V semiconductor surfaces is to remove the inherent native oxide on the surface. The removal of oxides is primarily achieved through two routes, by using either a wet chemical etch or a dry etch. In a wet chemical etch surface atoms are oxidized (or reduced) into a product that can be subsequently dissolved away from the surface. GaAs and GaP can be etched with either strongly acidic or basic solutions. Some common etchants for these two materials are H_2SO_4, H_3PO_4, HNO_3, HF, HCl, Br_2 in methanol, and NH_3, among others.[16,17] For example GaAs is etched according to this general equation in the presence of an acid and hydrogen peroxide:

$$GaAs + H_2O_2 + \text{“HA”} \rightarrow \text{“GaA” complex} + H_3AsO_4 + 4\ H_2O$$

However, GaN is inert to acid etchants and requires a strong base (such as NaOH or KOH) at high temperatures.[18] The advantages of using wet chemical etch methods are their relatively low cost, high-through put, and reliability if the experimental conditions (temperature, pH, duration) are carefully controlled. However, there is the potential problem that a wet chemical etch will etch the surface anisotropically. When there are two different types of surface atoms it is likely that one type of atom will etch faster than the other. For example, with GaAs, As-rich surfaces etch at a much faster rate than Ga-rich surfaces. Also, since the nature of the wet etch is diffusion limited, anisotropy can arise if the solubilized product is not removed from the near surface area fast enough or if there is a reduction in the concentration of the etchant at the surface. This particular issue can be avoided by keeping the sample size small and the concentration of the etchant high. Wet chemical etchants necessitate the disposal of and safety hazards associated with large volumes of strongly acidic solutions. Finally, bubble formation at the surface during the etching process can lead to local unetched regions. The resultant surface after a wet chemical etch can no longer be described as an atomically flat surface. During the process the surface is roughened, exposing both atom types.[16]

The most common dry etch method is through reactive ion etching (RIE). During an RIE process, a plasma is generated by strong rf frequencies between two charged plates. The reactive ions in the plasma hit the semiconductor surface and react to form etch products, which are further dislocated from the surface by the bombardment of additional reactive ions. Chlorine-based etchants are most commonly used for Ga-based III-V semiconductors, although CH_3-, bromine- and iodine- based etchants have also been used. When GaAs is etched using a chlorine etchant, the process follows this general profile:[17]

$$GaAs + Cl(etchant) \rightarrow GaCl_{x(ads)}, AsCl_{y(ads)} \rightarrow GaCl_{x(g)}, AsCl_{y(g)}$$

where x and y can range between 1 and 3 and are determined by the plasma experimental conditions, mainly the plasma temperature. The advantage of a dry etching method is that the etching profile can be perfectly anisotropic, meaning vertical sidewalls with no erosion can be achieved. Also, very small etch features can be carefully controlled due to the lack of surface tension or wettability effects that are a problem with wet etch methods. A final advantage is that a very small amount of waste is produced. However, dry etch techniques require very sophisticated instrumentation.

After etching away the native oxide to expose a clean semiconductor surface, the introduction of protective organic groups can be achieved. Perhaps one of the most well known wet chemical passivation strategies for Ga-based III-V semiconductor surfaces is through sulfide/thiol bonding. Yablonovitch, et al. first demonstrated this technique in 1987 by using aqueous sodium sulfide to passivate GaAs(100).[19] The effect of the sulfide group on the electronic properties of the GaAs(100) surfaces was probed using room temperature and low temperature photoluminescence and transient photoconductivity. Sulfide passivated surfaces demonstrated an improvement of 2800x in the photoluminescence signal over native GaAs surfaces. This corresponded to a change in the surface recombination velocity from 1×10^7 cm/s to 1×10^4 cm/s after sulfide treatment.[20] A surface with no surface recombination (ie. no surface states) would have a surface recombination velocity of 0 cm/s. The maximum surface recombination velocity is limited by the thermal velocity of carriers in a material. In GaAs, the upper limit on

surface recombination is approximately 1 x 10^7 cm/s. In order to accurately measure surface recombination velocities, recombination at the surface must be decoupled from recombination pathways that occur within the bulk (Auger, radiative recombination).[21] This necessitates the requirement of a high-purity material, where the concentration of bulk defects or contaminants is extremely low, therefore suppressing bulk recombination processes. Unfortunately, bulk III-V semiconductors with the requisite purity are exceedingly difficult to prepare and are presently unattainable commercially with an orientation in the [111] direction.

The passivation of GaAs with an aqueous sulfide has since been widely studied. Although an initial decrease in surface electronic defects has been inferred, the sulfide-treated GaAs surface quality degrades quickly in air and under sunlight.[22] The mechanism for degradation is thought to involve the breaking of the As-S or Ga-S covalent bond, which is then replaced with the formation of an oxide.[23] Variations in the pH of the sulfide solution, or more directly the sulfide concentration, do not seem to improve the longevity or packing density of the passivating layer.[23] Oxygen impurities are also prevalent when using an aqueous sulfide, though it has been shown that by changing the cation, this can be slightly controlled. GaAs surfaces that were passivated with ammonium sulfide possessed a lower concentration of oxygen impurities compared to surfaces similarly treated with sodium sulfide.[24]

The choice of solvent, much like the choice of cation, affects the quality of the passivating layer. It has been shown on GaN(0001),[25] GaAs(100),[26] and most recently with n-GaP(100)[27] that the quality of the sulfide layer can be greatly enhanced by using an alcoholic solution, or a solvent with a low dielectric constant. In the most recent case with GaP a lower carbon contamination (up to three times lower) was also reported. Unfortunately, long-term stability of sulfide layers in ambient or aqueous conditions has not been reported to date.

The passivation of Ga-based III-V surfaces with thiol groups has also been investigated. Thiol groups readily form self-assembled monolayers on GaAs, GaP and GaN at room temperature. The self-assembly process proceeds in two steps. First, thiol groups will rapidly form disordered layers, with the organic group laying close to the surface. After a few hours an equilibrium establishes and densification occurs. The final

resultant thiol monolayer can be very densely packed, with near perpendicular orientation to the surface.[28] Thiol layers are more stable against environmental degradation and surface oxidation when compared to analogous sulfide treated surfaces.[29]

There have also been many reports of the passivation of GaAs and GaP with nitrogen or nitrogen containing organic compounds. This passivation strategy was inspired by the rugged chemical inertness of GaN films, and a desire to incorporate GaAs into metal-insulator-semiconductor devices. It was hypothesized that a Ga-N interface may have less electronic defect sites than the Ga-O interface. Nitridation has been explored through both dry and wet chemical passivation methods. One example of a dry passivation technique involves immersing GaAs(100) surfaces into a plasma containing N_2(g). First the plasma serves to etch away any residual native oxide, preparing a clean GaAs surface. Then the N_2(g) reacts to form new bonds at the surface. The resultant surfaces did have a lower electronic trap site density, as compared to the starting surface.[30,31] Hydrazine (N_2H_2) was also a popular reagent for the nitridization of GaAs. Hydrazine has been used in both dry and wet chemical routes. Organic vapor deposition of hydrazine onto GaAs(111)B surfaces that were first wet etched with H_2O_2, presumably to remove the top As surface atoms, produced a Ga-N layer with improved electronic properties.[32] Characterization of these passivated surfaces revealed that hydrazine molecules adsorb to the surface in a side-on orientation.[30]

Wet chemical nitridization occurs under milder conditions and has been demonstrated on GaAs(100). Wet chemical passivation with hydrazine yields a thin homogeneous GaN layer that demonstrates improved chemical and electronic stability.[33] The addition of very small amounts of sulfide to the hydrazine solution effects more dramatic passivation on GaAs(100) surfaces because the sulfide removes the As surface atoms, facilitating direct bonding of Ga-N. GaN films prepared on GaAs(100) through this method are chemically and electronically stable for years![34,35] Interestingly, when this same hydrazine/sulfide solution is applied to GaAs(111)A or GaAs(111)B surfaces the result is entirely different. Hydrazine molecules replace the atop surface As atoms on the GaAs(111)B surface, which is expected. However, the GaAs(111)A surface is completely passivated through Ga-S bonds, even thought the concentration of hydrazine

(20 M) is significantly higher than that of the sulfide (10^{-2} M).[36] This demonstrates that the polarity of the surface has a huge effect on the surface reactivity.

GaP(100) surfaces have also been passivated with organic azides by Richards, et al. with the goal of using the azide groups to prevent leaching into aqueous and saline solutions.[37,38] Unfortunately, these surface groups do not exhibit the same chemical passivation as seen with hydrazine or nitrogen gas on GaAs(100). GaP(100) bound to organic azides are not stable for long in the presence of ambient or aqueous environments. This could possibly be due to the fact that organic azides are less nucleophilic than hydrazine or nitrogen gas.

V. Overview of Dissertation

The work presented in this dissertation involves developing a new wet chemical reaction strategy to covalently bind organic molecules to the Ga-rich surface of GaAs, GaN, and GaP. The ultimate goal of this work is to covalently bind organic groups to the surfaces of these materials that will impart both chemical and electronic stability, while also affording the possibility of further modification through secondary reactions.

Chapter Two reports the first application of a two-step chlorination/Grignard reaction sequence to Ga-rich GaAs(111)A and GaN(0001) surfaces. The reactivity of these surfaces towards alkylation is discussed and compared to previous work with Ga-rich GaP(111)A surfaces (Appendix I). The chemical stability of functionalized GaAs(111)A surfaces in ambient and aqueous conditions is characterized through X-ray photoelectron spectroscopy (XPS) and grazing-angle attenuated total reflectance (GATR) Fourier transform infrared (FTIR) spectroscopy. Raman spectroscopy is used to qualitatively characterize the density of electronic defects of alkyl-terminated GaAs(111)A as compared to the native surface.

In Chapter Three the two-step chlorination and Grignard reaction sequence is used to covalently bind allyl groups, with a terminal reactable olefin to the surface of GaP(111)A. The presence of this group is characterized by XPS and GATR-FTIR. The terminal olefin is then further reacted though Heck cross-coupling metathesis, hydrosilylation, and electrophilic addition of bromine reactions. The reactivity of a

freshly prepared allyl-terminated surface compared to a surface that has been aged in ambient conditions is compared.

A reaction strategy for the covalent attachment of a molecular catalyst to the surface of GaP(111)A is presented in Chapter Four. The GaP surface is initially passivated with pentenyl groups, containing a terminal olefin. The olefin is then reacted with dilute bromine, to produce a bromine-terminated monolayer. The bromine-terminated organic layer then undergoes a nucleophilic substitution reaction with sodium azide to produce an azide-terminated layer. Lastly, the azide groups are reacted *via* a Huisgen 1,3 dipolar cycloaddition or "Click" reaction to covalently bind an alkyne derivatized iron-based catalyst for proton reduction.

VI. References

(1) Gatos, H. C. *Surf. Sci.* **1994**, *300*.

(2) Kittel, C. *Introduction to Solid State Physics*; 6th ed.; John Wiley: New York, 1986.

(3) Nuss, M. C.; Auston, D. H.; Capasso, F. *Phys. Rev. Lett.* **1987**, *58*.

(4) Leitner, J.; Strejc, A.; Sedmidubsku, D.; Ruzicka, K. *Thermochim. Acta* **2003**, *401*, 169.

(5) Shibata, H.; Waseda, Y.; Ohta, H.; Kiyomi, K.; Shimoyama, K.; Fujito, K.; Nagaoka, H.; Kagamitani, Y.; Simura, R.; Fukufa, T. *Mater. Trans.* **2007**, *48*, 6.

(6) Dora, Y.; Chakraborty, A.; McCarthy, L.; Keller, S.; DenBaars, S. P.; Mishra, U. K. *Electron Device Lett. IEEE* **2006**, *27*, 713.

(7) Finklea, H. O. *Semiconductor Electrodes*; Elsevier: Amsterdam, 1984.

(8) Tomkiewicz, M.; Woodall, J. M. *Science* **1977**, *196*, 990.

(9) Dean, P. J.; Herbert, D. C. *J. Lumin.* **1976**, *14*, 24.

(10) Yamaguchi, T.; Niina, T.; Niina, T. *IEEE Trans. Electron Devices* **1981**, *28*, 588.

(11) Pande, K. P.; Morrison, S. R. *Appl. Phys. Lett.* **1985**, *46*.

(12) Thurmond, C. D.; Schwarts, G. P.; Kammlott, G. W.; Schwartz, B. *J. Electrochem. Soc.* **1980**, *127*.

(13) Frese Jr., K. W.; Morrison, S. R. *Appl. Surf. Sci.* **1981**, *8*, 11.

(14) Lester, S. D.; Streetman, B. G. *Superlattices Microstruct.* **1986**, *2*, 8.

(15) Heller, A. *ACS Symp Ser* **1981**, *146*, 20.

(16) Mukherjee, J.; Erickson, B.; Maldonado, S. *J. Electrochem. Soc.* **2010**, *157*, H487.

(17) Pearton, S. J. *Handbook of Compound Semiconductors: Growth, Processing, Characterization and Devices*; Elseveier, 1996.

(18) Zhuang, D.; Edgar, J. H. *Mater. Sci. Eng., R* **2005**, *48*, 1.

(19) Skromme, B. J.; Sandroff, C. J.; Yablonovitch, E.; Gmitter, T. *Appl. Phys. Lett.* **1987**, *51*, 2022.

(20) Yablonovitch, E.; Bhat, R.; Harbison, J. P.; Logan, R. A. *Appl. Phys. Lett.* **1987**, *50*, 1197.

(21) Bullis, W. M. *Measurement of carrier lifetime in semiconductors*, 1968.

(22) Sandroff, C. J.; Hegde, M. S.; Chang, C. C. *J. Vac. Sci. Technol. B* **1989**, *7*, 841.

(23) Lunt, S. R.; Ryba, G. N.; Santangelo, P. G.; Lewis, N. S. *J. Appl. Phys.* **1991**, *70*, 7449.

(24) Besser, R. S.; Helms, C. R. *J. Appl. Phys.* **1989**, *65*, 4306.

(25) Huh, C.; Kim, S.-W.; Kim, H.-S.; Lee, I.-H.; Park, S.-J. *J. Appl. Phys.* **2000**, *87*, 4591.

(26) Bessolov, V. N.; Lebedev, M. V.; Zahn, D. R. T. *J. Appl. Phys.* **1997**, *82*, 2640.

(27) Lebedev, M. V.; Mayer, T. *Phys. Status Solidi. A* **2014**, n/a.

(28) McGuiness, C. L.; Shaporenko, A.; Mars, C. K.; Uppili, S.; Zharnikov, M.; Allara, D. L. *J. Am. Chem. Soc.* **2006**, *128*, 5231.

(29) Dorsten, J. F.; Maslar, J. E.; Bohn, P. W. *Appl. Phys. Lett.* **1995**, *66*, 1755.

(30) Apen, E.; Gland, J. L. *Surf. Sci.* **1994**, *321*.

(31) Gourrier, L.; Smit, P.; Friedel, P.; Larsen, P. K. *J. Appl. Phys. Lett.* **1983**, *54*.

(32) Gaskill, D. K.; Bottka, N.; Lin, M. C. *Appl. Phys. Lett.* **1986**, *48*, 1449.

(33) Berkovits, V. L.; Ulin, V. P.; Losurdo, M.; Capezzuto, P.; Bruno, G.; Perna, G.; Capozzi, V. *Appl. Phys. Lett.* **2002**, *80*, 3739.

(34) Berkovits, V. L.; Paget, D.; Karpenko, A. N.; Ulin, V. P.; Tereshchenko, O. E. *Appl. Phys. Lett.* **2007**, *90*.

(35) Berkovits, V. L.; Ulin, V. P.; Losurdo, M.; Capezzuto, P.; Bruno, G. *J. Electrochem. Soc.* **2005**, *152*.

(36) Berkovits, V. L.; Ulin, V. P.; Tereshchenko, O. E.; Paget, D.; Rowe, A. C. H.; Chiaradia, B.; Doyle, P.; Nannarone, S. *Phys. Rev. B* **2009**, *80*.

(37) Richards, D.; Luce, P.; Zemlyanov, D.; Ivanisevic, A. *Scanning* **2012**, *34*, 332.

(38) Richards, D.; Zemlyanov, D.; Ivanisevic, A. *Langmuir* **2010**, *26*, 8141.

Chapter 2

Wet Chemical Functionalization of III-V Semiconductor Surfaces: Alkylation of Gallium Arsenide and Gallium Nitride by a Grignard Reaction Sequence

* This chapter was adapted from a published work.
Peczonczyk, S. L.; Mukherjee, J.; Carim, A. I.; Maldonado, S. *Langmuir,* **2012**, *28,* 4672

I. Introduction

Gallium-based III-V semiconductors such as gallium arsenide (GaAs) and gallium nitride (GaN) are the key materials in many existing and emerging optoelectronic technologies for chemical sensing, lighting, and solar energy conversion. One common drawback to these materials is that the quality of their native surfaces is easily compromised under ambient conditions. Relative to the vast wet chemical reaction sequences available for group IV semiconductor surfaces,[1-8] there are comparatively few established wet chemical methodologies for modifying the native surfaces of GaAs and GaN.[9-14] The most effective and most common type of wet chemical reactions for functionalizing GaAs and GaN surfaces involves immersion in solutions with sulfur-containing reagents (e.g. Na_2S or alkanethiols),[15-23] which affects the observable wetting properties, the surface energetics (i.e., the conduction and valence band edge electrochemical potentials), and/or surface trap density.[24-28] Although a comprehensive analysis of thiol/sulfide treatments is outside the scope of this chapter, the main conclusions to be drawn from decades of research are that these wet chemical strategies were not designed from a detailed molecular-level understanding of the surface reactivity and are accordingly not adequate in many optoelectronic applications. For example, thiol-

based treatments are inferior to epitaxial surface capping layers (e.g., $Al_xGa_{1-x}As$, SiN_x)[29-33] for ameliorating surface defects long-term. To determine whether any wet chemical strategy for III-V surfaces can supplant costly and complex solid-state surface treatments, better insight on the wet chemical reactivity of these semiconductor interfaces is needed.

For GaAs, the (111) surface plane features atop surface atoms with three bonding orbitals involved in bulk lattice bonding and one available bonding orbital directed normal to the surface. Unreconstructed GaAs(111) surfaces that feature only partially coordinated Ga atop atoms are denoted as GaAs(111)A (Figure 2.1a). Similarly, crystalline Wurtzite GaN ideally features only partially coordinated atop Ga atoms on the (0001) surface plane (Figure 2.1a). Provided that nonoxidized, chemically uniform GaAs(111)A and GaN(0001) surfaces can first be prepared through etching/cleaning treatments, the chemical reactivity of these two surface planes should largely reflect the reactivity of the atop Ga atoms.

We have recently demonstrated that alkyl chains can be covalently grafted onto single-crystalline GaP(111)A surfaces *via* a two-step chlorination/alkylation reaction sequence using Grignard reagents (See Appendix I).[34] The resultant GaP surfaces were resistant to surface oxidation, consistent with the presence of a protective organic group bound through a Ga-C covalent linkage. Herein, I present data that explores this reaction sequence applied to GaAs(111)A and GaN(0001) surfaces. The primary hypothesis of this chapter are that atop Ga atoms at these interfaces are selectively reactive toward nucleophilic alkylation reagents and that this surface bonding motif can address some of the deficiencies of native GaAs and GaN interfaces. Specifically, I have collected data that explore the viability of Grignard reagents (Figure 2.1b) for modifying GaAs(111)A and GaN(0001) surfaces. I will present a series of spectroscopic and electrical data that collectively describe chemically modified GaAs and GaN surfaces, highlighting this wet chemical strategy for controlling the properties of these semiconductor interfaces.

II. Experimental

Materials and Chemicals Unless noted otherwise, chemicals were purchased from Aldrich. Methanol (low water content, JT Baker), ethanol (95%, Fischer), acetone

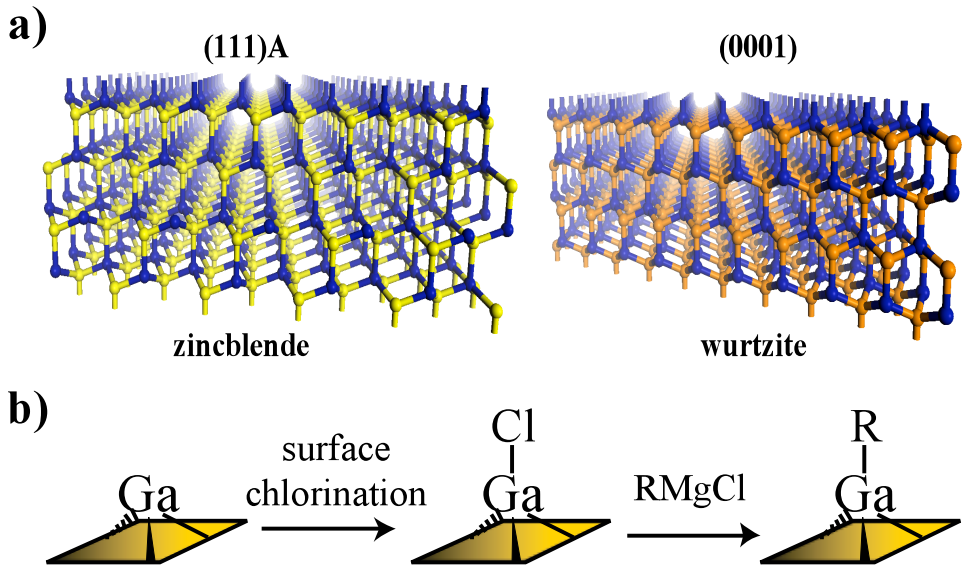

Figure 2.1. (a) Graphical representation of (left) Zincblende GaAs and (right) Wurtzite GaN crystal slabs. The (111)A and (0001) faces are at the top of each slab, respectively, and feature an atop Ga atom with one bonding orbital not participating in lattice bonding. Blue spheres depict Ga atoms, yellow spheres depict As atoms, and orange spheres depict N atoms. (b) Reaction scheme of wet chemical functionalization of atop Ga atoms at GaAs(111)A and GaN(0001) surfaces through surface Ga-C bonds produced through sequential chlorination and reaction with a Grignard reagent.

(HPLC grade, Fisher), tetrahydrofuran (anhydrous, Acros), CH_3MgCl (3.0 M solution in THF), C_2H_5MgCl (2.0 M solution in THF), C_4H_7MgCl (2.0 M solution in THF), $C_8H_{17}MgCl$ (2.0 M solution in THF), $C_{14}H_{29}MgCl$ (1.0 M solution in THF), $C_{18}H_{37}MgCl$ (0.5 M solution in THF), C_6H_4FMgBr (1.0 M in THF,), $C_{18}H_{37}SH$ (98%,), HCl (2.0 M solution in diethyl ether), HCl (aq), NH_4OH (30% NH_3 in H_2O), PCl_5 (95%), chlorobenzene (anhydrous 99.8%), doubly distilled H_2SO_4 (95-98%), tert-butyl alcohol (99%), Na_2S (90%) and KOH (85%, Acros) were used as received. Benzoyl peroxide (≥ 97%) was purchased from Fluka and dried under a vacuum of <200 mTorr for 24 h. Water with a resistivity > 18 MΩ·cm (Barnsted Nanopure system) was used throughout. GaAs(111) wafers (ITME) doped with Zn at 3.1 x 10^{17} cm^{-3} with a thickness of 400 ± 20 μm were used for physicochemical characterization. GaAs(111) wafers (ITME) doped with Si at 2.6 x 10^{16} cm^{-3} with a thickness of 500 ± 25 μm were used for electrical measurements. GaAs(111) wafers (ITME) doped with Te at 1.1 x 10^{18} cm^{-3} with a thickness of 385 ± 25μm were used for Raman measurements. Undoped N-polar GaN(0001) films on c-plane sapphire (5 μm ± 2 μm) were purchased from Kyma Technologies.

Etching Prior to use, samples were cut into square ~ 0.5 cm^2 sections and degreased by sequential rinsing in water, methanol, acetone, methanol and water. To remove native oxides, GaAs(111) samples were etched in concentrated doubly distilled H_2SO_4(aq) for 30 s, while GaN(0001) samples were etched in 1 M KOH(aq) at 70°C for 2 min. Etched samples were rinsed with copious amounts of water and dried with a stream of N_2(g) before further use.

Chlorine Activation and Grignard Reaction All reactions were performed in a MBraun LABstar glove box purged and pressurized with dry N_2(g). The residual O_2 and H_2O content in the glovebox were assessed using diethyl zinc and an exposed tungsten filament.[35,36] An open container of diethyl zinc in the glovebox did not combust, or substantially fume. Separately, an exposed tungsten filament remained lit for > 7 min, indicating that H_2O and O_2 levels were at 100 ppm or lower after purging with dry N_2(g). Chlorination of GaN(0001) was performed at 95ºC for 50 min in a saturated solution of PCl_5 in chlorobenzene containing a few grains of benzoyl peroxide.[34,37] This treatment macroscopically roughened both GaAs(111) surface planes. Attempts were made to

perform this reaction at lower temperatures and for shorter time periods but PCl_5 in chlorobenzene effected bulk etching of GaAs under all investigated reaction conditions. Accordingly, GaAs(111)A surfaces were immersed in a 2 M solution of HCl in diethyl ether for 50 min. The sample was then rinsed with anhydrous THF. For samples used for further functionalization, the substrates were directly reacted with the next reagent without exposure to ambient. For XP analysis, Cl-activated surfaces were exposed briefly (<15 s) to ambient before insertion into the X-ray photoelectron spectrometer.

Reactions with Grignard reagents were performed at 145-150ºC for 3 h in a closed, pressurized thick glass vessel. These vessels were heated with a solid metal heating block. Following reaction, samples were rinsed sequentially with anhydrous THF and anhydrous methanol. Samples were subject to an additional sonication step in methanol for 2 minutes to remove any physisorbed Cl- and Mg-containing species.

X-ray Photoelectron Spectroscopy All X-ray photoelectron spectra were acquired with a PHI 5400 analyzer using an Al Kα (1486.6 eV) source without a monochromator. Spectra were recorded without charge neutralization at a base pressure of < 2.5×10^{-9} torr. A 6 mA emission current and 10 kV anode HT were used. Survey scans were acquired at a pass energy of 117.40 eV. High-resolution XP spectra of Ga 3d, As 3d, C 1s, and Cl 2p regions were recorded at a pass energy of 23.5 eV. The binding energy of all spectra were corrected using the difference between the observed peak energy of the C 1s signal and the expected binding energy for adventitious carbon at 284.6 eV.[38] Average times for acquiring high-resolution spectra (100 scans) for each element ranged from 30-45 minutes. Samples did not undergo any observable degradation upon exposure to the X-ray source under these conditions.

Spectra were fit and analyzed using CasaXPS Version 2.313 software. A Shirley background correction was applied to all spectra. As 3d peaks were fit using a 70% Gaussian and 30% Lorentzian line shape, a pair of doublets that were mutually constrained to have an area ratio of 3:2 and the same full width at half maxima (ranging from 0.9-1.2), and peak separation of 0.69 eV.[39,40] Fractional monolayer coverage of oxidized GaAs surfaces were calculated using the simplified substrate-overlayer model (Equation 2.1).[39]

$$d = \lambda_{ov} \ln\left(1 + \frac{I_{overlayer}}{I_{substrate}} \frac{I^0_{substrate}}{I^0_{overlayer}}\right) \sin\phi \qquad (2.1)$$

where d is the thickness of the oxide overlayer in nm, λ_{ov} is escape depth of the emitted electrons through the oxide overlayer, ϕ is the take-off angle (54.6º), $I_{substrate}$ is the integrated area of As 3d signal from the bulk crystal, $I_{overlayer}$ is the integrated area of the oxide As 3d signals, $I^0_{substrate}$ is the integrated intensity of As 3d signals obtained from a GaAs surface etched with H_2SO_4(aq) for 30 s, and $I^0_{overlayer}$ is the integrated intensity of the As 3d oxide signatures from a pure oxide of GaAs. To determine this value, thick thermal oxides were not tenable,[41,42] so $I^0_{overlayer}$ was estimated with a heavily chemically oxidized substrate. The escape depths of As 3d electrons were estimated from Eq 2.2,

$$\lambda = 0.41 A^{3/2} E^{1/2} \qquad (2.2)$$

where α is the diameter of the atoms in the overlayer in nm and E is the kinetic energy of the ejected core electron in electronvolts.[39] The escape depth was 2.1 nm for As 3d electrons. The surface coverage of Cl-terminated GaAs(111)A and GaN(0001) was calculated using the full substrate overlayer model.[39]

$$\left(\frac{I_{ov}}{I_{sub}}\right) = \left(\frac{SF_{ov}}{SF_{sub}}\right)\left(\frac{\rho_{ov}}{\rho_{sub}}\right)\left(\frac{1 - e^{\frac{-d_{ov}}{\lambda_{ov}\sin\phi}}}{e^{\frac{-d_{ov}}{\lambda_{sub}\sin\phi}}}\right) \qquad (2.3)$$

where SF_{sub} is the instrument sensitivity factor for the element of interest in the substrate, SF_{ov} is the instrument sensitivity factor for the element of study in the overlayer, ρ_{sub} is the molar density of the element of interest in the substrate (mol cm^{-3}), ρ_{ov} is the density of the element of interest in the overlayer (mol cm^{-3}), and the other symbols are defined as above.

For time-dependent oxide growth measurements, modified samples were first introduced into the XPS load-lock chamber immediately following functionalization. Subsequent measurements were taken by exposing the sample to laboratory ambient for a

designated period of time in the spectrometer load-lock chamber and then re-insertion back into the XPS chamber. For water studies, samples were immersed in water, removed and dried under flowing N_2(g), and then re-introduced into the XPS load-lock chamber.

Fourier Transform Infrared Spectroscopy Infrared spectra were acquired using a Thermo-Fisher 6700 FT-IR spectrometer equipped with a grazing angle attenuated total reflectance (GATR) accessory. A Ge hemisphere was used with p-polarized light at an incidence angle of 65°. Ge crystal was cleaned with methyl ethyl ketone prior to each data collection. All spectra were referenced to a bare freshly cleaned Ge crystal spectrum.

Static Sessile Drop Contact Angle Measurements A water droplet (~ 2.2 μL) was dispensed onto the surface of each interrogated sample. Each contact angle formed between the droplet and sample interface was recorded with a CAM 100 optical contact angle meter (KSV instrument, Helsinki, Finland). Images of the droplets were acquired and analyzed using the KSV software analysis package. The reported values are the average equilibrium contact angles (θ_0), which were calculated from the advancing contact angle (θ_A) and receding contact angle (θ_R) (Equation 2.4).[43,44] The uncertainties in θ_0 are reported as sample deviations.

$$\theta_0 = \arccos\left(\frac{\sqrt[3]{\frac{\sin^3\theta_A}{2-3\cos\theta_A+\cos^3\theta_A}}\cos\theta_A + \sqrt[3]{\frac{\sin^3\theta_R}{2-3\cos\theta_R+\cos^3\theta_R}}\cos\theta_R}{\sqrt[3]{\frac{\sin^3\theta_A}{2-3\cos\theta_A+\cos^3\theta_A}} + \sqrt[3]{\frac{\sin^3\theta_R}{2-3\cos\theta_R+\cos^3\theta_R}}}\right) \quad (2.4)$$

Raman Spectroscopy Raman spectra were acquired with a Renishaw inVia spectrometer arranged in a 180˚ backscatter geometry and equipped with a Leica microscope, Leica 100x N Plan EPI objective (*NA* = 0.85), dielectric edge filter, 1800 lines/mm grating and a CCD detector. The 457.9 nm line of a Ar^+ laser (Coherent Innova 307) was used as the excitation with a radiant power of 160 μW incident on the sample. Optical excitation was directed along the $\langle 111 \rangle$ direction and polarized along the $\left\langle 11\bar{2}0 \right\rangle$ direction. No polarization optics were used for the detection of scattered light. This excitation is strongly absorbed by GaAs ($\alpha_{GaAs,\ 458\ nm} = 1.9 \times 10^5\ cm^{-1}$),[45] that is, the Raman

scatter arises from the near surface region. The use of an objective with a high numerical aperture also ensured that the collection of scattered light was predominantly from the near surface region. Hence, these spectral acquisition conditions were chosen specifically to collect Raman spectra that reported on the surface to near-surface regions of heavily doped GaAs samples. Unfortunately, an appropriate excitation wavelength for GaN that would similarly effect surface-sensitive Raman signals was not available and so no attempt was made to acquire Raman spectra for GaN. Integrated areas of the Γ(TO) and Γ(LO) modes were determined through spectra fitting with Wire 3.1 software. The best fits were obtained for each signature using a line shape composed of 55% Gaussian and 45% Lorentzian lineshapes. For comparison, GaAs(111)A samples were also treated by immersion in a 10% (v/v) Na_2S solution in tert-butanol for 6-8 h in a N_2(g) purged glovebox, then analyzed under ambient conditions.[46-48]

Hg/GaAs Heterojunctions Several methods for preparing ohmic back contacts were explored. Initial efforts followed the procedure of G. Nesher et al.[25] First, the backside was gently scratched with a diamond scribe and then immediately coated with a thin layer of InGa eutectic. Spot contacts separated by 2-3 mm showed a total resistance of 100-120 ohms but the current-potential responses between these spot contacts were decidedly non-linear, i.e. these contacts did not exhibit ideal ohmic behavior. Therefore, an alternative contacting strategy was used.[34] Briefly, the backside was scratched, etched in H_2SO_4(aq), and then coated with a thin layer of In solder. The sample was purged in a tube furnace with Ar for 50 minutes at a flow rate of 1000 $cm^3 \bullet min^{-1}$, annealed at 400°C for 10 minutes in a stream of Ar(g) and forming gas (5:95 H_2(g):N_2(g), v/v at a flow rate of 50 $cm^3 \bullet min^{-1}$) and slowly cooled to room temperature in Ar(g). For functionalization only the non-soldered part of the crystal was exposed to reagents so that the ohmic contact remained uncompromised. For functionalization with $C_{18}H_{37}S$- moieties, the non-soldered part of sample was etched and immediately immersed for 24 h in a freshly prepared ethanolic solution of 0.003 M $C_{18}H_{37}SH$ and 0.01 M NH_4OH.[20] The solution was deaerated and degassed in dry N_2(g) prior to use. After surface passivation, the wafer was thoroughly rinsed in ethanol and immediately used for further studies. A Hg droplet was placed on the front surface of a GaAs wafer section resting on a stainless steel support that acted as the back contact. A Viton o-ring was used to define the junction area

(0.063 cm^2) between GaAs and the Hg droplet. A Pt wire was used to make electrical contact to the Hg droplet. Current-voltage responses were measured in the dark, with a CH Instruments potentiostat/galvanostat at a scan rate of 0.05 $V \bullet s^{-1}$.

Atomic Force Microscopy Atomic force microscopy (AFM) images were acquired using a Veeco 3100 NanoMan AFM in tapping mode with a scan rate of 0.8 Hz. Bruker Tespa tips were used for image acquisition. Data analysis was preformed in a separate image analysis sorftware package (Gwyddion) after first flattening and plane fitting the raw images. The AFM images presented are representative 2 μm x 2 μm images all plotted with the same z-scale. The surface roughness average (R_a) and root mean square roughness (RMS) were calculated using equations 2.5 and 2.6, respectively.

$$R_a = \frac{1}{n}\sum_{i=1}^{n}|y_i| \tag{2.5}$$

$$RMS = \sqrt{\frac{1}{n}\sum_{i=1}^{n}y_i^2} \tag{2.6}$$

III. Results

GaAs Unlike our earlier report on chlorine-termination of GaP(111)A interfaces (See Appendix I),[34] wet chemical chlorination of GaAs(111)A surfaces through immersion in dissolved PCl_5 in chlorobenzene consistently effected severe etching/ macroscopic pitting. Aqueous HCl(aq) has previously been used to introduce surficial Cl at GaAs(111)A.[40] To avoid the possibility of residual Ga surface hydroxides from an aqueous chlorination step,[40,49] HCl in diethyl ether facilitated surface chlorination in a controlled environment in a N_2(g) glovebox. Figure 2.2a shows high-resolution XP spectra highlighting the Cl 2p doublet near the As 3s signal. Selective chlorination of GaAs(111)A over GaAs(111)B surfaces was observed, with no detectable level of Cl at GaAs(111)B surfaces. The Cl signatures in Figure 2.2a could be fit accurately with a single doublet.

Following chlorination, GaAs(111)A substrates were immediately exposed to dissolved Grignard reagents in THF. High-resolution XP spectra of chlorinated GaAs(111)A surfaces after reaction with $C_{18}H_{37}MgCl$ in THF are shown in Figures 2.2a and 2.2b. Following this sequence, a decrease in surficial Cl from 0.41 ± 0.04 monolayers (ML) to 0.18 ± 0.04 ML was observed. For samples that were not immersed in CH_3OH following exposure to Grignard reagents, detectable levels of Mg, presumably from residual Grignard reagent, were noted. Brief sonication in CH_3OH effectively removed these signatures (detection limit of Mg < 1 at %). Additionally, after reaction with linear chain alkyl Grignard reagents ($C_nH_{2n+1}MgCl$, $n \geq 4$), the measured C 1s intensity was consistently larger than for etched or chlorinated samples. Two separate factors complicated quantitative analysis of the collected C 1s spectra. First, the broad As LLM Auger signal at slightly smaller binding energies than 284 eV masked any possible low-energy shoulder indicative of Ga-C.[17] Second, the presence of adventitious carbon precluded direct determination of surface group content from the intensity of the C 1s signal. Although adventitious carbon was always detected on every measured GaAs surface condition, a pronounced and systematic increase in C 1s signal intensity following exposure to solutions of long alkyl chain Grignard reagents was never observed for GaAs(111)B surfaces. To separately probe the carbon content of GaAs(111)A surfaces before and after reaction with $C_{18}H_{37}MgCl$, infrared spectra were obtained with a grazing-angle attenuated total reflectance (GATR) accessory. After functionalization, the pronounced increase in the intensities of the CH_3- and CH_2- asymmetric and symmetric vibrational modes was consistent with introduction of long alkyl chains to GaAs(111)A specifically *via* the two-step Grignard reaction sequence (Figure 2.3).

To assess the physicochemical properties of GaAs(111)A surfaces following chlorine activation and reaction with alkyl Grignard reagents, the wetting properties of reacted surfaces were measured (Table 2.1). Figure 2.4a shows the measured sessile drop contact angles between a water droplet and GaAs(111)A surfaces after reaction with several different alkyl Grignard reagents. Freshly etched GaAs(111)A interfaces consistently showed the smallest sessile drop contact angles (45 ± 3°). Etched samples that were then immersed in hot THF without dissolved Grignard reagents showed modestly higher sessile drop contact angle values (‘control’, 60 ± 4°). Reaction with short

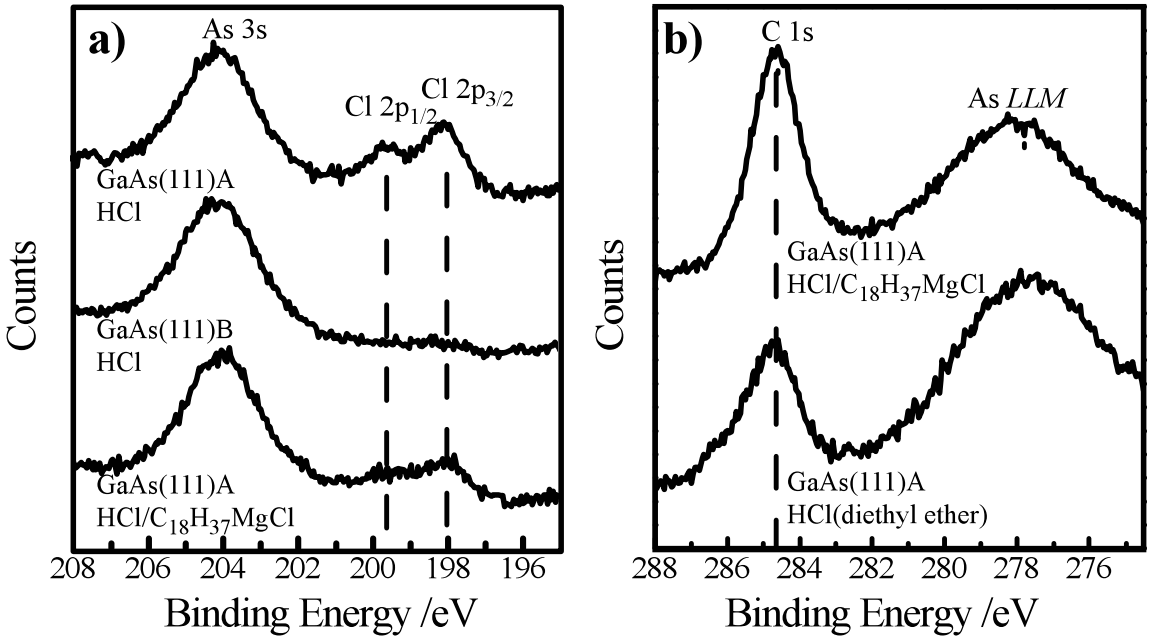

Figure 2.2. (a) High-resolution XP spectra of Cl 2p region for (top) GaAs(111)A after reaction with HCl in diethyl ether, (middle) GaAs(111)B after reaction with HCl in diethyl ether, and (bottom) GaAs(111)A after sequential reaction first with HCl in diethyl ether and then $C_{18}H_{37}MgCl$ in THF. (b) High-resolution C 1s XP spectra for GaAs(111)A after reaction in (top) HCl in diethyl ether followed by $C_{18}H_{37}MgCl$ in THF and (bottom) HCl in diethyl ether. Spectra are offset for clarity.

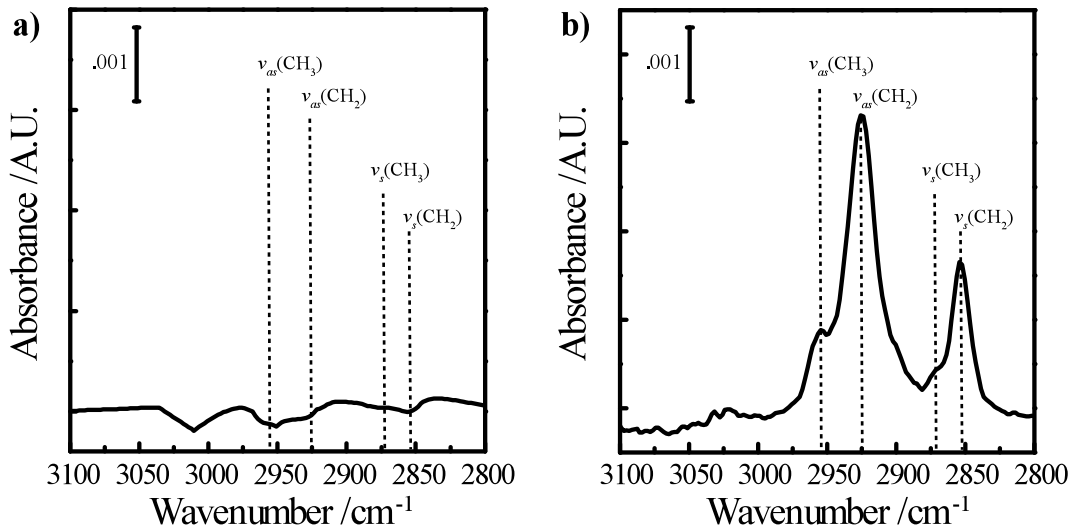

Figure 2.3. GATR-FTIR spectra of GaAs(111)A surfaces after (a) etching with H_2SO_4(aq) or (b) after sequential reaction with HCl in diethyl ether solution and then $C_{18}H_{37}MgCl$. Dashed lines denote asymmetric and symmetric CH_3- and CH_2- vibrational stretches.

Table 2.1. Water Contact Angle Measurements (°)

Treatment	GaAs(111)A	GaP(111)A	GaN(0001)
etched[a]	≤ 20	45 ± 3	36 ± 6
control[b]	≤ 40	60 ± 4	45 ± 4
$C_{18}H_{37}MgCl$[c]	119 ± 6	107 ± 11	78 ± 3

a.degreased and etched to remove native oxide
b.same as (a), then Cl-activated, then immersed in hot THF
c.same as (a), then Cl-activated, then immersed in THF with Grignard reagent

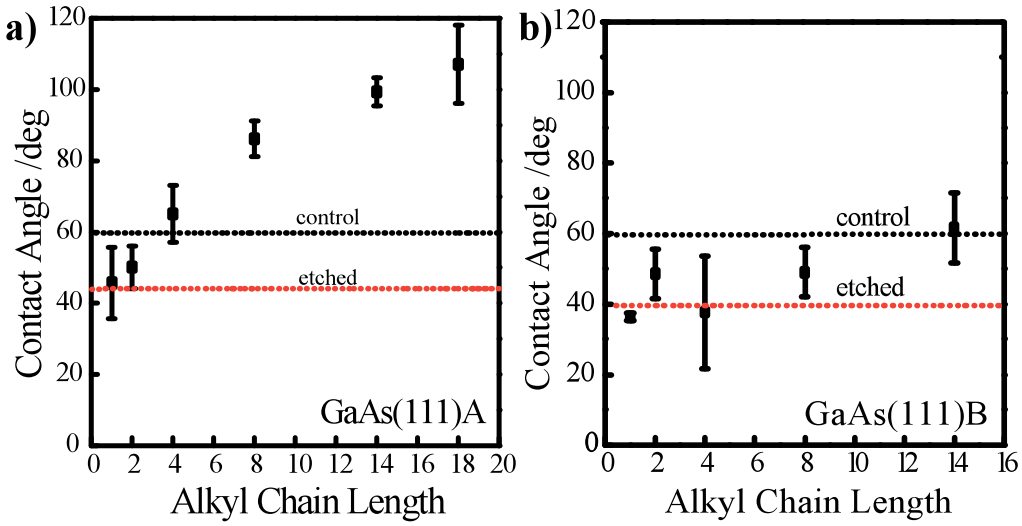

Figure 2.4. Measured contact angle between sessile water droplet and (a) GaAs(111)A or (b) GaAs(111)B after sequential reaction first with HCl in diethyl ether and then with $C_nH_{2n+2}MgCl$ (n= 1, 2, 4, 8, 14, 18) in THF.

alkyl Grignard reagents ($n \leq 2$) did not increase the measured sessile drop contact angle values relative to control samples. Reaction with longer alkyl Grignard reagents ($n \geq 4$) did result in a pronounced increase in hydrophobicity that was larger than the control sample, with longer alkyl Grignard reagents effecting larger sessile drop contact angle values. Measurements for GaAs(111)B interfaces treated in the same manner did not show either a systematic increase in hydrophobicity or values larger than control samples (Figure 2.4b). These observations support the contention that alkyl groups are selectively attached to GaAs surfaces through a linkage that is specifically favored at the GaAs(111)A face over the GaAs(111)B surface plane.

The amount of residual oxide after reaction with Grignard reagents was determined through high-resolution As 3d XP spectra (Figure 2.5). Samples that were reacted only with HCl in diethyl ether consistently showed As 3d spectra indicating no detectable surface oxide. The rates of surface oxidation following surface treatment [either etching for 30 s with concentrated H_2SO_4(aq)[50] or the two-step Grignard reaction sequence] were then measured. GaAs(111)A surfaces etched in H_2SO_4(aq) consistently showed a detectable level of surface oxides inferred from the As 3d spectra (0.23 nm). Prolonged exposure to air resulted in rapid and further oxidation of GaAs(111)A surfaces. After 90 min, both an increase in As_2O_3-type surface oxides and the appearance of spectral features at slightly higher binding energies indicative of As_2O_5-type surface oxides were noted (Figure 2.5a). In contrast, GaAs(111)A surfaces that had been reacted with $C_{18}H_{37}MgCl$ exhibited a suppressed rate of surface oxidation (Figure 2.5b). Specifically, after 90 min of exposure to ambient air, the surface oxide content inferred from the As 3d spectra for GaAs(111)A reacted with $C_{18}H_{37}MgCl$ was eight-fold lower than the surface oxide content on etched GaAs(111)A exposed to ambient air for the same period of time (Figure 2.5c). The GaAs(111)A surfaces were stable in air for prolonged periods, exhibiting less than a monolayer of oxide after 35 days (Figure 2.5d), but the apparent oxidation rate for these GaAs(111)A surfaces were higher than the oxidation rate for GaP(111)A surfaces treated with the same Grignard reagents.[34] GaAs(111)A surfaces reacted with CH_3MgCl also showed a slightly higher rate of surface oxidation in ambient air (Figure 2.6) as compared to similarly treated GaP(111)A surfaces.[34]

High-resolution As 3d XP spectra were also collected to assess the susceptibility of GaAs to chemical attack during immersion in water. GaAs(111)A interfaces were studied that were initially etched in concentrated H_2SO_4(aq) and then immersed in oxygenated water for a total of 27 h. After this period of time, the native surface became visibly roughened, appearing dull and dark brown. High-resolution XP spectra (Figure 2.7a) exhibited two important features. First, the intensity of the signature corresponding to oxidized As species (shown in dashed box) exceeded the intensity of the signature for As from the bulk, indicating the surface has become substantially oxidized by water. Second, the overall intensity of the As 3d spectra decreased, as evidenced by the significantly poorer signal-to-noise ratio under the same collection conditions as the data for the initially etched sample. Corresponding survey scans of these two surface types showed that the GaAs(111)A surfaces are Ga-rich i.e. the surfaces become depleted specifically of As (oxidized and reduced) in the near surface region of the samples (Figure 2.7b). These observations are consistent with the known solubility of oxidized As species in water.[51] In contrast, GaAs(111)A surfaces that were treated with the two-step chlorination-alkylation reaction sequence showed substantial resistance to chemical attack from water. These surfaces remained smooth (mirror polished) even after immersion in water for 27 h, with no visible discoloration. The collected As 3d XP spectra correspondingly showed no appreciable change after 27 h in water (Figure 2.7c). Specifically, no perceptible increase in signatures indicative of oxidized As species were apparent in the high-resolution As 3d XP spectra and the As content inferred from the survey scan was the same before and after water immersion (Figure 2.7d).

Additional experiments were performed to assess the electrical properties of GaAs(111)A surfaces following reaction with Grignard reagents. Figure 2.8 and Table 2.2 display the first-order Raman spectral features recorded for GaAs(111)A samples under the spectral acquisition conditions defined above. According to the selection rules for a Zincblende crystal structure in the absence of an applied electric field and with optical excitation normal to the (111) surface plane, a pronounced Γ(TO) phonon mode at 268 cm^{-1} is independent of carrier density and the presence/absence of an electric field.[52] Conversely, the Γ(LO) phonon mode at 291 cm^{-1} is strongly sensitive to the magnitude of an electric field, with increased intensity under larger electric fields.[53,54] Specifically, so-

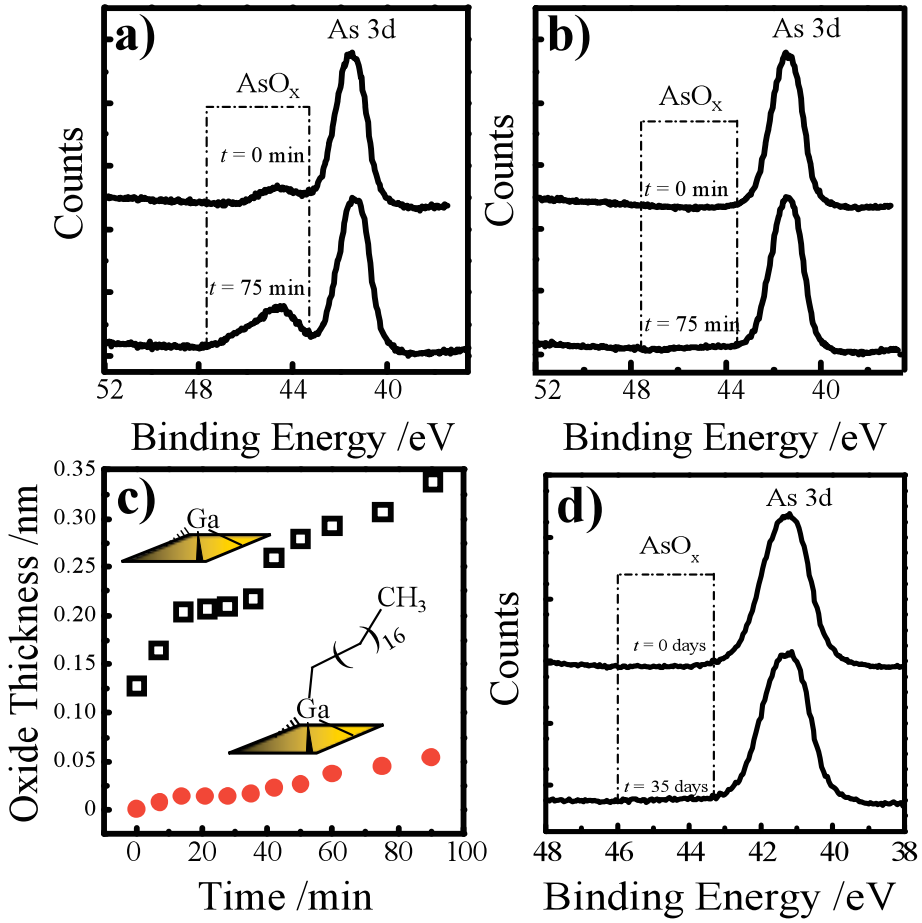

Figure 2.5. Time-dependent high-resolution As 3d XP spectra for GaAs(111)A surfaces (a) after etching with H_2SO_4(aq) and (b, d) after sequential reaction first with HCl in diethyl ether solution and then $C_{18}H_{37}MgCl$ in THF. Spectra are offset for clarity. (c) Measured time-dependent oxide growth from As 3d spectra over time for GaAs(111)A surfaces (open square) etched in H_2SO_4(aq) and (red circles) after sequential reaction first with HCl in diethyl ether and then with $C_{18}H_{37}MgCl$ in THF.

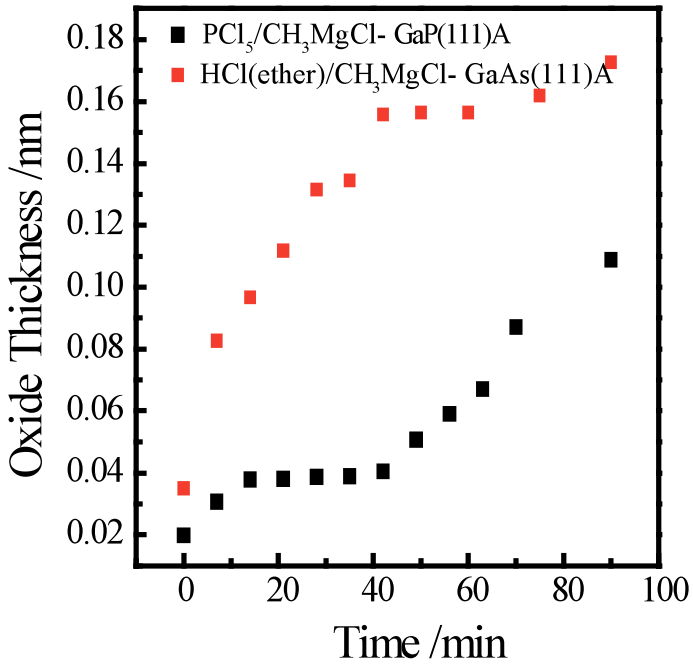

Figure 2.6. Oxide thickness of (red squares) GaAs(111)A surfaces after sequential reaction with HCl in diethyl ether solution and CH_3MgCl in THF and (black squares) GaP(111)A surfaces after sequential reaction with PCl_5 in chlorobenzene and CH_3MgCl in THF as a function of time exposed to ambient. Oxide thickness calculated from high-resolution Ga 3d spectra.

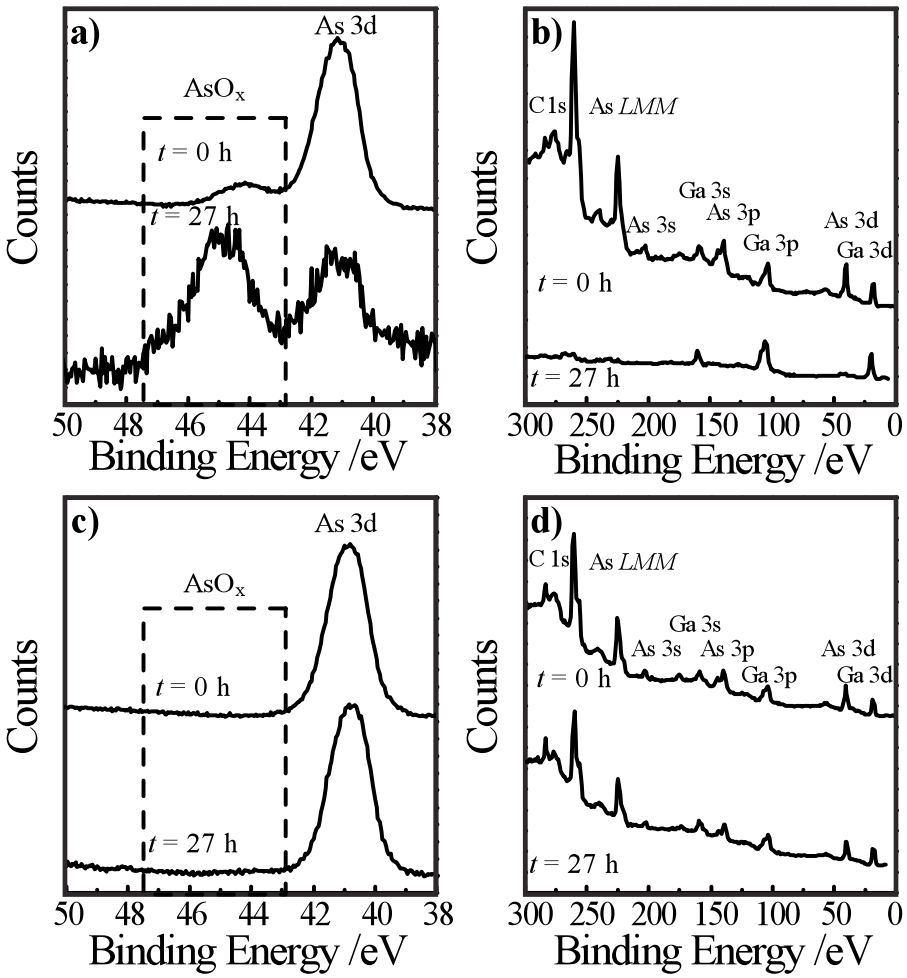

Figure 2.7. (a, b) XP spectra, (a) high-resolution As 3d and (b) survey, for GaAs(111)A surfaces that were etched in H_2SO_4(aq). The top spectra in panels a and b were obtained immediately after etching, and the bottom spectra were collected after sustained immersion in water for 27 h. (c, d) XP spectra, (c) high-resolution As 3d and (d) survey, for GaAs(111)A surfaces that were sequentially reacted with HCl in diethyl ether solution and then $C_{18}H_{37}MgCl$ in THF. The top spectra in panels c and d were obtained immediately after preparation, and the bottom spectra were collected after sustained immersion of 27 h.

called electric-field-induced Raman scattering (EFIRS)[55-58] can be observed at semiconductor surfaces under strong depletion and can be used to gauge the level of band bending and surface defects when (1) the length scale of the depletion layer is on par with the optical probing depth of the Raman experiment and (2) the resultant electric field is large (two conditions satisfied with the experimental condition employed here). Figure 2.8a shows that both Γ(TO) and Γ(LO) phonon modes are readily apparent in the spectra for GaAs(111)A surfaces featuring a native oxide. Native oxides at GaAs interfaces possess a high density of electrical defects, which trap charge and render a significant potential drop across the near-surface region (i.e. appreciable band bending occurs).[18,52,55] Figures 2.8b and 2.8c depict the presence and absence of surface depletion for ideal n-type semiconductors featuring a high density and absence of a significant density of surface defects, respectively. Under certain experimental conditions, the logarithm of the integrated intensity of the Γ(LO) mode, I_{LO}, is directly proportional to the product of the depletion layer width, W, in the semiconductor and the absorptivity of the excitation wavelength, $\alpha(\lambda)$.[48,59] In the work shown here, adequate polarization optics on the collection side were not available and so the contribution to the intensity of the Γ(LO) mode from deformation-potential scattering[52] was not determined, preventing explicit calculation of the magnitude of band bending within each sample. Nevertheless, by using the integrated intensity of the Γ(TO) mode, I_{TO}, as an 'internal standard', the ratio I_{TO}/I_{LO} does report on the extent of band bending and, by association, the presence of mid-gap surface defects that effect depletion conditions. Table 2.2 shows the values of I_{TO}/I_{LO} for GaAs(111)A substrates coated with a native oxide. Table 2.2 also shows the value of I_{TO}/I_{LO} recorded for samples treated with 10% Na_2S in tert-butanol, a proven (albeit temporary) wet chemical passivation strategy that eliminates surface defects. For comparison, Figure 2.8d shows a representative Raman spectrum for a GaAs(111)A surface treated with $C_{18}H_{37}MgCl$. In marked contrast to Figure 2.8a, the intensity of the Γ(LO) phonon mode is substantially suppressed. As indicated by I_{TO}/I_{LO} for alkyl-terminated samples (Table 2.2), GaAs(111)A samples treated with these Grignard reagents showed responses comparable to those measured for Na_2S(tert-butanol)-treated GaAs(111)A surfaces. These data suggest that alkyl terminated GaAs(111)A surfaces do not possess the same high density of mid-gap surface trap states that native oxides on

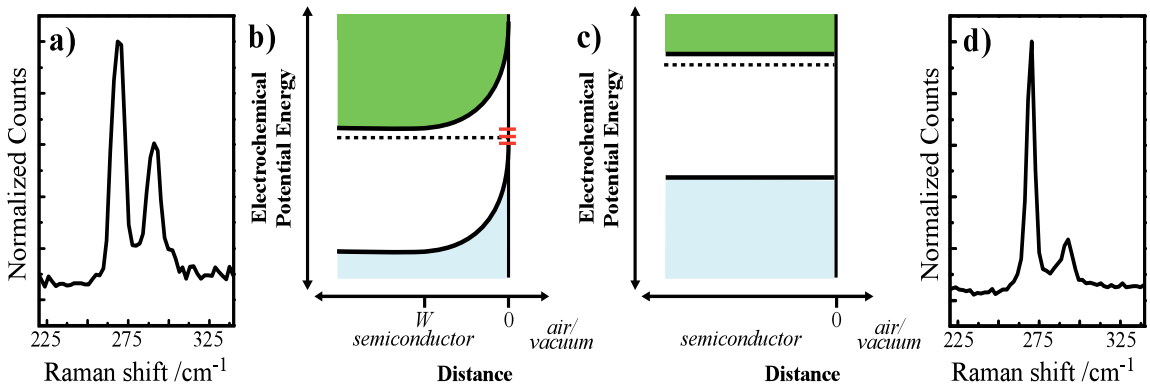

Figure 2.8. (a) First-order Raman spectrum for GaAs(111)A featuring a native oxide. (b) Idealized depiction of an n-type semiconductor under depletion conditions caused by a high density of surface states. (c) Idealized depiction of the depletion condition of an n-type semiconductor in the absence of surface states. (d) First-order Raman spectrum for GaAs(111)A after sequential reaction first with HCl in diethylether then $C_{18}H_{37}MgCl$ in THF. Spectra in panels a and d are both normalized to the same y-axis scale.

Table 2.2. Measured Ratio of Phonon Intensity in First-Order Raman Spectra for GaAs(111)A Surface

Surface Treatment	I_{TO}/I_{LO} [a,b]
native oxide	1.98 ± 0.03 (N=7)
Na_2S(*t* -butanol)	3.04 ± 0.11 (N=7)
HCl(diethyl ether)/CH_3MgCl	3.04 ± 0.16 (N=7)
HCl(diethyl ether)/$C_8H_{17}MgCl$	2.72 ± 0.26 (N=5)
HCl(diethyl ether)/$C_{14}H_{29}MgCl$	3.68 ± 0.51 (N=5)
HCl(diethyl ether)/$C_{18}H_{37}MgCl$	2.89 ± 0.08 (N=5)

a. Measured ratio of integrated intensities for Γ(TO) and Γ(LO)
b. Errors reported as standard deviation for N sample measurements

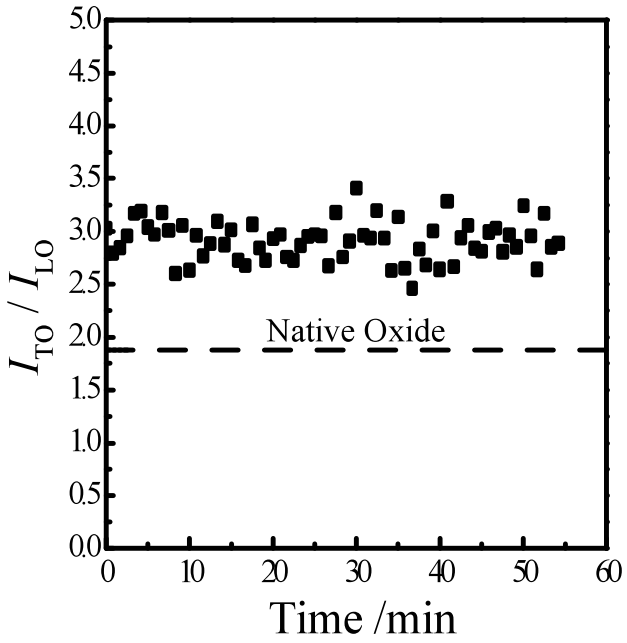

Figure 2.9. Ratio of integrated intensities of the I_{TO} and I_{LO} phonon modes obtained from first-order Raman spectra over time for GaAs(111)A surfaces after sequential reaction with HCl in diethyl ether solution and then $C_{18}H_{37}MgCl$ in THF. Dashed line denotes the average intensity ratio for a native surface of GaAs(111)A.

GaAs(111)A have. Further, the Raman spectra suggest that the electrical quality of alkyl terminated GaAs(111)A is comparable to GaAs(111)A surfaces treated with Na_2S(tert-butanol), the most effective known wet chemical treatment.[48] A distinct feature of the GaAs(111)A surfaces following reaction with $C_{18}H_{37}MgCl$ is that the Raman signal is stable (Figure 2.9). Over the course of 50 min, the measured values of I_{TO}/I_{LO} remained unchanged for GaAs(111)A surfaces treated first with HCl(diethyl ether) then $C_{18}H_{37}MgCl$. By contrast, the beneficial surface properties induced by immersion in a Na_2S solution are known to be fleeting.[20,48]

A separate probe of the electrical properties of GaAs(111)A surfaces following the two-step chlorination/Grignard reaction sequence was performed through the analysis of Hg/GaAs Schottky heterojunctions.[60] We note that the back contacting scheme described by G. Nesher et. al[25] yielded heterojunctions whose properties were only partially sensitive to surface changes and so an alternative ohmic contacting approach was used. Several types of Hg/GaAs(111)A junctions, including freshly etched GaAs(111)A surfaces, GaAs(111)A surfaces reacted with $C_{18}H_{37}SH$ in ethanol, and GaAs(111)A surfaces reacted with HCl(diethyl ether)/$C_{18}H_{37}MgCl$, were studied. Figure 2.10a shows representative current density-potential responses for these three types of Hg/GaAs contacts. All three types exhibited strongly rectifying responses, with the etched GaAs(111)A surfaces resulting in the lowest applied bias needed to support a given current density. The Hg/GaAs(111)A heterojunctions featuring surface alkyl chains both showed more strongly rectifying responses. In principle, both of these heterojunctions feature a similar organic barrier layer between Hg and GaAs consisting of $C_{18}H_{37}$- groups. The observed current density-potential profiles for these two contact types were similar, indicating that both types of long alkyl chain surface groups acted as comparable tunneling barriers that impeding heterogeneous charge transfer between GaAs and Hg. The different surface bonds linking the alkyl chains to GaAs (i.e. ‘Ga-C’ vs ‘Ga-S) apparently was not the defining feature impacting heterogeneous charge transfer in these systems. Figure 2.10b highlights a secondary difference between these two specific contact types. Figure 2.10b shows the applied potential required to drive an arbitrary current density of 0.02 A cm^{-2} across the Hg/GaAs heterojunction. Upon repeated cycling between 0 and 1.2 V, a decrease in the applied potential required to

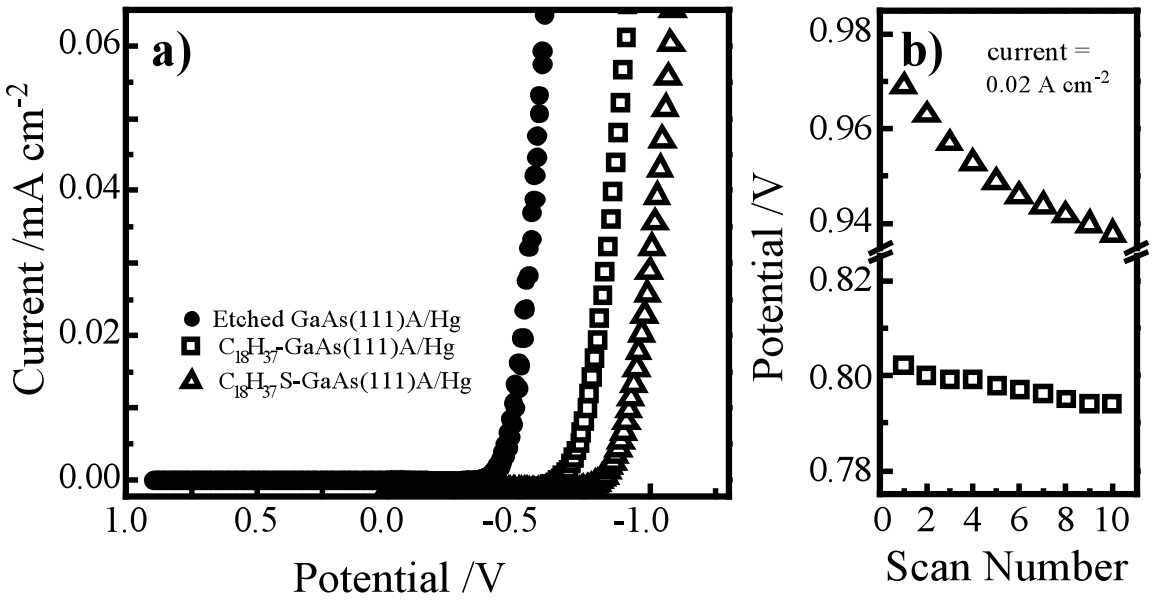

Figure 2.10. (a) Measured potential-dependent current density for Hg/GaAs heterojunctions featuring (circle) GaAs(111)A etched in H_2SO_4(aq), (triangle) GaAs(111)A functionalized with $C_{18}H_{37}SH$ in ethanol, and (square) GaAs(111)A functionalized with $C_{18}H_{37}MgCl$ in THF. (b) Change in necessary applied bias to drive 0.02 A•cm^{-2} across Hg/GaAs heterojunctions as a function of potential scan number for (triangle) GaAs(111)A functionalized with $C_{18}H_{37}SH$ in ethanol and (square) GaAs(111)A functionalized with $C_{18}H_{37}MgCl$ in THF.

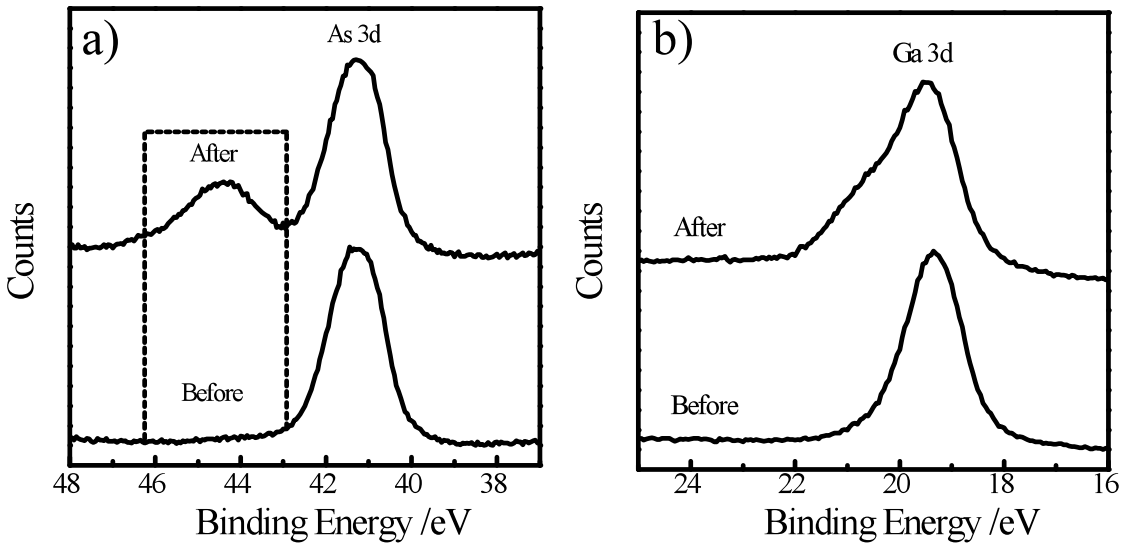

Figure 2.11. High-resolution (a) As 3d and (b) Ga 3d regions for GaAs(111)A after reaction with $C_{18}H_{37}SH$ in ethanol. Bottom spectra were acquired immediately after functionalization, and top spectra were obtained after the passage of charge at 0.02 A•cm^{-2} for 10 scans. Spectra are offset for clarity.

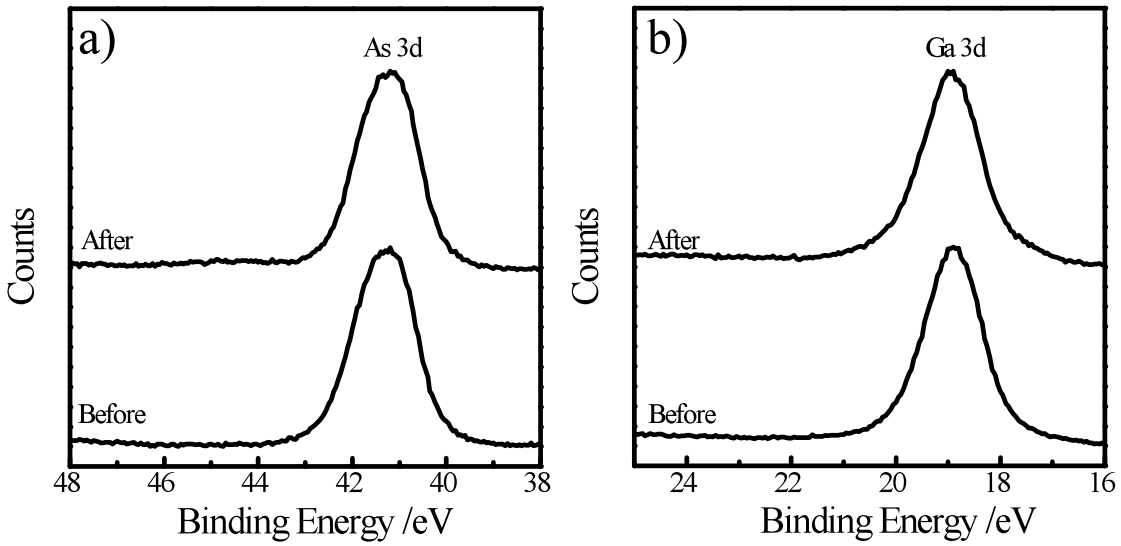

Figure 2.12. High-resolution (a) As 3d and (b) Ga 3d regions for GaAs(111)A after sequential reaction with HCl in diethyl ether solution and then $C_{18}H_{37}MgCl$ in THF. Bottom spectra were acquired immediately after functionalization, and top spectra were obtained after the passage of charge at 0.02 A•cm^{-2} for 10 scans. Spectra are offset for clarity.

drive this current density was observed for the thiol-modified heterojunctions ($\frac{\Delta Potential}{\Delta Scan\ Number}$ = 3.3x10-3 V $scan^{-1}$). A possibility for the lowered applied potential needed to supply the desired current could be loss of the thiol surface group and an increasing fraction of direct Hg/GaAs contact area.[25,26] Degradation of $C_{18}H_{37}S$-terminated GaAs(111)A after passage of charge at this current density for 10 scans was confirmed through XP spectra. High-resolution Ga 3d and As 3d spectra both showed GaAs(111)A surfaces with substantial levels of oxide (0.32 nm from As 3d; Figure 2.11). For GaAs(111)A surfaces reacted with $C_{18}H_{37}MgCl$, the change in applied bias required to sustain 0.02 A cm^{-2} after repeated cycling was noticeably smaller ($\frac{\Delta Potential}{\Delta Scan\ Number}$ = 8.7x10^{-4} V $scan^{-1}$). Corresponding XP spectra for these surfaces after passage of current showed minimal surface oxidation (0.06 ± .01nm from As 3d; Figure 2.12).

GaN Figure 2.13 shows a high-resolution Cl 2p XP spectrum for a GaN(0001) surface chlorinated using PCl_5 in dichlorobenzene. In contrast to GaAs but similar to GaP,[34] this wet chemical chlorination scheme did not induce macroscopic surface pitting of GaN(0001), in accord with the previously recognized chemical inertness of GaN towards corrosive environments.[61-63] Reaction of GaN(0001) with PCl_5 in chlorobenzene did effect a slight increase in the measured surface topography, as indicated through atomic force microscopy (Figure 2.14). Corresponding Cl 2p XP spectra showed the presence of surficial Cl higher than attainable with HCl in diethyl ether (1.2 ± 0.2 vs 0.6 ± 0.2 ML, respectively). For this reason, PCl_5 was used for reactions with Grignard reagents in THF as described above. After reaction with $C_{18}H_{37}MgCl$, GaN(0001) films became noticeably more hydrophobic. Sessile drop contact angles with water increased relative to either the etched or control treatments (Table 2.1). The measured value of 78°± 3° for GaN(0001) reacted with $C_{18}H_{37}MgCl$ was consistent with a surface featuring hydrophobic groups but was less than the corresponding value for similarly treated GaAs(111)A and GaP(111)A[34] wetting contact angles.

XP spectra of GaN(0001) surfaces following exposure to Grignard reagents were collected. Even though there were no overlapping Auger signals near 284 eV for GaN

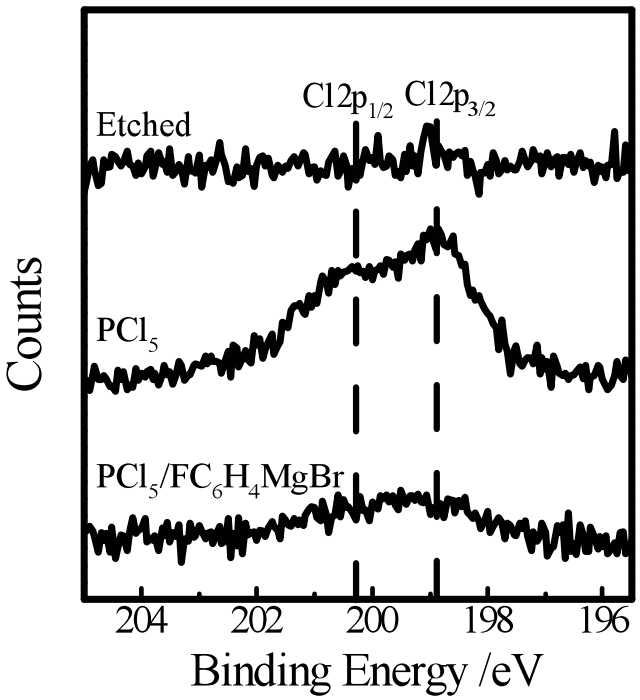

Figure 2.13. High-resolution Cl 2p XP spectra for GaN(0001) surfaces, (top) after etching in KOH(aq), (middle) after reaction with PCl_5 in chlorobenzene, and (bottom) after sequential reaction first with PCl_5 in chlorobenzene and then C_6H_4FMgBr in THF. Spectra are offset for clarity.

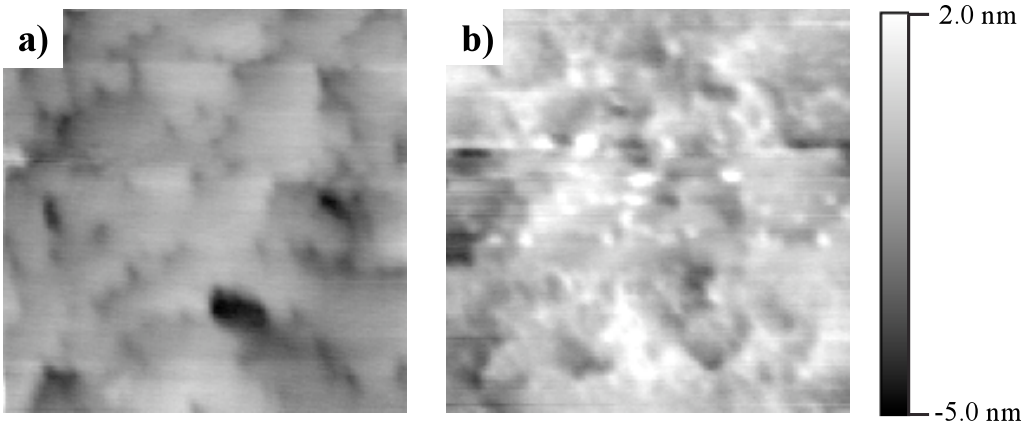

Figure 2.14. 2μm x 2μm AFM images of GaN(0001) surfaces treated with either (a) H_2SO_4(aq) or (b) PCl_5 in chlorobenzene.

samples, analyses of the C 1s XP spectra were still complicated. Conclusive determination of Ga-C surface bonds was problematic since GaN(0001) samples produced through chemical vapor deposition (CVD) from organogallium precursors natively show a detectable and inhomogeneous content of residual Ga-C containing species within the probing volume of our X-ray photoelectron spectrometer. Specifically, Ga-bound carbon impurities in CVD-based GaN films show a spectroscopic feature that mimics the low binding energy shoulder ascribed to surficial Ga-C bonding.[34] For this reason, commercial GaN films without residual organic contaminants were employed. For these samples, no signatures at binding energies more positive than 284 eV were observed in the C 1s spectra for etched or control experiments. However, the high-resolution C 1s spectra for GaN(0001) samples that were first reacted with PCl_5 and then CH_3MgCl did show a shoulder at 282.7 eV (Figure 2.15). The integrated intensity of this spectral feature corresponded to a CH_3- surface coverage of 0.47 ± 0.02 ML, less than previously observed for similarly treated GaP(111)A.[34] High-resolution F 1s spectra for GaN(0001) surfaces were also obtained following etching, chlorination, and reaction with C_6H_4FMgBr to determine whether surface functionalization occurred at GaN(0001) surfaces under the employed conditions (Figure 2.16). As seen with GaAs(111)A surfaces, the apparent carbon content (as indicated by the C 1s signal intensity) increased significantly after exposure to Grignard reagent. Figure 2.17 highlights the difference in increase in the C 1s signature of GaN(0001) surfaces reacted with C_6H_4FMgBr compared to similarly treated surfaces with CH_3MgCl. Larger organic groups effected a more substantial increase. Concomitantly, the measured Cl 2p intensities were significantly attenuated (Figure 2.13). The remaining Cl signature after reaction with Grignard reagent could still be fit with the same doublet, although the low signal intensity made it difficult to analyze these data. This trend was observed consistently for both this aryl-Grignard reagent and linear chain alkyl Grignard reagents, although the total C 1s intensity varied somewhat due to the residual carbon contamination in the films. High-resolution F 1s spectra are shown in Figure 2.16b. Fluorine is not present in either adventitious carbon or carbon contaminant from film deposition. Therefore, detection of F signatures is a direct indicator that the Grignard reaction sequence results in FC_6H_4- groups attached to the surface. Figure 2.16b shows that a detectable F 1s singlet was only obtained only after

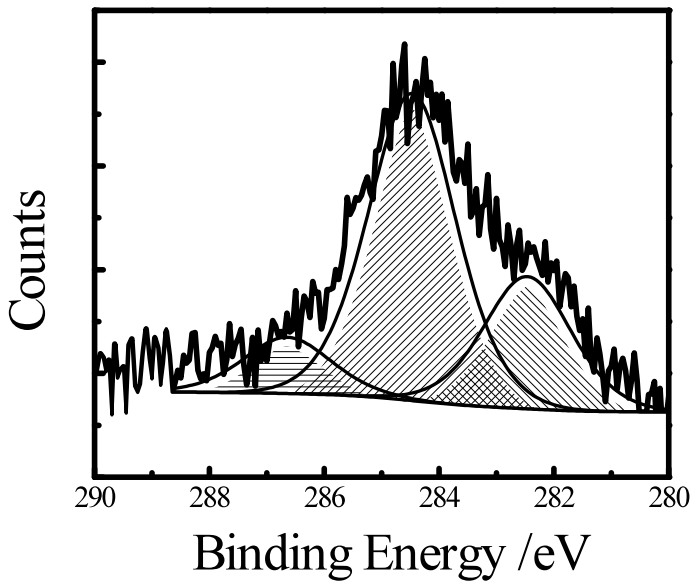

Figure 2.15. High-resolution C 1s XP spectrum of a GaN(0001) surface after sequential reaction with PCl_5 in chlorobenzene and then CH_3MgCl in THF.

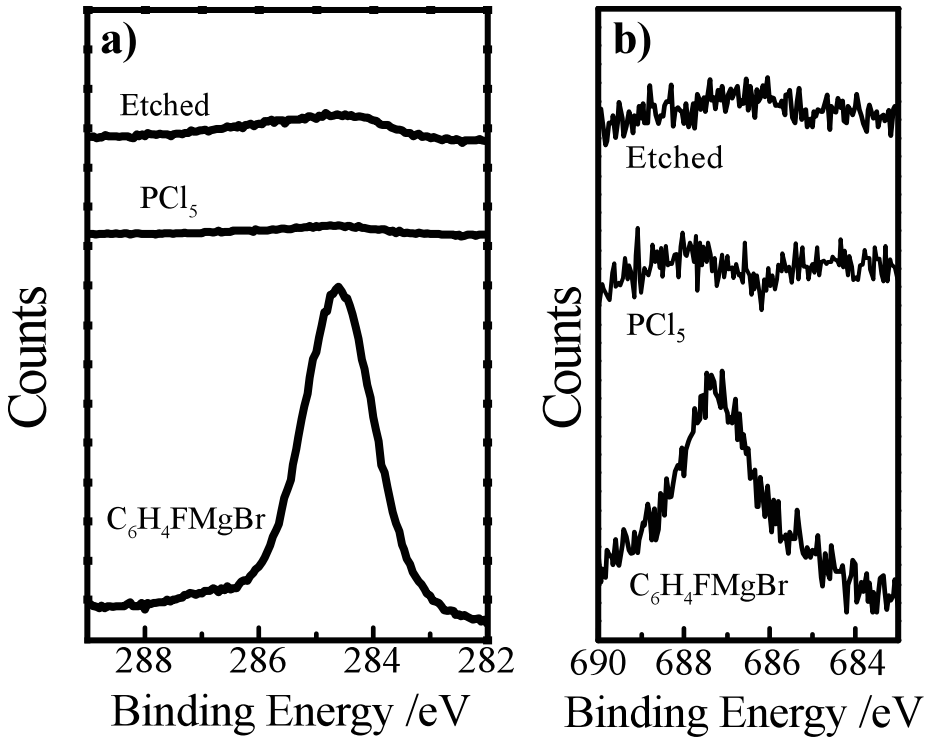

Figure 2.16. High-resolution (a) C 1s and (b) F 1s XP spectra for GaN(0001) surfaces (top) after etching in 1 M KOH(aq), (middle) after reaction with PCl_5 in chlorobenzene, and (bottom) after sequential reaction first with PCl_5 in chlorobenzene and then with C_6H_4FMgBr in THF.

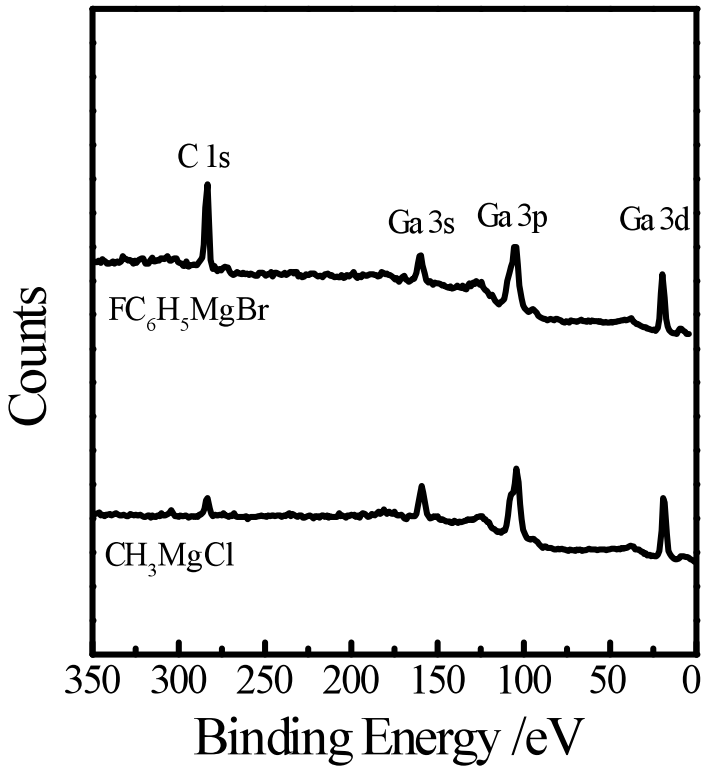

Figure 2.17. XP survey spectra of GaN(0001) surfaces after sequential reaction first with PCl_5 and then (top) C_6H_4FMgCl or (bottom) CH_3MgCl.

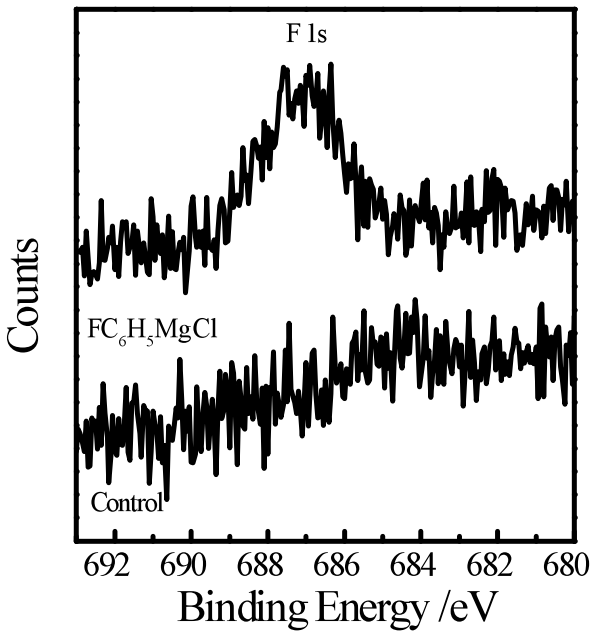

Figure 2.18. High-resolution F 1s XP spectra of GaN(0001) (top) after sequential reaction with PCl_5 in chlorobenzene and then C_6H_4FMgCl or (bottom) immersed in control solution. Control solution does not contain C_6H_4FMgCl.

exposure to C_6H_4FMgBr, consistent with the premise that this reaction sequence produces covalently grafted C_6H_4F- groups onto GaN(0001) surfaces. The high-resolution F 1s spectrum of the control sample is presented in Figure 2.18. The magnitude of the F 1s signal was invariant towards repeated washing/sonication in neat methanol, indicating the signal did not arise purely from physisorbed and unreacted reagents. Makowski et. al.[11] have also recently shown the functionalization of GaN surfaces with organic groups. However, the surface functionalization approach in that work required the use of an initial H_2 plasma activation step and C 1s spectroscopic evidence of a Ga-C surface bond was not shown. The data shown here represent organic groups grafted to unoxidized GaN(0001) interfaces using purely wet chemical treatments.

IV. Discussion

The cumulative results from this report on GaAs and GaN interfaces, in conjunction with our earlier study of GaP surfaces, indicate that the atop Ga atom at the surfaces of binary III-V semiconductors are reactive towards alkylation reagents. The net process mirrors both the classic, homogeneous inorganic synthesis of organogallium compounds from $GaCl_3$ and alkyl Grignard reagents[64-66] and the more recently studied heterogeneous Si and Ge surface Grignard reaction chemistry.[7,67-71] Hence, the data shown here for atop Ga atoms at the GaAs(111)A, GaP(111)A, and GaN(0001) surface planes, in conjunction with relatively low reaction yields observed with the GaAs(111)B and GaP(111)B surface planes, support the contention that organic groups can be grafted specifically through surface Ga-C bonds.

The demonstration of wet chemical strategies that covalently link functional groups to non-oxidized Ga-containing III-V semiconductor interfaces has both applied and fundamental implications. Surface modification strategies utilizing oxidized surfaces (e.g. silanization, phosphonate chemisorption)[72-75] are problematic for GaAs, GaP, and GaN surfaces in many optoelectronic applications. Oxidized Ga-based III-V semiconductor interfaces unavoidably contain large quantities of electronic surface traps (i.e. $\geq$ 1013 defects per cm^{-2}).[76,77] For example, in the context of solar energy conversion, surface-mediated charge recombination at interfacial defects is a deleterious, parasitic

pathway.[78] Modification schemes based on oxidized surfaces are wholly inappropriate and incompatible. The analysis of Schottky junctions performed here indicate that the wet chemical chlorination-Grignard reaction sequence produces GaAs heterojunctions with stability towards the passage of current, in contrast to other wet chemical strategies.[13] Surface groups coordinated through σ-bonds are believed to be particularly effective for electronic passivation.[18,79] The presented Raman data support the notion that a GaAs(111)A interface featuring a layer of alkyl groups introduced *via* Grignard reaction chemistry constitutes a surface with a much lower density of mid-gap electrical traps than a GaAs(111)A surface with a native oxide. Separate time-resolved photoluminescence or photoconductivity measurements,[18,32,33,80,81] performed with high quality (i.e. long bulk lifetime) GaAs materials, would be useful to determine the specific level of mid-gap surface defects and trap-based recombination before and after the two-step chlorination/Grignard reaction sequence. The Raman spectra shown here should serve as impetus for such work. Nevertheless, the measured I_{TO}/I_{LO} values shown here suggest that the presence of alkyl chains results in GaAs surface electronic properties comparable to GaAs interfaces following wet chemical sulfide treatments with respect to trap sites that arise from the presence of a native oxide. This feature is in contrast to other wet chemical routes that functionalize surfaces without passivating surface defects.[10,13,20] The measured I_{TO}/I_{LO} values does not suggest that electronic trap sites can not arise from trace amounts of residual Mg^{+2}, which are undetectable with our spectrometer. Since the prevailing thought in GaAs surface science is surface traps at the native surface are As-based in nature,[18] the observation that surface reactions directed towards bonding at atop Ga lowers surface defect density may be surprising. However, the data shown here are consistent with the premise that coordination of surficial Ga indirectly imparts stability on surface As atoms, limiting (or severely slowing) the extent of As-based surface reactions. This observation may prove useful since surface As species are notoriously reactive.[18] For GaN (and GaP), the extent that surface alkylation through putative Ga-C bonds lowers surface defect density remains undefined.

An important conclusion from the present studies is that surface alkylation improves surface stability with respect to oxidation. The XP spectra shown here and previously[34] demonstrate that GaAs and GaP interfaces featuring alkyl groups are

markedly less susceptible to undesirable surface oxidation under ambient conditions. The observed chemical stability likely arises from a high density of surface groups that sterically impede surface attack. The measured contact angles with water droplets for GaAs(111)A and GaP(111)A surfaces following reaction with $C_{18}H_{37}MgCl$ suggests that the introduced surface layer is more dense than on GaN(0001) after reaction with $C_{18}H_{37}MgCl$.[20,82,83] These observations are in accord with the distance between adjacent Ga atop atoms at GaAs(111)A and GaP(111)A surfaces (0.399 and 0.385 nm, respectively)[84,85] which are better matched to the areal footprint of a linear alkane chain than the 0.319 nm surface atom spacing at GaN(0001). However, for GaN, a lower density of surface groups may not be as critical since GaN surfaces are more naturally resistant to chemical attack.[86,87]

Reactions between nucleophilic reagents and electrophilic Ga atoms that produce stable bonds has precedent in homogeneous and heterogeneous reaction chemistries. Although simple organogallium compounds like $Ga(CH_3)_3$ are typically not stable in air or moisture, exceedingly stable Ga-C bonds have been achieved in N-heterocyclic carbene-$GaCl_3$ adducts. These compounds show indefinite stability in air and in solution[88] and feature a four-coordinate Ga atom bound by a strong σ-donor ligand. It is presently unclear whether the putative surficial Ga-C bonds effected through the reaction of III-V semiconductors and Grignard reagents more closely resemble the bonding in these adducts or in simple compounds like $Ga(CH_3)_3$. The data suggest the former. To be clear, the stability indicated by the data in this work exceeds that achieved with other nucleophilic reagents like PCl_3 and N_2H_4.[9,14,89,90] In addition to stability in ambient and wet conditions, an advantage of surface passivation layers from Grignard reagents over passivation reagents like PCl_3 and N_2H_4 is the possibility of secondary surface functionalization when partially unsaturated organic surface groups are introduced.[91] Although versatile and attractive for practical reasons, Grignard reagents are neither the only nor the most nucleophilic reagents for alkylation. For example, organolithium and organozinc reagents tend to show greater and weaker nucleophilicity, respectively[37,66]. Surface alkylation through nucleophilic attack may be a general wet chemical reaction pathway for III-V surfaces and additional types of alkylation reagents should be explored. Regarding Grignard reagents, the principal mechanism by which surface reaction occurs

is not clear. None of the presented experiments provide direct insight on whether the surface bonding formation is mechanistically related to either homogeneous organogallium reactions or heterogeneous Group IV semiconductor passivation. Since Ga-Cl bond exchange for putative Ga-C surface bonds should be sensitive to surface site spacing and the covalent character of Ga-V bonds, the differences in wettability and stability across GaN(0001), GaP(111)A, and GaAs(111)A surfaces noted in this work are not surprising. Still, the premise that Cl-termination provides a consistent, reproducible, and metastable surface reactive condition appears valid for GaAs, GaN, and GaP. Studies that explore whether the extent of surface coverage and/or resultant surface properties is affected noticeably by the nucleophilic character of the alkylation reagent and or halide termination step would be useful. To date, few experiments have been performed that directly probe the wet chemical reactivity of a family of related semiconductor surfaces towards σ-bonding reagents. In this regard, the data shown here complete a report on the wet chemical reactivity between an alkylating reagent and a family of related III-V semiconductor surfaces.

V. Summary

Crystalline gallium arsenide (GaAs) and gallium nitride (GaN) surfaces have been functionalized with alkyl groups *via* a sequential wet chemical Cl-activation, Grignard reaction process. These results, in conjunction with previous studies on GaP, show that atop Ga atoms on structurally related Ga-based binary III-V semiconductors can be deliberately functionalized with putative Ga-C surface bonds. For GaAs, the collected Raman spectra specifically indicate a lowering of deleterious electrical surface defects, that arise from the presence of surface oxides, at a level comparable to the existing state-of-the-art in chemical passivation techniques. For GaN, the cumulative data illustrate a purely wet chemical method for modifying interfacial characteristics. Overall, these results highlight the largely unexplored possibilities of using nucleophilic alkylation reagents for modifying, improving, and controlling the physicochemical and electrochemical properties of both GaAs and GaN.

VI. References

(1) Bent, S. F. *Surf. Sci.* **2002**, *500*, 879.
(2) Filler, M. A.; Bent, S. F. *Prog. Surf. Sci.* **2003**, *73*, 1.
(3) Linford, M. R.; Fenter, P.; Eisenberger, P. M.; Chidsey, C. E. D. *J. Am. Chem. Soc.* **1995**, *117*, 3145.
(4) Buriak, J. M. *Chem. Rev.* **2002**, *102*, 1271.
(5) Buriak, J. M. *Chem. Comm.* **1999**, 1051.
(6) Hamers, R. J. In *Annu. Rev. Anal. Chem.* 2008; Vol. 1, p 707.
(7) Gerlich, D.; Cullen, G. W.; Amick, J. A. *J. Electrochem. Soc.* **1962**, *109*, 133.
(8) Hamers, R. J.; Coulter, S. K.; Ellison, M. D.; Hovis, J. S.; Padowitz, D. F.; Schwartz, M. P.; Greenlief, C. M.; Russell, J. N. *Acc. Chem. Res.* **2000**, *33*, 617.
(9) Berkovits, V. L.; Ulin, V. P.; Losurdo, M.; Capezzuto, P.; Bruno, G.; Perna, G.; Capozzi, V. *Appl. Phys. Lett.* **2002**, *80*, 3739.
(10) Cohen, R.; Kronik, L.; Shanzer, A.; Cahen, D.; Liu, A.; Rosenwaks, Y.; Lorenz, J. K.; Ellis, A. B. *J. Am. Chem. Soc.* **1999**, *121*, 10545.
(11) Makowski, M. S.; Zemlyanov, D. Y.; Ivanisevic, A. *Appl. Surf. Sci.* **2011**, *257*, 4625.
(12) Seker, F.; Meeker, K.; Kuech, T. F.; Ellis, A. B. *Chem. Rev.* **2000**, *100*, 2505.
(13) Stewart, M. P.; Maya, F.; Kosynkin, D. V.; Dirk, S. M.; Stapleton, J. J.; McGuiness, C. L.; Allara, D. L.; Tour, J. M. *J. Am. Chem. Soc.* **2003**, *126*, 370.
(14) Traub, M. C.; Biteen, J. S.; Brunschwig, B. S.; Lewis, N. S. *J. Am. Chem. Soc.* **2008**, *130*, 955.
(15) Adlkofer, K.; Tanaka, M. *Langmuir* **2001**, *17*, 4267.
(16) Baum, T.; Ye, S.; Uosaki, K. *Langmuir* **1999**, *15*, 8577.
(17) Jun, Y.; Zhu, X.-Y.; Hsu, J. W. P. *Langmuir* **2006**, *22*, 3627.
(18) Lunt, S. R.; Ryba, G. N.; Santangelo, P. G.; Lewis, N. S. *J. Appl. Phys.* **1991**, *70*, 7449.
(19) McGuiness, C. L.; Shaporenko, A.; Mars, C. K.; Uppili, S.; Zharnikov, M.; Allara, D. L. *J. Am. Chem. Soc.* **2006**, *128*, 5231.
(20) McGuiness, C. L.; Shaporenko, A.; Zharnikov, M.; Walker, A. V.; Allara, D. L. *J. Phys. Chem. C.* **2007**, *111*, 4226.
(21) Shaporenko, A.; Adlkofer, K.; Johansson, L. S. O.; Tanaka, M.; Zharnikov, M. *Langmuir* **2003**, *19*, 4992.
(22) Shaporenko, A.; Adlkofer, K.; Johansson, L. S. O.; Ulman, A.; Grunze, M.; Tanaka, M.; Zharnikov, M. *J. Phys. Chem. B.* **2004**, *108*, 17964.
(23) Sheen, C. W.; Shi, J.-X.; Mirtensson, J.; Parikh, A. N.; Allara, D. **L.** *J. Am. Chem. Soc.* **1992**, ***114***, **1514**.
(24) Ashkenasy, G.; Cahen, D.; Cohen, R.; Shanzer, A.; Vilan, A. *Acc. Chem. Res.* **2002**, *35*, 121.
(25) Nesher, G.; Shpaisman, H.; Cahen, D. *J. Am. Chem. Soc.* **2007**, *129*, 734.
(26) Nesher, G.; Vilan, A.; Cohen, H.; Cahen, D.; Amy, F.; Chan, C.; Hwang, J.; Kahn, A. *J. Phys. Chem. B.* **2006**, *110*, 14363.
(27) Salomon, A.; Bo1cking, T.; Gooding, J. J.; Cahen, D. *Nano Lett.* **2006**, *6*, 2873.
(28) Vilan, A.; Shanzer, A.; Cahen, D. *Nature* **2000**, *404*, 166.

(29) Gila, B. P.; Thaler, G. T.; Onstine, A. H.; Hlad, M.; Gerger, A.; Herrero, A.; Allums, K. K.; Stodilka, D.; Jang, S.; Kang, B.; Anderson, T.; Abernathy, C. R.; Ren, F.; Pearton, S. J. *Solid-State Electron.* **2006**, *50*, 1016.
(30) Tomioka, K.; Motohisa, J.; Hara, S.; Hiruma, K.; Fukui, T. *Nano Lett.* **2010**, *10*, 1639.
(31) Vetury, R.; Zhang, N. Q. Q.; Keller, S.; Mishra, U. K. *IEEE Trans. Electron Devices* **2001**, *48*, 560.
(32) Yablonovitch, E.; Bhat, R.; Harbison, J. P.; Logan, R. A. *Appl. Phys. Lett.* **1987**, *50*, 1197.
(33) Yablonovitch, E.; Gmitter, T. J. *Solid-State Electron.* **1992**, *35*, 261.
(34) Mukherjee, J.; Peczonczyk, S.; Maldonado, S. *Langmuir* **2010**, *26*, 10890.
(35) Mao, O.; Altounian, Z.; StromOlsen, J. O. *Rev. Sci. Instrum.* **1997**, *68*, 2438.
(36) Shriver, D. F.; Drezdzon, M. A. *The Manipulation of Air-Sensitive Compounds*; Wiley: New York, 1986.
(37) Bansal, A.; Li, X.; Yi, S. I.; Weinberg, W. H.; Lewis, N. S. *J. Phys. Chem. B.* **2001**, *105*, 10266.
(38) Wagner, C. D.; Riggs, W. M.; Davis, L. E.; Moulder, J. F.; Muilenberg, G. E. *Handbook of X-ray Photoelectron Spectroscopy*; Perkin Elmer Corporation: Eden Prairie 1979.
(39) Briggs, D.; Seah, M. P. *Practical Surface Analysis by Auger and X-ray Photoelectron Spectroscopy*; John Wiley & Sons: New York 1984.
(40) Traub, M. C.; Biteen, J. S.; Michalak, D. J.; Webb, L. J.; Brunschwig, B. S.; Lewis, N. S. *J. Phys. Chem. B* **2006**, *110*, 15641.
(41) Butcher, D. N.; Sealy, B. J. *Electron. Lett.* **1977**, *13*, 558.
(42) Wasilewski, Z. R.; Baribeau, J.-M.; Beaulieu, M.; Wu, X.; Sproule, G. I. *J. Vac. Sci. Technol. B* **2004**, ***22***, 1534.
(43) Chibowski, E.; Terpilowski, K. *J. Colloid Interface Sci.* **2008**, *319*, 505.
(44) Tadmor, R. *Langmuir* **2004**, *20*, 7659.
(45) Aspnes, D. E.; Studna, A. A. *Phys. Rev. B* **1983**, *27*, 985.
(46) Bessolov, V. N.; Lebedev, M. V. *Semiconductors* **1998**, *32*, 1141.
(47) Bessolov, V. N.; Lebedev, M. V.; Ivankov, A. F.; Bauhofer, W.; Zahn, D. R. T. *Appl. Surf. Sci.* **1998**, *133*, 17.
(48) Bessolov, V. N.; Lebedev, M. V.; Zahn, D. R. T. *J. Appl. Phys.* **1997**, *82*, 2640.
(49) Lu, Z. H.; Lagarde, C.; Sacher, E.; Currie, J. F.; Yelon, A. *J. Vac. Sci. Technol. A.* **1989**, *7*, 646.
(50) Yao, H.; Yau, S. L.; Itaya, K. *Appl. Phys. Lett.* **1996**, *68*, 1473.
(51) Aspnes, D. E.; Studna, A. A. *Appl. Phys. Lett.* **1985**, *46*, 1071.
(52) Geurts, J. *Surf. Sci. Rep.* **1993**, *18*, 1.
(53) Nakamura, T.; Katoda, T. *J. Appl. Phys.* **1984**, *55*, 3064.
(54) Olego, D. J.; Schachter, R.; Baumann, J. *J. Vac. Sci. Technol. B.* **1985**, *3*, 1097.
(55) Cape, J. A.; Tennant, W. E.; Hale, L. G. *J. Vac. Sci. Technol.* **1977**, *14*, 921.
(56) Fleury, P. A.; Worlock, J. M. *Phys. Rev. Lett.* **1967**, *18*, 665.
(57) Pinczuk, A.; Burstein, E. *Phys. Rev. Lett.* **1968**, *21*, 1073.
(58) Scott, J. F.; Fleury, P. A.; Worlock, J. M. *Phys. Rev.* **1969**, *177*, 1288.
(59) Chen, X.; Si, X.; Malhotra, V. *J. Electrochem. Soc.* **1993**, *140*, 2085.

(60) Maldonado, S.; Plass, K. E.; Knapp, D.; Lewis, N. S. *J. Phys. Chem. C.* **2007**, *111*, 17690.
(61) Basak, D.; Verdu, M.; Montojo, M. T.; SanchezGarcia, M. A.; Sanchez, F. J.; Munoz, E.; Calleja, E. *Semicond. Sci. Technol.* **1997**, *12*, 1654.
(62) King, S. W.; Barnak, J. P.; Bremser, M. D.; Tracy, K. M.; Ronning, C.; Davis, R. F.; Nemanich, R. J. *J. Appl. Phys.* **1998**, *84*, 5248.
(63) Zhuang, D.; Edgar, J. H. *Mater. Sci. Eng., R* **2005**, *48*, 1.
(64) Andrews, P. C.; Junk, P. C.; Nuzhnaya, I.; Spiccia, L.; Vanderhoek, N. *J. Organomet. Chem.* **2006**, *691*, 3426.
(65) Jones, A. C.; Holliday, A. K.; Colehamilton, D. J.; Ahmad, M. M.; Gerrard, N. D. *J. Cryst. Growth* **1984**, *68*, 1.
(66) Robinson, G. H. *Gallium: Organometallic Chemistry*; John Wiley & Sons, Ltd, 2006.
(67) Bansal, A.; Li, X.; Lauermann, I.; Lewis, N. S.; Yi, S. I.; Weinberg, W. H. *J. Am. Chem. Soc.* **1996**, *118*, 7225.
(68) Fellah, S.; Boukherroub, R.; Ozanam, F.; Chazalviel, J. N. *Langmuir* **2004**, *20*, 6359.
(69) Fellah, S.; Teyssot, A.; Ozanam, F.; Chazalviel, J. N.; Vigneron, J.; Etcheberry, A. *Langmuir* **2002**, *18*, 5851.
(70) Rivillon, A. S.; Michalak, D. J.; Chabal, Y. J.; Wielunski, L.; Hurley, P. T.; Lewis, N. S. *J. Phys. Chem. C* **2007**, *111*, 13053.
(71) Vegunta, S. S.; Ngunjiri, J. N.; Flake, J. C. *Langmuir* **2009**, *25*, 12750.
(72) Baur, B.; Steinhoff, G.; Hernando, J.; Purrucker, O.; Tanaka, M.; Nickel, B.; Stutzmann, M.; Eickhoff, M. *Appl. Phys. Lett.* **2005**, *87*.
(73) Bolts, J. M.; Wrighton, M. S. *J. Am. Chem. Soc.* **1979**, *101*, 6179.
(74) Kang, B. S.; Ren, F.; Wang, L.; Lofton, C.; Tan, W. W.; Pearton, S. J.; Dabiran, A.; Osinsky, A.; Chow, P. P. *Appl. Phys. Lett.* **2005**, *87*.
(75) Kim, H.; Colavita, P. E.; Paoprasert, P.; Gopalan, P.; Kuech, T. F.; Hamers, R. J. *Surf. Sci.* **2008**, *602*, 2382.
(76) Ahrenkiel, R. K.; Dunlavy, D. J. *Solid-State Electron* **1984**, *27*, 485.
(77) Faraz, S. M.; Ashraf, H.; Arshad, M. I.; Hageman, P. R.; Asghar, M.; Wahab, Q. *Semicond. Sci. Technol.* **2010**, *25*.
(78) Fonash, S. *Solar Cell Device Physics*; 2nd ed.; Academic Press: Burlington, MA, 2010.
(79) Bent, S. F. *Nanomater.* **2007**, *1*, 10.
(80) Dmitruk, N. L.; Lyashenk.Vi; Tereshen.Ak; Spektor, S. A. *Phys. Status Solidi. A* **1973**, *20*, 53.
(81) Hovel, H. J.; Guidotti, D. *IEEE Trans. Electron Devices* **1985**, *32*, 2331.
(82) Rodriguez, L. M.; Gayone, J. E.; Sanchez, E. A.; Grizzi, O.; Blum, B.; Salvarezza, R. C.; Xi, L.; Lau, W. M. *J. Am. Chem. Soc.* **2007**, *129*, 7807.
(83) Rosu, D. M.; Jones, J. C.; Hsu, J. W. P.; Kavanagh, K. L.; Tsankov, D.; Schade, U.; Esser, N.; Hinrichs, K. *Langmuir* **2009**, *25*, 919.
(84) Massa, W. *Crystal Structure Determination*; 2 ed.; Springer: New York, 2002.
(85) Smart, L. E.; Moore, E. A. *Solid State Chemistry; An Introduction* 3ed.; Taylor & Francis Group: New York, 2005.

(86) Mileham, J. R.; Pearton, S. J.; Abernathy, C. R.; MacKenzie, J. D.; Shul, R. J.; Kilcoyne, S. P. *J. Vac. Sci. Technol. A.* **1996**, *14*, 836.
(87) Minsky, M. S.; White, M.; Hu, E. L. *Appl. Phys. Lett.* **1996**, *68*, 1531.
(88) Marion, N.; Escudero-Adan, E. C.; Benet-Buchholz, J.; Stevens, E. D.; Fensterbank, L.; Malacria, M.; Nolan, S. P. *Organometallics* **2007**, *26*, 3256.
(89) Kropewnicki, T. J.; Kohl, P. A. *J. Vac. Sci. Technol.* **1998**, *16*, 139.
(90) Singh, N. K.; Doran, D. C. *Surf. Sci.* **1999**, *422*, 50.
(91) Plass, K. E.; Liu, X.; Brunschwig, B. S.; Lewis, N. S. *Chem. Mater.* **2008**, *20*, 2228.

Chapter 3

Secondary Functionalization of Allyl-Terminated GaP(111)A Surfaces *via* Heck Cross-Coupling Metathesis, Hydrosilylation and Electrophillic Addition of Bromine

***** This chapter was adapted from a published work.
Peczonczyk, S. L.; Brown, E. S.; Maldonado, S. *Langmuir,* **2014**, *30,* 156

I. Introduction

Gallium phosphide (GaP) is a potential photoelectrode material for photoelectrochemical energy storage.[1-4] However, a disadvantage with native GaP interfaces is a susceptibility towards rapid surface degradation, impacting both the electrochemical properties and the ability to design rational strategies for controlling physicochemical properties.[5,6] Modification of GaP surfaces with specific molecular protecting groups that are resistant to chemical attack has been recently demonstrated.[7-9] To date, wet chemical surface passivation strategies such as thiol/sulfide binding,[9,10] photochemical grafting of alkenes[9] or reaction with organic azides[8] have been successfully demonstrated but have yet to produce GaP interfaces rigorously free of surface oxidation while also retaining the capacity for secondary functionalization. Hence, the development of surface reaction schemes that are both amenable to protecting the underlying surface quality and to adding a secondary reaction handle to the surface is a challenge.

We have previously demonstrated that the (111) surface plane of GaP featuring partially coordinated Ga atoms (i.e. GaP(111)A) can be covalently modified with alkyl chains attached through a surface Ga-C bond using a two-step chlorination/Grignard

reaction sequence.[7] The attached alkyl chains did not appreciably oxidize after more than 50 days in air or after passage of current in a Schottky diode. This report herein expands the two-step Grignard reaction approach for GaP to covalently bond an allyl group with a terminal reactive olefin (Scheme 1). Allyl groups are targeted here in light of known difficulties preserving shorter unsaturated moieties on semiconductor surfaces.[11,12] Three primary hypotheses are investigated here with respect to the properties of allyl termination of GaP surfaces. First, an allyl-terminated GaP(111)A surface has improved chemical stability relative to the native surface. Second, an allyl-terminated GaP(111)A surface can be further reacted through at least one of three separate pathways (Scheme 1), indicating versatility in available reaction pathways for secondary GaP surface modification. Third, the reactivities of pristine and aged allyl-terminated GaP(111)A surfaces are distinct. The cumulative data supporting these hypotheses are discussed in terms of prospects for design of tailored GaP photoelectrode interfaces.

II. Experimental

Materials and Chemicals All chemicals were purchased from Aldrich unless otherwise noted. Methanol (anhydrous, 99.8%), acetone (HPLC-grade, Fisher), tetrahydrofuran (anhydrous, ≥99.9%), CH_3MgCl (2.0 M solution in THF), C_3H_5MgCl (2.0 M in THF), C_3H_7MgCl (2.0 M in THF), PCl_5 (95%), chlorobenzene (anhydrous, 99.8%), dichloromethane (anhydrous, ≥98.7%), ethanol (anhydrous, 99.9%), isopropanol (anhydrous, 99.5%), doubly distilled H_2SO_4(aq) (95-98%), tributylamine (≥98.5%), 4-iodobenzotrifluoride (97%), bromine (99+%, Acros Organics), and trichlorosilane (99%) were all used as received. Benzoyl peroxide (≥97%, Fluka), tris(dibenzylideneacetone)dipalladium ($Pd_2(dba)_3$, 97% wt/wt), and chloroplatinic acid (H_2PtCl_6) were dried under a vacuum of <200 mTorr for at least 24 h. Water with a resistivity of >18 MΩ•cm (Barnsted Nanopure system) was used throughout. Polished n-type GaP(111)A wafers doped with sulfur at 1.6 x 10^{18} cm^{-3} with a thickness of 350 ± 10 μm were used for XP and IR spectroscopic measurements. Polished p-type GaP(111)A

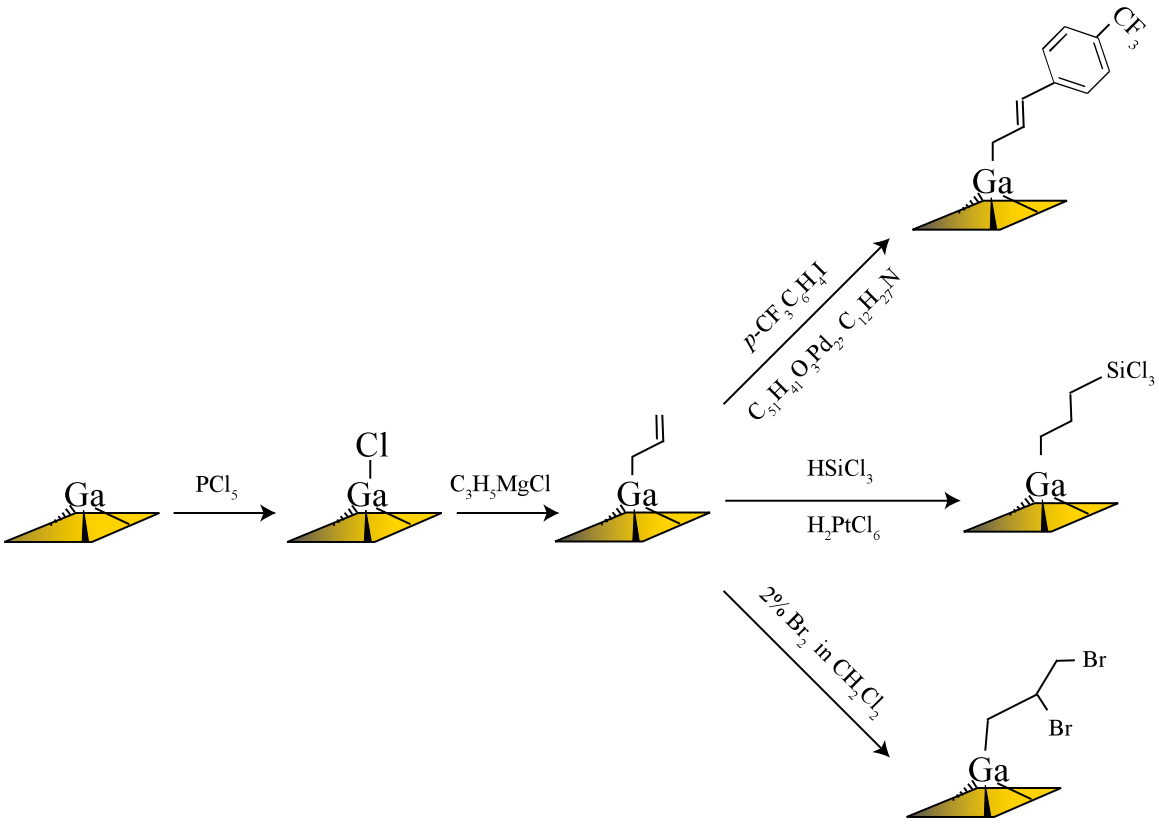

Scheme 1. Reaction scheme of primary wet chemical functionalization of atop Ga atoms of GaP(111)A using a two-step chlorination/Grignard reaction strategy to covalently bond allyl groups. Three secondary reactions with terminal olefin are also shown. (top) Heck cross-coupling metathesis, (middle) hydrosilylation and (bottom) electrophilic addition of bromine.

wafers doped with Zn at 2.7 x 10^{18} cm^{-3} with a thickness of 350 ± 25 μm were used for impedance measurements. GaP wafers were purchased from ITME.

Etching GaP(111)A wafers were cut into ~ 0.5 - 1.5 cm^2 sections. Samples were first degreased by sequential sonication in water, methanol, acetone, methanol, and water for 3 minutes each. The samples were then etched in H_2SO_4(aq) for 30 sec, rinsed copiously with water, and dried with a stream of N_2(g).

Primary Functionalization. *Chlorination and Grignard Reaction.* Allyl, methyl, or propyl groups were grafted to GaP(111)A surfaces using the previously described chlorination/Grignard reaction sequence.[7] Briefly, GaP(111)A samples were degreased then etched with H_2SO_4(aq) and introduced into a N_2(g) purged glovebox where all subsequent reaction steps were carried out. GaP(111)A surfaces were chlorinated by immersion into a saturated solution of PCl_5 in chlorobenzene with a few grains of benzoyl peroxide for 50 min at 90°C. The sample was subsequently rinsed with fresh chlorobenzene and dried in the glovebox. The sample was then transferred into a pressure-tolerant glass reaction vessel and immersed in the desired Grignard reagent. The vessel was then heated using a metal heating block to 150-160°C for 3 h for CH_3MgCl and C_3H_7MgCl or 110-120°C for 6 h for C_3H_5MgCl. The samples were then rinsed with fresh anhydrous THF and CH_3OH and dried in the glovebox before further functionalization or characterization.

Secondary Functionalization. *Heck Cross Coupling Metathesis Reaction.* Functionalized GaP(111)A samples were immersed in a solution of $Pd_2(dba)_3$ (3 mg mL^{-1}) in THF in a pressure-tolerant glass reaction vessel. Equal amounts (0.4 mL) of dried tributylamine and *p*-$CF_3C_6H_4I$ were added to the solution. The reaction mixture was then heated to 100-120°C for 16-18 h. The samples were then rinsed with copious amounts of THF, CH_2Cl_2, and CH_3OH inside the glovebox. The samples were then sonicated in THF, CH_2Cl_2 and CH_3OH for 3 min each. The samples were then dried in a stream of N_2(g).

Hydrosilylation Reaction. Functionalized GaP(111)A samples were immersed in a solution of trichlorosilane in chlorobenzene (4 M) with a catalytic amount of H_2PtCl_6 in isopropanol in a glass reaction vessel and heated to 110-120°C for 24 h. The samples

were then rinsed with a copious amount of fresh chlorobenzene and then sonicated in chlorobenzene and dried under a stream of N_2(g) before further characterization.

Electrophilic Addition of Bromine Reaction. Functionalized GaP(111)A samples were immersed in a 2% solution of Br_2 in CH_2Cl_2 for 2 h at room temperature. The samples were then rinsed with fresh CH_2Cl_2, CH_3OH and C_2H_5OH. The samples were then rinsed with 40 mL of boiling CH_2Cl_2 and sonicated in methanol and ethanol for 3 min each. Finally the samples were rinsed with 1 M H_2SO_4(aq) and dried in a stream of N_2(g)

X-ray Photoelectron Spectroscopy All X-ray photoelectron (XP) spectra were acquired with a PHI 5400 analyzer using an Al Kα (1486.6 eV) source without a monochromator. Spectra were recorded without charge neutralization at a base pressure of $<3.0 \times 10^{-9}$ Torr. A 6 mA emission current and 10 kV anode HT were used. Survey scans were acquired at a pass energy of 117.40 eV. High-resolution XP spectra of P 2p, Ga 3d, F 1s, C 1s, Si 2s and Br 3d were recorded at a pass energy of 23.5 eV. The binding energy of all spectra were corrected by using the difference between the observed peak energy of the C 1s and the peak energy of adventitious carbon (284.6 eV).[13,14] Average times for acquiring high-resolution spectra (100 scans) were 30 - 45 min. Samples did not undergo any observable degradation (as evidenced by diminution of surface signatures) upon prolonged exposure to X-ray source under these conditions.

Spectra were fit with a Shirley type background using CASAXPS version 2.313 software. P 2p spectra were fit with a doublet using 80% Gaussian and 20% Lorentzian line shapes with an area ratio of 0.5, a full width at half maximum (fwhm) constrained within 0.8 - 1.2 eV, and a peak separation of 0.85 eV. Fractional monolayer coverage of oxidized GaP surfaces were calculated using the simplified substrate-overlayer model (eq 3.1).[15]

$$d = \lambda_{ov} \ln\left(1 + \frac{I_{overlayer}}{I_{substrate}} \frac{I^0_{substrate}}{I^0_{overlayer}}\right) \sin\phi \qquad (3.1)$$

where d is the thickness of the oxide overlayer in nanometers, λ_{ov} is the escape depth of emitted electrons through the oxide layer, ϕ is the takeoff angle between the analyzer

and the surface normal (54.6°), $I_{substrate}$ is the integrated area of the P 2p signal obtained from the bulk crystal, $I_{overlayer}$ is the integrated area of the oxide P 2p signals, $I^0_{substrate}$ is the integrated area of P 2p signal from the bulk crystal of a sample that was freshly etched with H_2SO_4(aq) and $I^0_{overlayer}$ is the integrated area of the oxide P 2p signals from a thermal oxide. The escape depth of P 2p electrons through the oxide overlayer was estimated using eq 3.2.

$$\lambda_{ov} = 0.41A^{3/2}E^{1/2} \tag{3.2}$$

where A is the mean diameter of one unit in the overlayer in nanometers and E is the kinetic energy of the ejected core electron in electron volts.[15] λ_{ov} was calculated to be 1.66 nm for P 2p core electrons assuming a surface oxide density equivalent to $GaPO_4$ (3.56 g cm^{-3}).[16,17]

The surface monolayer coverages on GaP(111)A samples after additional modification reactions were calculated using a two-layer overlayer model (eq 3.3).[18]

$$\left(\frac{I_{ov}}{I_{sub}}\right) = \left(\frac{SF_{ov}}{SF_{sub}}\right)\left(\frac{\rho_{ov}}{\rho_{sub}}\right)\left(\frac{1 - e^{\frac{-d_{ov}}{\lambda_{ov}\sin\phi}}}{e^{\frac{-d_{ov}}{\lambda_{sub}\sin\phi}}}\right) \tag{3.3}$$

where I_{ov} is the measured intensity of the element of interest in the second overlayer, I_{sub} is the measured intensity of the element of interest in the substrate, SF_{ov} and SF_{sub} are the sensitivity factors of the element of interest in the second overlayer and substrate, respectively. ρ_{ov} and ρ_{sub} are the molar densities (mol/cm^3) of the overlayer and substrate, respectively. d_o' is the thickness of the second overlayer in nanometers, d_o is the thickness of the whole overlayer in nanometers, λ_{ov} and λ_{sub} are the escape depths from the overlayer and the substrate. Escape depths after secondary reaction were estimated following earlier precedent in the chemically modified surface literature.[19] Specifically, the model described by Laibinis[19] was chosen due to the uncertainty in the effective scattering within an organic film[20] and to more precisely localize the signal from the terminal functional group (ie. CF_3, $SiCl_3$ or Br).[18,21] Bond lengths were estimated with

Chemdraw using the assumption that the bound molecules are oriented perpendicular to the surface and possess an all-trans conformation.[22] The overlayer thicknesses for the resultant surface groups are as follows: *p*-$CF_3C_6H_4C_3H_4$-: 9.9 Å, $BrCHBrCHCH_2$-: 6.5 Å and $SiCl_3C_3H_5$-: 5.6 Å.

For the Heck cross coupling metathesis reaction, monolayer coverage was calculated from both F 1s and C 1s spectra. F 1s spectra were fit with a singlet with a fwhm constrained between 1.5 and 2.5 using 45 % Gaussian and 55% Lorentzian line shapes. The C 1s peak at 292.9 eV was fit with a singlet constrained to a fwhm between 1.0 and 2.0 using 45 % Gaussian and 55% Lorentzian line shapes. Monolayer coverage of surfaces after hydrosilylation reaction was determined from high-resolution Si 2s spectra, with a singlet with a fwhm constrained between 0.6 and 1.8 using 80% Gaussian and 20% Lorentzian line shapes. Monolayer coverage after reaction with Br_2 was calculated from both Br 3d and C 1s spectra. The Br 3d peak was fit with a doublet with an area ratio of 0.667, peak separation of 1.05 eV, and a fwhm constrained between 0.6 and 1.3 using 80% Gaussian and 20 % Lorentzian line shapes. The C 1s peak was fit with a singlet with a fwhm constrained between 0.8 and 2.1 using 45% Gaussian and 55% Lorentzian line shapes.

Infrared Spectroscopy Infrared spectra were collected using a Thermo-Fisher 6700 FT-IR spectrometer with a deuterated triglycerine sulfate (DTGS) detector. The spectrometer was equipped with a grazing angle attenuated total reflectance (GATR) accessory with a Ge hemisphere. The incident light was *p*-polarized and fixed at an incident angle of 65°. All samples were approximately 1.5 cm x 1.5 cm, covering the majority area of the Ge crystal. Reported spectra were recorded with 4 cm^{-1} resolution. All spectra were referenced to a background spectrum of the cleaned Ge hemisphere.

Electrode Preparation Ohmic contact was made to the backside of GaP(111)A wafers by lightly scratching the surface with a diamond scribe and soldering a thin film of In metal. The samples were then annealed at 400°C for 10 min in forming gas and argon gas. Electrodes were prepared by attaching the backside of GaP wafer to a tinned copper wire threaded through a glass tube using silver print (EC Electronics). Electrodes were then sealed using inert epoxy (Hysol C). Prior to reaction with Grignard reagents, exposed epoxy was securely wrapped with Teflon tape.

Impedance Measurements Impedance measurements were acquired using a Schlumberger Sl1286 electrochemical interface and a Schlumberger Sl1250 frequency response analyzer modulated by CorrWare and ZPlot software. Frequency responses were measured with a sinusoidal AC potential waveform (10 mV amplitude) superimposed onto a DC bias that was stepped to increasingly more negative potentials. Impedance measurements were acquired in the dark using a three-electrode electrochemical cell. Three N_2(g) purged electrolyte solutions with varying pH were used (pH = 4.0, 1 M KCl, 20 mM $EuCl_2$, 20 mM $EuCl_3$, 1 mM HCl; pH = 6.5, 1 M KCl, 20 mM $EuCl_2$, 20 mM $EuCl_3$; pH = 7.5, 1 M KCl, 20 mM $EuCl_2$, 20 mM $EuCl_3$, 1 mM KOH). Differential capacitance values were obtained assuming a simple parallel RC equivalent circuit. Frequency (*f*) ranges were deemed acceptable when an average Bode slope (log Z vs log *f*) between -0.95 and -1 was obtained. For etched electrodes a frequency range of 413 Hz to 16 Hz was used. For allyl-terminated electrodes a frequency range of 52 Hz to 10 Hz was used. The capacitance was calculated from Z" (imaginary) using equation 4:

$$Z'' = \frac{1}{2\pi f C} \tag{3.4}$$

The intercept on the x-axis of the Mott-Schottky plot (E_0) was used to calculate the flat-band potential (E_{fb}) for p-GaP electrodes using equation 5:

$$E_0 = E_{FB} - \frac{k_b T}{q} \tag{3.5}$$

Where k_b is the Boltzman constant and q is the charge of an electron.

III. Results

Preparation of Allyl-terminated GaP(111)A Reaction of clean GaP(111)A surfaces with C_3H_5MgCl through the sequence described in Scheme 1 resulted in a

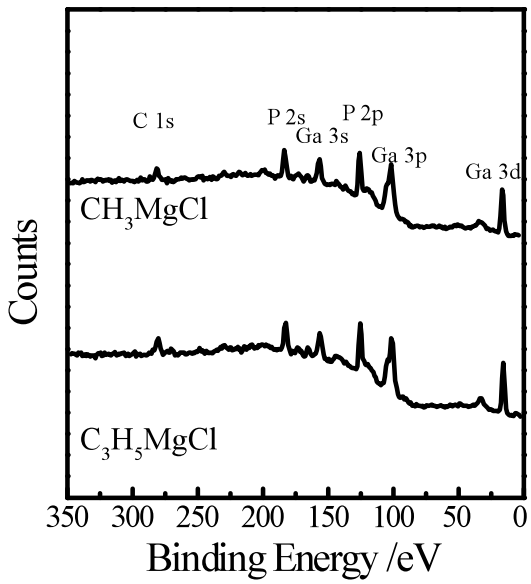

Figure 3.1. Survey XP spectra of GaP(111)A surfaces after sequential reaction with PCl_5 in chlorobenzene and then either (bottom) C_3H_5MgCl in THF or (top) CH_3MgCl in THF. Signatures for Mg species are not detectable. Spectra are offset for clarity.

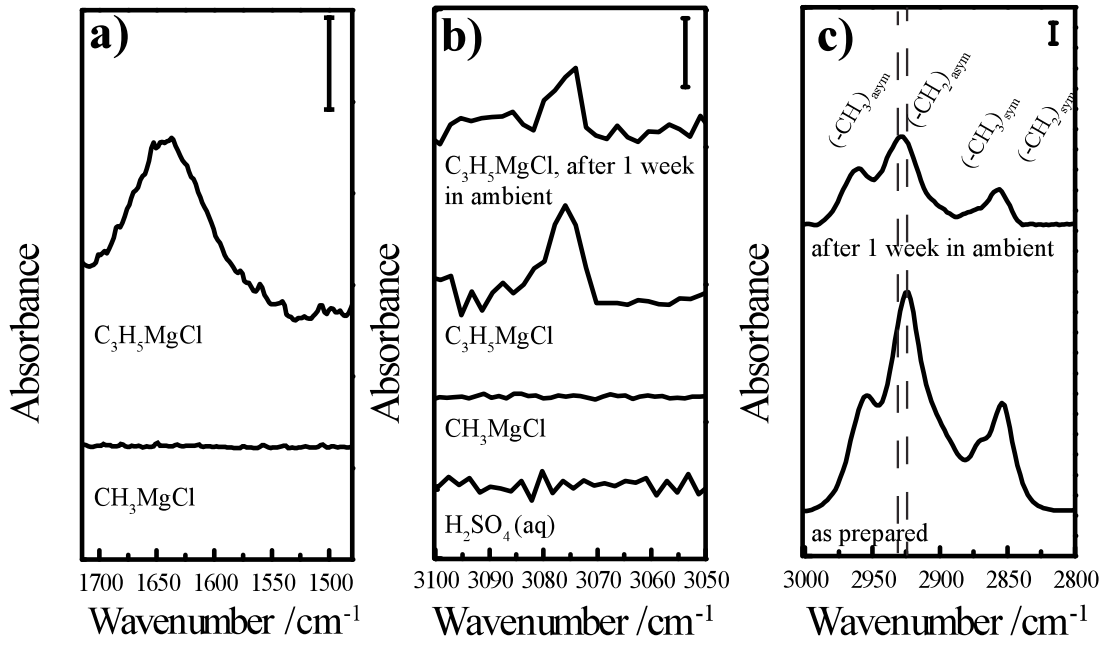

Figure 3.2. (a) GATR-FTIR spectra in the region for the C=C stretch for GaP(111)A after reaction with PCl_5 in chlorobenzene and then (top) C_3H_5MgCl in THF or (bottom) CH_3MgCl in THF. Vertical scale bar = 1 x 10^{-3} absorbance units. (b) GATR-FTIR spectra in the region for the C=C-H asymmetric stretch for GaP(111)A after various treatments: (bottom) etched with H_2SO_4 (aq), (2^{nd} from bottom) sequentially reacted with PCl_5 in chlorobenzene and then CH_3MgCl in THF, (3^{rd} from bottom) sequentially reacted with PCl_5 in chlorobenzene and then C_3H_5MgCl in THF, (top) Allyl-terminated GaP(111)A after exposure to ambient for 1 week. Vertical scale bar = 1 x 10^{-4} absorbance units. (c) GATR-FTIR spectra in the region for CH_3- and CH_2- symmetric and asymmetric stretches for GaP(111)A after sequential reaction with PCl_5 in chlorobenzene and C_3H_5MgCl in THF either (top) after the sample was exposed to laboratory ambient for 1 week or (bottom) immediately after Grignard reaction. Vertical scale bar = 1 x 10^{-3} absorbance units. Spectra are offset for clarity.

Table 3.1. IR Spectral Assignments and Oxide Thicknesses for Allyl-Terminated GaP(111)A Following Various Treatments

Condition	**C=C-H$_{asym}$ /cm^{-1}**	**CH$_{2,asym}$ /cm^{-1}**	**Oxide Thickness /nm**[b]
As prepared	3075	2923	0.07 ± 0.04
1 week in ambient	3076	2928	0.21 ± 0.13
30 minutes in water	3076	2926	0.13 ± 0.05
After Heck Reaction	3050	----[c]	0.17 ± 0.06
After Hydrosilylation	----[c]	2927	0.07 ± 0.03

a. N = 3 for all measurements

b. Calculated from P 2p spectra using simplified substrate-overlayer model

c. no peak observed

persistently hydrophobic surface with a water contact angle value of 73° ± 2° (*N*= 3), which was slightly larger than the value for reactions with CH_3MgCl (67° ± 4°, *N*= 3) and comparable to the value for reactions with C_3H_7MgCl (74° ± 5°, *N*= 3). XP survey spectra taken after reaction with Grignard reagents showed no evidence of physisorbed Mg-containing species (detection limit of Mg < 1 at%) (Figure 3.1) . Figure 3.2a presents IR spectra of GaP(111)A surfaces following various surface treatments. The signature for the C=C stretch is only apparent after samples treated with C_3H_5MgCl. Figure 3.2b separately displays the spectral region corresponding to the C=C-H asymmetric bond stretch.[23] Only GaP(111)A samples treated with C_3H_5MgCl showed a sharp peak at 3075 cm^{-1} (Table 3.1) consistent with this vibrational mode. Accordingly, Figures 3.2a and 3.2b support the premise that allyl groups are grafted to GaP(111)A surfaces specifically through reaction with C_3H_5MgCl. Although the oscillator strength of the C=C-H asymmetric stretch is weaker than the C=C bond stretching modes,[24,25] the C=C-H mode was a more convenient reporter on the surficial allyl groups because of the much sharper peak width and lack of overlap with signatures for ambient water and CO_2. Accordingly, Figure 3.2b also shows the C=C-H stretch for a GaP(111)A surface that had been reacted with C_3H_5MgCl and then allowed to sit in lab ambient for one week. The intensity of the signal relative to the background decreased somewhat and the peak position shifted slightly to 3076 cm^{-1}. Both features suggested a decrease in pristine allyl surface groups after aging in air. Corresponding spectral features for the CH_2- symmetric and asymmetric bond stretches are shown in Figure 3.2c. The peak position of the CH_2- asymmetric stretch for GaP(111)A surfaces reacted with C_3H_5MgCl shifted from 2923 cm^{-1} to 2928 cm^{-1} after aging in air for a week. For reference, crystalline (ordered) alkanes show the asymmetric methylene stretch at 2920 cm^{-1} while liquid (disordered) alkanes show a signature at 2928 cm^{-1}.[26-28] A red shift in the CH_2- asymmetric stretch to 2926 cm^{-1} was also observed after immersion of a GaP(111)A surface immediately after reaction with C_3H_5MgCl for 30 minutes in oxygenated water (Table 3.1).

The effect of changes to the surface attached allyl-groups on GaP(111)A on the chemical resistance of allyl-terminated GaP(111)A surfaces was investigated. Figure 3.3 compares the high-resolution P 2p XP spectra after allyl-terminated GaP(111)A surfaces were exposed to laboratory ambient for 1 week or immersed in water for 30 min. A broad

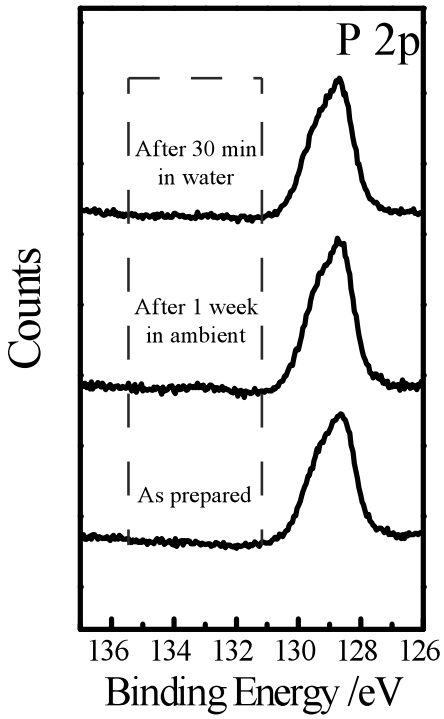

Figure 3.3. High-resolution P 2p XP spectra of GaP(111)A samples after sequential reaction with PCl_5 in chlorobenzene and C_3H_5MgCl in THF: (top) 30 minutes in oxygenated water, (middle) after exposure to laboratory ambient for 1 week, (bottom) immediately after Grignard reaction. Spectra are offset for clarity.

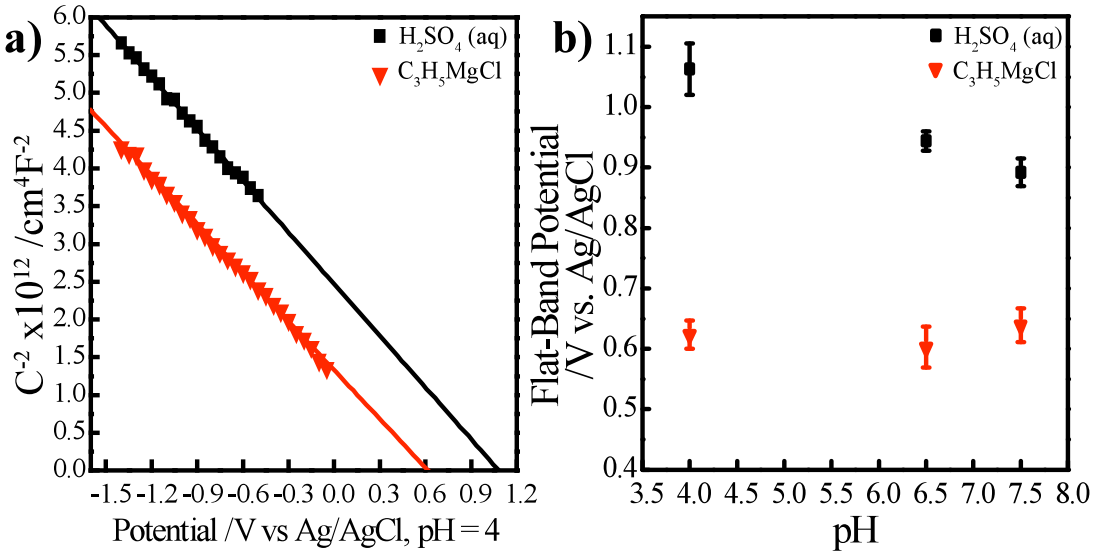

Figure 3.4. (a) Representative capacitance-voltage data for p-GaP(111)A electrodes that were either etched with H_2SO_4(aq) (black squares) or sequentially reacted with PCl_5 in chlorobenzene and then C_3H_5MgCl in THF (red triangles). Electrodes were immersed in a N_2(g) purged solution of 1M KCl, 20 mM $EuCl_2$, 20 mM $EuCl_3$ and 1 mM HCl. Measurements were acquired in the dark at 32 Hz. (b) Comparison of calculated flatband potentials of etched (black squares) and allyl-terminated (red triangles) p-GaP(111)A electrodes with respect to pH. Error bars are the standard error mean (*N*=4).

shoulder at higher binding energies suggestive of oxidized P (i.e. PO_x) was not observed in any of the spectra, indicating the protecting capacity of the allyl termination layer did not change irrespective of any apparent changes in the vibrational spectra. Table 3.1 summarizes the calculated surface oxide thickness of allyl groups for these three conditions.

Electrochemical impedance measurements were acquired to probe the effect of covalently attached allyl groups on the surface band energetics of GaP in acidic and basic solutions. Figure 3.4a compares representative Mott-Schottky plots of etched and allyl-terminated GaP(111)A in an acidic (pH= 4) solution. The intercept on the x-axis of Mott-Schottky plot was used to calculate the flat-band potential. Figure 3.4b compares the flat-band potentials of etched and allyl-terminated GaP(111)A over a range of pHs. The flat-band potential of etched electrodes change by 0.059 V/pH unit while the flat-band potential of allyl-terminated electrodes stay nominally the same.

Heck Cross-Coupling Metathesis with Allyl-terminated GaP(111)A Surfaces

Allyl-terminated GaP(111)A surfaces were used as reactants in a Heck cross coupling metathesis reaction to attach additional surface functionalities to the end of the terminal olefin group. For proof of principle, *p*-$CF_3C_6H_4I$ was chosen as the other reagent (Scheme 1), with the target -$C_6H_5CF_3$ surface groups readily detectable in XP spectra. To assess the specificity of these reactions towards allyl-terminated GaP(111)A, methyl-terminated GaP(111)A surfaces were used as controls. Figures 3.5a and 3.5b show high-resolution F 1s XP spectra of allyl- and methyl-terminated GaP(111)A, respectively, after reaction with *p*-$CF_3C_6H_4I$. For both surface types, the initial surfaces showed no signatures suggestive of F, as there was no fluorinated reagents used in any previous steps nor does fluorine typically constitute adventitious carbon.[29] After undergoing the Heck reaction with tris(dibenzylideneacetone)dipalladium(0) as the coupling catalyst, only allyl-terminated GaP showed a definitive C-F signature (centered at 687.6 eV) above the baseline. Methyl-terminated GaP(111)A consistently yielded spectra before and after attempts at Heck coupling reactions that were indistinguishable. C 1s XP spectra were also collected to separately corroborate the presence of $–CF_3$ (Figure 3.5c and 3.5d). For allyl-terminated GaP(111)A, performing the Heck reaction resulted in the appearance of a new peak in the C 1s spectra at 292.9 eV, consistent with C bonded to F

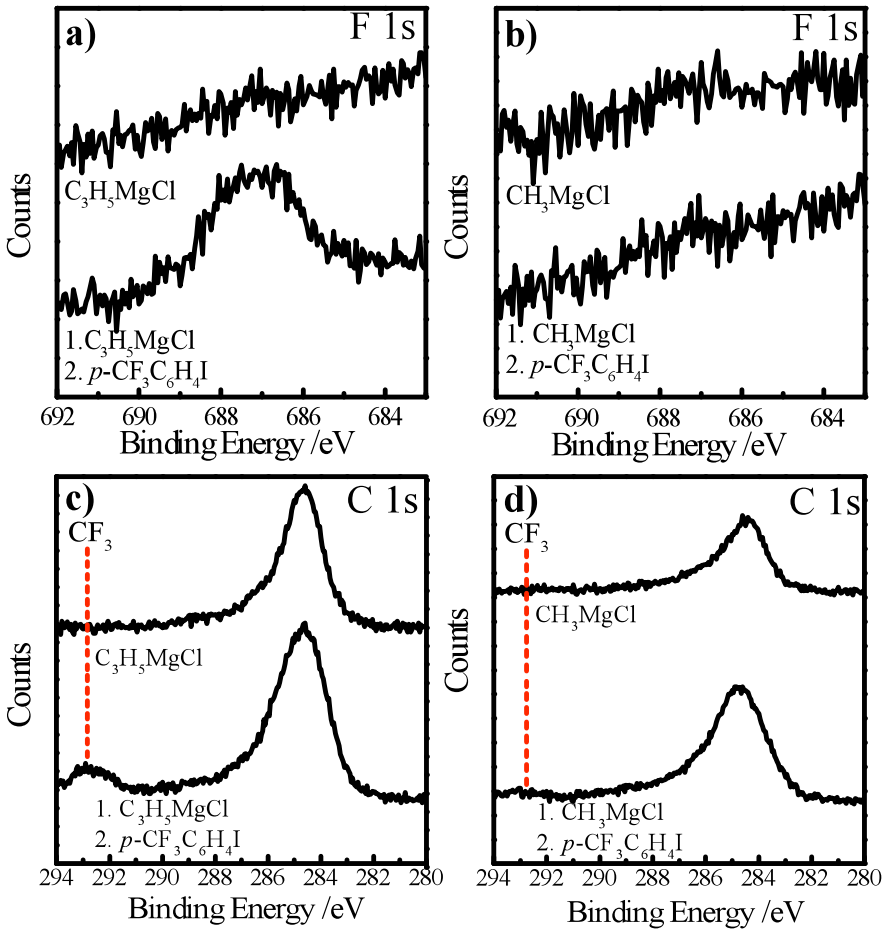

Figure 3.5. High-resolution F 1s XP spectra for GaP(111)A after reaction with PCl_5 in chlorobenzene and then either (a) C_3H_5MgCl or (b) CH_3MgCl in THF. High-resolution C 1s XP spectra of GaP(111)A after reaction with PCl_5 in chlorobenzene and then either (c) C_3H_5MgCl or (d) CH_3MgCl in THF. The spectra on top were acquired immediately after Grignard reaction. The spectra on the bottom were acquired after secondary Heck reaction with *p*-$CF_3C_6H_4I$. Spectra are offset for clarity.

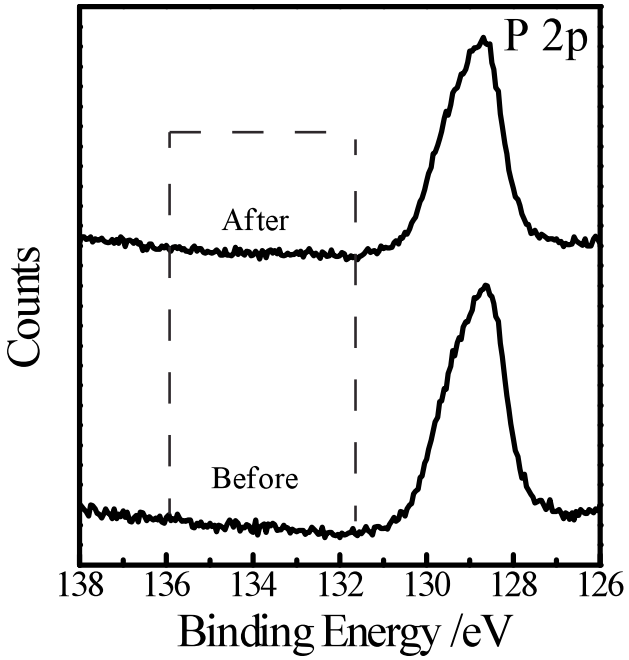

Figure 3.6. High-resolution P 2p XP spectra of GaP(111)A samples after sequential reaction with PCl_5 in chlorobenzene and then C_3H_5MgCl in THF. Bottom spectrum was acquired immediately after Grignard reaction. Top spectrum was acquired after reaction with *p*-$CF_3C_6H_4I$. spectra are offset for clarity.

in -CF_3 groups.[20] CH_3-terminated GaP(111)A showed no change in C 1s spectra before and after exposure to Heck reaction conditions. For allyl-terminated GaP(111)A, the monolayer coverage of -$C_6H_5CF_3$ groups calculated from the F 1s peak is 0.8 ± 0.2 monolayers (MLs) while the surface coverage calculated from the C 1s peak at 293 eV was 0.6 ± 0.2 ML. The discrepancy between the two estimates could be due to subtle errors in the model parameters (*vide supra*) but both measurements indicated a total surface coverage less than a full monolayer. Variations in reaction conditions (e.g. time, temperature, concentration) only resulted in lower measured surface coverage. With the optimal conditions, P 2p XP spectra showed a minimal increase in surface oxide content for allyl-terminated GaP(111)A surfaces after undergoing the Heck reaction (Figure 3.6).

IR spectra of allyl-terminated GaP(111)A surfaces after undergoing the Heck reaction are presented in Table 1 and Figure 3.7. IR spectra of the C=C-H asymmetric stretching region (Figure 3.8) showed a single sharp peak at 3050 cm^{-1} after Heck reaction (Table 1), a red shift of 25 cm^{-1} relative to the signal observed for pristine allyl-terminated GaP(111)A. Similar red-shifts are known for terminal olefins modified with an aryl group.[30,31] Figure 3.7 highlights the -CF_3 stretching region, comparing the spectra for allyl-terminated GaP(111)A immediately after undergoing the Heck reaction and a reference spectrum for *p*-$CF_3C_6H_4I$. The -CF_3 symmetric stretch (1324 cm^{-1}) and the two fundamentals of the -CF_3 asymmetric stretch (1128 cm^{-1} and 1102 cm^{-1}) are evident in both spectra.[32] A spectrum for a CH_3-terminated GaP(111)A control sample conversely showed no features diagnostic of the aryl moiety.

The effect of aging in air of allyl-terminated GaP(111)A surfaces on the apparent reactivity towards the Heck reaction was investigated. Allyl-terminated GaP(111)A samples were first exposed to laboratory ambient for 1 week before attempting Heck reaction. Figure 3.9 shows high-resolution F 1s and C 1s spectra for fresh and aged allyl-terminated GaP(111)A after Heck reaction. Samples that were allowed to age in air for 1 week showed evidence for surface attached F-containing species, albeit at lower surface coverages than pristine allyl-terminated GaP(111)A. Calculated monolayer coverages for -$C_6H_5CF_3$ moieties were 0.6 ± 0.2 ML, and 0.5 ± 0.2 ML from the F 1s and C 1s spectra in Figure 3.9, respectively, indicating a nominal 20% decrease in reaction yield relative to new allyl-terminated GaP(111)A surfaces.

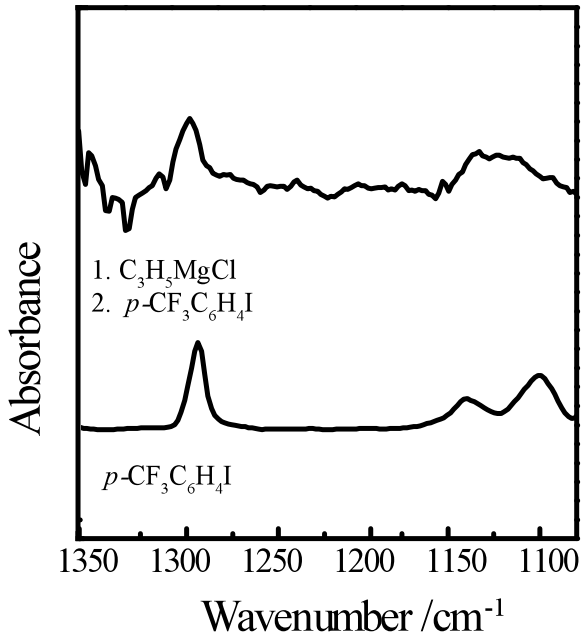

Figure 3.7. GATR-FTIR spectra for (top) GaP(111)A after reaction with PCl_5 in chlorobenzene, then C_3H_5MgCl in THF, and then p-$CF_3C_6H_4I$ and (bottom) for neat p-$CF_3C_6H_4I$. Spectra offset for clarity

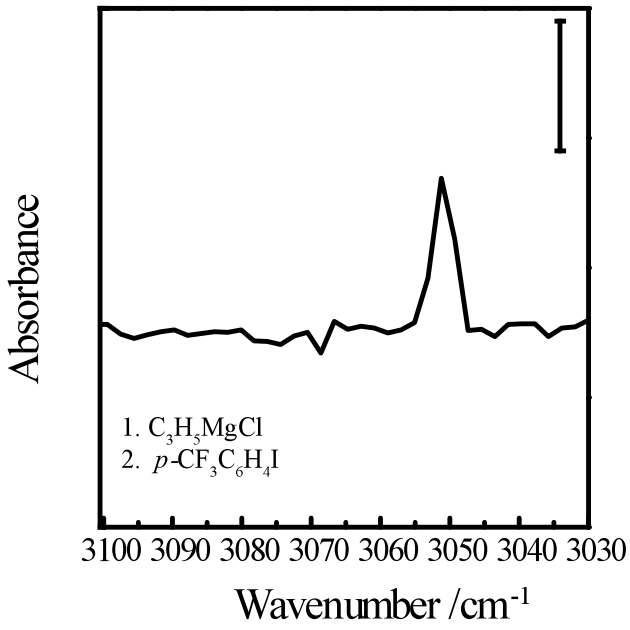

Figure 3.8. GATR-FTIR spectrum of a GaP(111)A sample after sequential reaction with PCl_5 in chlorobenzene and then C_3H_5MgCl in THF followed by Heck reaction with *p*-$CF_3C_6H_4I$.

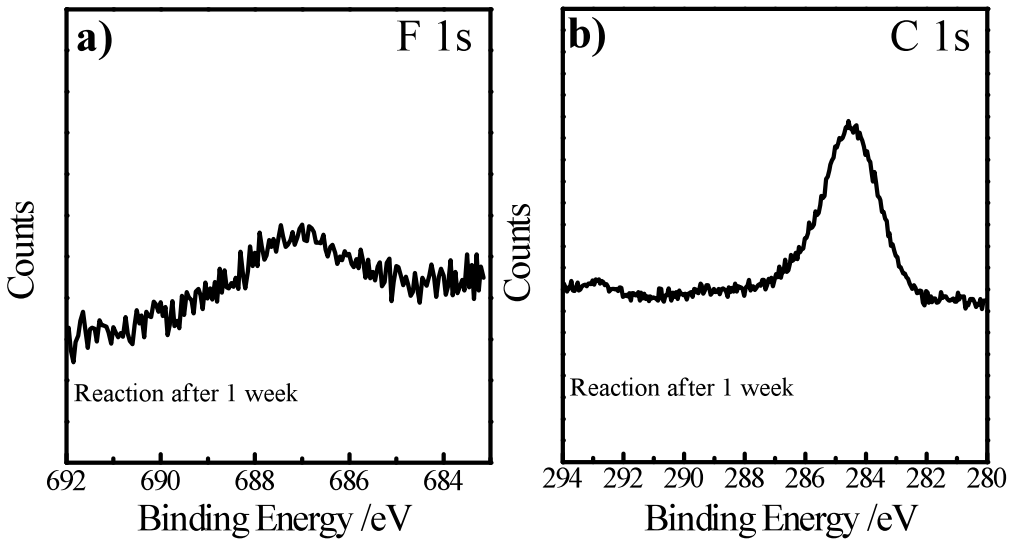

Figure 3.9. High-resolution (a) F 1s and (b) C 1s XP spectra of GaP(111)A sequentially reacted with PCl_5 in chlorobenzene, then C_3H_5MgCl in THF, exposed to ambient for 1 week, and then Heck reaction with *p*-$CF_3C_6H_4I$.

Hydrosilylation with Allyl-Terminated GaP(111)A Allyl-terminated GaP(111)A surfaces were separately used as reactants in a catalyzed hydrosilylation reaction. Figure 3.10 shows the high-resolution XP spectra before and after attempting hydrosilylation reaction with $HSiCl_3$ and either freshly prepared allyl- or CH_3-terminated GaP(111)A surfaces. Analysis for Si quantification was limited to binding energies for Si 2s since the expected Si 2p peaks could not be definitively resolved from the overlap with the Ga 3p signal. Figure 3.10a shows the marked signal intensity increase of the Si 2s spectra for allyl-terminated GaP(111)A. The peak at 153.8 eV was consistent with Si in the oxidation state expected for an *n*-propyl-$SiCl_3$ group.[33] From these data, the monolayer coverage of $–SiCl_3$ groups introduced by the hydrosilylation reaction was 0.8 ± 0.2 ML. The inferred thickness of the surface oxide after the hydrosilylation reaction was 0.07 ± 0.03 nm (Figure 3.11). In contrast, the CH_3-terminated GaP(111)A samples showed no change in the collected Si 2s spectra between the pristine surface and after exposure to hydrosilylation reaction conditions, indicating no chemisorption of $–SiCl_3$.

The IR spectrum of an allyl-terminated GaP(111)A surface after catalyzed reaction with $HSiCl_3$ is presented in Figure 3.12. The broad band at 1258 cm^{-1} was consistent with a Si-CH_2 stretch.[30] There were no observable signals at 1090 cm^{-1} or 795 cm^{-1} to suggest silica formation[34] through condensation of physisorbed $HSiCl_3$. The inset highlights that spectral region near 3100 cm^{-1} showed no signature suggestive of a C=C-H asymmetric stretch after reaction with $HSiCl_3$.

Reaction of Br_2 with Allyl-Terminated GaP(111)A Surfaces Allyl-terminated GaP(111)A surfaces were immersed in a solution of dilute Br_2 in dichloromethane to test the hypothesis that bromine addition will occur across the allyl group (Scheme 1). Figure 3.13 summarizes the collected high-resolution Br 3d spectra following immersion in a Br_2 solution for a freshly etched GaP(111)A sample, a GaP(111)A sample that had undergone the two-step chlorination/alkylation reaction with C_3H_7MgCl to impart surface propyl groups, and an allyl-terminated GaP(111)A sample. All surface types were susceptible to attack by Br_2. The Br 3d signal for freshly etched GaP(111)A was fit adequately with one 3d doublet featuring the $3d_{5/2}$ position at 68.5 eV, demonstrating the XP signature for direct attack of GaP by Br_2. The Br 3d spectra for the propyl-terminated GaP(111)A showed identical spectral features, indicating direct attack of the underlying

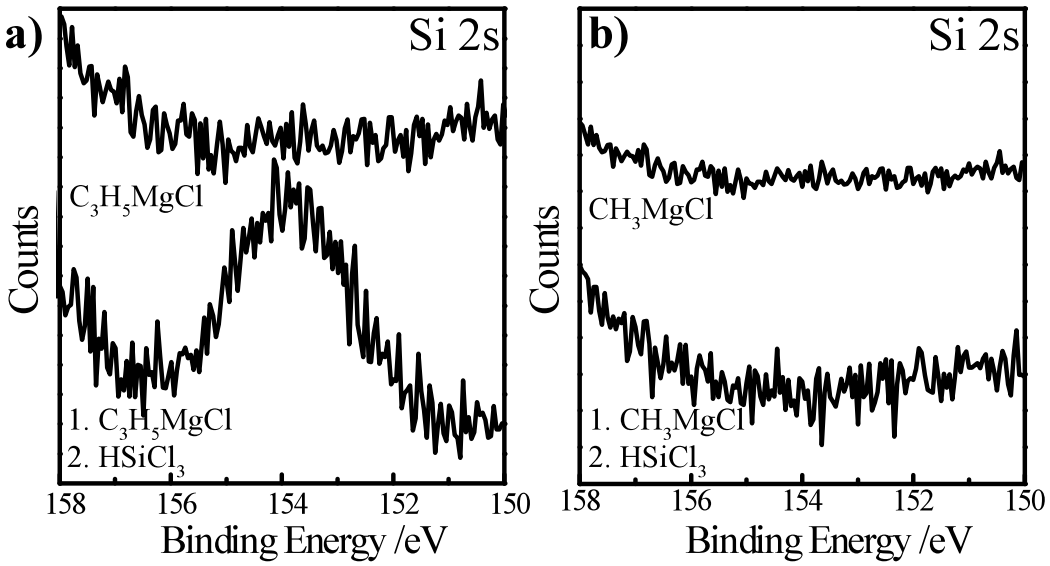

Figure 3.10. Comparison of high-resolution Si 2s XP spectra of (a) allyl-terminated and (b) methyl-terminated GaP(111)A samples after reaction with $HSiCl_3$. Spectra are offset for clarity.

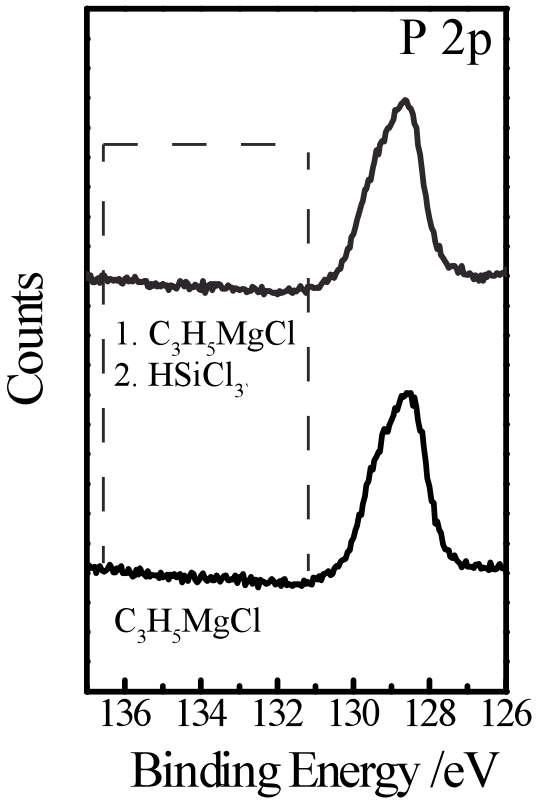

Figure 3.11. High-resolution P 2p spectra of GaP(111)A samples after sequential reaction with PCl_5 in chlorobenzene and then C_3H_5MgCl in THF. (bottom) Immediately after Grignard reaction. (top) After secondary reaction with $HSiCl_3$. Spectra are offset for clarity.

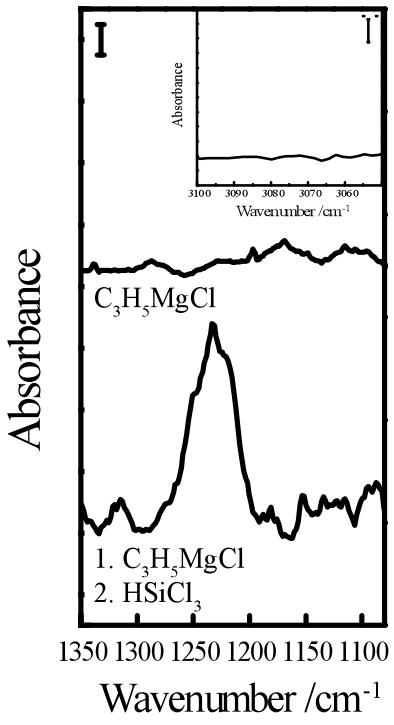

Figure 3.12. GATR-FTIR spectra of GaP(111)A that was first reacted with PCl_5 in chlorobenzene and then C_3H_5MgCl in THF: (top) immediately after Grignard reaction and (bottom) after reaction with $HSiCl_3$. Vertical scale bar = 1 x 10^{-4} absorbance units. Spectra are offset for clarity. Inset: GATR-FTIR spectra in the region for the C=C-H_{asym} stretch for allyl-terminated GaP(111)A after hydrosilylation reaction. Vertical scale bar = 1 x 10^{-4} absorbance units.

GaP surface by Br_2. The Br 3d peak for allyl-terminated GaP(111)A was more intense and required a fit with two separate doublets, one at 68.5 eV and another at 70.1 eV. The doublet at higher binding energies was consistent with the expected shift for Br-C bonding.[23] The surface coverage calculated from the higher binding energy doublet was 0.6 ± 0.3 ML. The relative intensity of the C-Br peak from the high-resolution Br 3d peak at 70.1 eV compared to the intensity of the C-Br shoulder in the high-resolution C 1s spectra at 287 eV (Figure 3.14) was 1.1 ± 0.1, suggesting a heterogeneous distribution of surface groups with some C bonded to more than one Br.

IV. Discussion

The presented data cumulatively show that it is possible to simultaneously impart both chemical stability and chemical reactability to a crystalline GaP surface through a simple wet chemical reaction sequence. Freshly etched GaP surfaces oxidize after only minutes of exposure to ambient conditions.[8] By attaching a short allyl group to a GaP(111)A surface, the resistance towards interfacial oxide growth in air and in water was substantially augmented. Although the limits of inertness were not defined in this work, the stability of the GaP(111)A surfaces modified with allyl groups seemed at least comparable to the measured oxide resistance of GaP(111)A surfaces covered with short alkyl groups.[7] Presently, the mechanistic steps involved in surface oxidation are not known, but the durability imparted by the allyl groups in this work likely arises from both steric blocking of oxidizing species (i.e. O_2, H_2O) to the underlying GaP surface and a strong surface Ga-C bond. This is supported by the lack of change in the flat-band potential of allyl-terminated GaP as pH is varied. Adsorption of H^+ and OH^- ions at the interface of etched GaP creates a charged double layer, thus causing a shift in flatband potential. Moreover, the salient feature of allyl groups on a surface is not solely as a protective barrier but their capacity to serve as reaction handles for secondary functionalization of the surface.

Allyl-terminated surfaces were tested as reaction platforms to determine whether the rich C=C coupling chemistry of olefins[35-37] could be used to further modify GaP. The

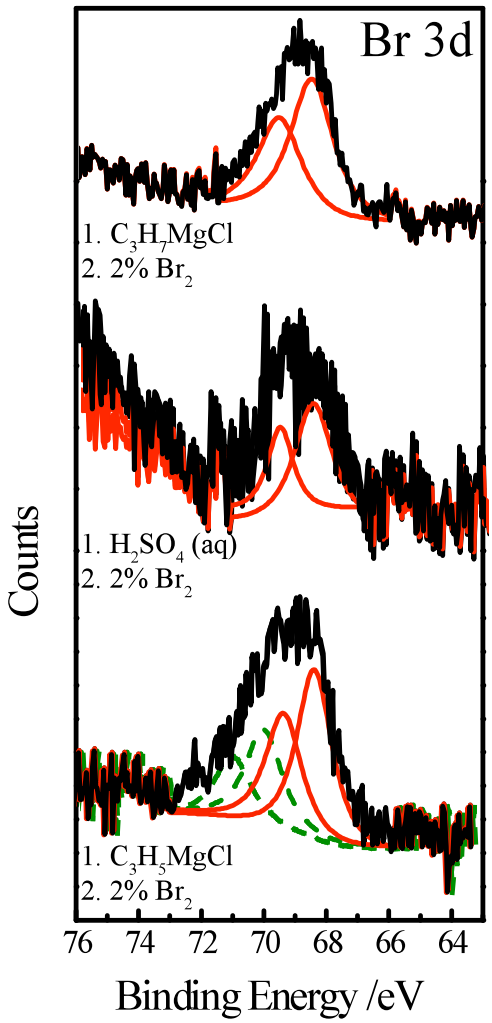

Figure 3.13. High-resolution Br 3d XP spectra of various GaP(111)A samples after immersion in 2% Br_2 in CH_2Cl_2: (top) first reacted with PCl_5 in chlorobenzene and then C_3H_7MgCl in THF, (middle) first etched with H_2SO_4 aq), or (bottom) first reacted with PCl_5 in chlorobenzene and then C_3H_5MgCl in THF. Spectra are offset for clarity.

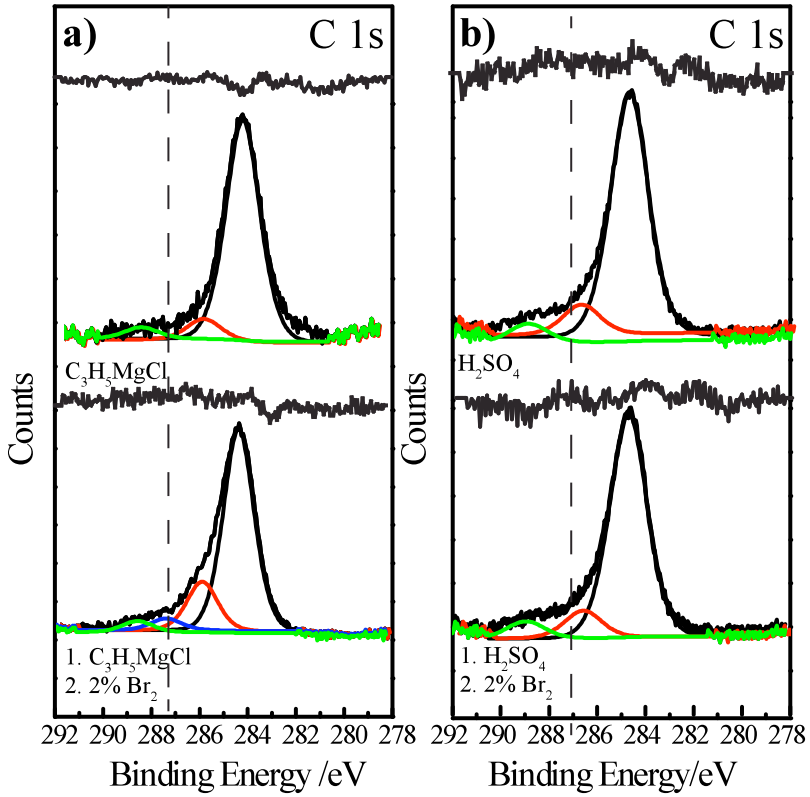

Figure 3.14. High-resolution C 1s spectra of GaP(111)A surfaces that were either (a) sequentially reacted with PCl_5 in chlorobenzene and then C_3H_5MgCl in THF or (b) etched in H_2SO_4(aq). Top spectra were taken immediately after initial surface treatment. Bottom spectra were taken after immersion in a dilute bromine solution. Dashed line denotes C-Br species.

general observations from the Heck cross coupling metathesis, hydrosilylation, and bromination reactions all indicated that allyl-terminated GaP(111)A possesses reactivity akin to a primary alkene. Specifically, the Heck cross coupling metathesis reaction extended the surface layer on GaP(111)A by one aryl group through the formation of a C-C bond. The sub-monolayer coverages determined here are consistent with the footprint of $-C_6H_4CF_3$ exceeding the atom-to-atom distance of atop Ga atoms on a GaP(111)A surface (3.85 Å).[38] Still, the relatively high fractional monolayer content of $-C_6H_4CF_3$ and low surface oxide content following the Heck metathesis shown here stand apart from an analogous report of the reaction chemistry of allyl-terminated Si(111) surfaces, where lower resultant density of surface groups, higher levels of persistent catalyst adsorption, and greater levels of surface oxidation after reaction were noted.[39] Although differences in surface roughness and the slightly larger lattice constant may partially account for the higher coverage of aryl groups grafted here to GaP(111)A, the lower surface contamination level of coupling catalyst (none was detected, detection limit of Pd < 0.03 at %) and decreased oxide content after reaction suggest that allyl-termination on GaP(111)A is not intrinsically equivalent to allyl-termination on Si(111). The origin for the more favorable properties observed here for GaP(111)A are not presently clear and indicate that more studies are needed to elucidate the microscopic details of surface bonding at these GaP(111)A surfaces.

One notable aspect that was highlighted here was that time in air negatively impacts the reactivity of allyl-terminated GaP(111)A. The data argue against the decreased reactivity arising purely from the loss of allyl groups from the surface since the surface oxide content stays low in the same time frame that the reactivity decreases. The collected infrared spectra instead suggest that the C=C groups are compromised in some manner. Although it is unlikely that all chemically grafted allyl groups are oriented initially as depicted in Scheme 1, time in air or water apparently disrupts the initial surface layer order. Interactions with adventitious carbon species in air may facilitate this occurrence. Irrespective, the data indicate that the reactivity of GaP(111)A surfaces with terminal allyl groups is quite time-sensitive. Accordingly, attempts at exploiting the reactivity of allyl-terminated GaP(111)A interfaces should be focused on freshly prepared surfaces.

Two important requirements for photoelectrodes in photoelectrochemical cells are stability and activity.[1,40] As mentioned above, the maximal stability enhancements afforded by allyl-termination have yet to be determined. To be clear, the results shown here are a significant enhancement over the extremely limited stability of native GaP (and most III-V semiconductor) surfaces. However, because allyl-terminated surfaces can be further reacted, subsequent secondary chemical reactions will be needed to further augment stability in solution for extended time scales. In a similar fashion, subsequent surface reactions should also be directed toward the activity of GaP for fuel-forming reactions.[41,42] For example, in a recent work, a photopolymerization approach was used, with electrical communication between GaP and each attached catalyst through a heterogeneous polymeric network. A surface attachment scheme as outlined here ought to provide more uniformity in the chemical environment of the catalyst, affording detailed studies of catalyzed photoelectrode operation. Although three different attachment pathways were shown here, in principle any coupling chemistry applicable to primary alkenes (e.g. Diels alder reaction, radical addition of hydrogen halides, hydroboration, etc.)[43-45] could be exploited for catalyst attachment. In this way, allyl-terminated GaP(111)A surfaces are model platforms to compare photoelectrochemical activity as a function of the chemical tether to identify effects of electronic coupling, stability, orientation, etc.

Similarly, p-type allyl-terminated GaP(111)A surfaces are excellent platforms to study dye-sensitized hole injection.[5] We have recently identified the capacity of p-GaP photoelectrodes function as sensitized photocathodes in water if they operate under depletion conditions.[1] Since the native surface is replete with high surface defects that negatively impact the quantum yield for sensitized charge injection, modified surfaces are necessary. The use of allyl-terminated GaP(111)A should allow for systematic variation in the details of electrode-dye coupling, enabling a more precise sensitized photocathode studies. The distinct characteristics of the band edge potentials of allyl-terminated GaP(111)A surfaces may also present a unique advantage for sensitization. Specifically, the possibility exists for solution pH as a factor to modulate the driving force/rate (and accordingly quantum yield) for sensitized hole injection from photoelectrochemical chromophores. Work in this direction is ongoing.

Finally, the work described here opens up new chemical strategies for further refining Ga-based semiconductor interfaces. For example, although hydrosilyation reactions have been extensively exploited for the modification of Group IV semiconductor surfaces,[46] this work represents first example of a hydrosilylation reaction with a III-V semiconductor acting as the olefin towards a silane compound in solution. As known for Si surface chemistry,[47] the method employed to graft a surface functionality matters as much (if not more) to the electrical properties of semiconductors as the chemical properties of the attached surface group. Hence, comparisons of the electrical properties of III-V surfaces modified with the same functional groups but attached through various ways would be informative. If applied to related semiconductors like GaAs and GaN, which have shown similar propensities for modification by Grignard reagents,[48] new improved chemical pathways may emerge for designing tailored heterojunctions involving III-V semiconductors for energy[49] and sensing[50] applications.

V. Summary

This work demonstrates the successful modification of GaP(111)A surfaces with allyl groups containing a terminal reactive olefin. Allyl-terminated GaP(111)A surfaces were found to be substantially more stable in ambient and aqueous environments than native GaP(111)A surfaces. These modified GaP(111)A surfaces showed reactivity akin to a primary alkene, demonstrating susceptibility to Heck, hydrosilyation, and bromination reactions. The versatility of the chemical reactivity imparted to GaP(111)A, in addition to the augmented chemical stability, defines a new toolbox that can be used for further studies involving chemically modified III-V semiconductors.

VI. References

(1) Chitambar, M.; Wang, Z.; Liu, Y.; Rockett, A.; Maldonado, S. *J. Am. Chem. Soc.* **2012**, *134*, 10670.
(2) Finklea, H. O. *Semiconductor Electrodes*; Elsevier: Amsterdam, 1984.
(3) Tomkiewicz, M.; Woodall, J. M. *Science* **1977**, *196*, 990.

(4) Ziegler, J.; Fertig, D.; Kaiser, B.; Jaegermann, W.; Blug, M.; Hoch, S.; Busse, J. *Energy Procedia* **2012**, *22*, 108.
(5) Gerischer, H. *J. Vac. Sci. Technol.* **1978**, *15*, 1422.
(6) Khaselev, O.; Turner, J. *J. Electrochem. Soc.* **1998**, *145*, 3335.
(7) Mukherjee, J.; Peczonczyk, S.; Maldonado, S. *Langmuir* **2010**, *26*, 10890.
(8) Richards, D.; Luce, P.; Zemlyanov, D.; Ivanisevic, A. *Scanning* **2012**, *34*, 332.
(9) Richards, D.; Zemlyanov, D.; Ivanisevic, A. *Langmuir* **2010**, *26*, 8141.
(10) Flores-Perez, R.; Zernlyanov, D. Y.; Ivanisevic, A. *J. Phys. Chem. C.* **2008**, *112*, 2147.
(11) Yamada, T.; Shirasaka, K.; Noto, M.; Kato, H. S.; Kawai, M. *J. Phys. Chem. B.* **2006**, *110*, 7357.
(12) Yang, F.; Hunger, R.; Roodenko, K.; Hinrichs, K.; Rademann, K.; Rappich, J. *Langmuir* **2009**, *25*, 9313.
(13) Haber, J. A.; Lewis, N. S. *J. Phys. Chem. B.* **2002**, *106*, 3639.
(14) Wagner, C. D.; Riggs, W. M.; Davis, L. E.; Moulder, J. F.; Muilenberg, G. E. *Handbook of X-ray Photoelectron Spectroscopy*; Perkin Elmer Corporation: Eden Prairie 1979.
(15) Briggs, D.; Seah, M. P. *Practical Surface Analysis by Auger and X-ray Photoelectron Spectroscopy*; John Wiley & Sons: New York 1984.
(16) Morota, H.; Adachi, S. *J. Appl. Phys.* **2007**, *101*, 113518.
(17) Pies, W.; Weiss, A. *Crystal Structure Data of Inorganic Compounds*; Springer-Verlag: Berlin, 1979; Vol. 7.
(18) Fadley, C. S. *Solid State- and Surface-Analysis by Means of Angular-Dependent X- Ray Photoelectron Spectroscopy*; Pergamon Press, 1976.
(19) Laibinis, P. E.; Bain, C. D.; Whitesides, G. M. *J. Phys. Chem.* **1991**, *95*, 7017.
(20) Hamers, R. J. In *Annu. Rev. Anal. Chem.* 2008; Vol. 1, p 707.
(21) Sturzenegger, M.; Prokopuk, N.; Kenyon, C. N.; Royea, W. J.; Lewis, N. S. *J. Phys. Chem. B* **1999**, *103*, 10838.
(22) Allen, F. H.; Kennard, O.; Watson, D. G.; Brammer, L.; Orpen, A. G.; Taylor, R. *J. Chem. Soc., Perkin Trans. 2* **1987**, *0*, S1.
(23) Toledano, T.; Biller, A.; Bendikov, T.; Cohen, H.; Vilan, A.; Cahen, D. *J. Phys. Chem. C* **2012**, *116*, 11434.
(24) Koizumi, H.; Yoshimi, T.; Shinsaka, K.; Ukai, M.; Morita, M.; Hatano, Y.; Yagishita, A.; Ito, K. *J. Chem. Phys.* **1985**, *82*, 4856.
(25) Van Den Bergh, H. E.; Callear, A. B. *Trans. Faraday Soc.* **1970**, *66*, 2681.
(26) Porter, M. D.; Bright, T. B.; Allara, D. L.; Chidsey, C. E. D. *J. Am. Chem. Soc.* **1987**, *109*, 3559.
(27) Seitz, O.; Bocking, T.; Salomon, A.; Gooding, J. J.; Cahen, D. *Langmuir* **2006**, *22*, 6915.
(28) Snyder, R. G.; Strauss, H. L.; Elliger, C. A. *J. Phys. Chem.* **1982**, *86*, 5145.
(29) Crist, B. V. *XPS Reports* **2007**, *1*, 1.
(30) Bellamy, L. J. *The Infrared Spectra of Complex Molecules*; 2nd ed.; Jon Wiley & Son: New York, 1961.
(31) Nakanishi, K.; Solomon, P. *Infrared Absorption Spectroscopy*; Holden-Day, Inc: San Francisco, 1962.
(32) Narasimham, N. A.; Nielsen, J. R.; Theimer, R. *J. Chem. Phys.* **1957**, *27*, 5.

(33) Iiimura, K.; Suzuki, N.; Kato, K. *Bull. Chem. Soc. Japan* **1996**, *61*, 10.
(34) Beganskiene, A.; Sirutkaitis, V.; Kurtinaitiene, M.; Juskenas, R.; Kareiva, A. *Mater. Sci.* **2004**, *10*, 287.
(35) Brown, R. S. *Acc. Chem. Res.* **1997**, *30*, 131.
(36) Heck, R. F.; Nolley, J. P. *J. Org. Chem.* **1972**, *37*, 2320.
(37) Ryan, J. W.; Speier, J. L. *J. Am. Chem. Soc.* **1964**, *86*, 895.
(38) Massa, W. *Crystal Structure Determination*; 2 ed.; Springer: New York, 2002.
(39) Plass, K. E.; Liu, X.; Brunschwig, B. S.; Lewis, N. S. *Chemistry of Materials* **2008**, *20*, 2228.
(40) Wen, W.; Carim, A. I.; Collins, S. M.; Price, M. J.; Peczonczyk, S. L.; Maldonado, S. *J. Phys. Chem. C* **2011**, *115*, 22652.
(41) Krawicz, A.; Yang, J.; Anzenberg, E.; Yano, J.; Sharp, I. D.; Moore, G. F. *J. Am. Chem. Soc.* **2013**, *135*, 11861.
(42) Moore, G. F.; Sharp, I. D. *J. Phys. Chem. Lett.* **2013**, *4*, 568.
(43) Burgess, K.; Ohlmeyer, M. J. *Chem. Rev.* **1991**, *91*, 1179. (44) Mayo, F. R.; Walling, C. *Chem. Rev.* **1940**, *27*, 351.
(45) Nicolaou, K. C.; Snyder, S. A.; Montagnon, T.; Vassilikogiannakis, G. *Angew. Chem. Int. Ed.* **2002**, *41*, 1668.
(46) Langner, A.; Panarello, A.; Rivillon, S.; Vassylyev, O.; Khinast, J. G.; Chabal, Y. J. *J. Am. Chem. Soc.* **2005**, *127*, 12798.
(47) Webb, L. J.; Lewis, N. S. *J. Phys. Chem. B* **2003**, *107*, 5404.
(48) Peczonczyk, S. L.; Mukherjee, J.; Carim, A. I.; Maldonado, S. *Langmuir* **2012**, *28*, 4672.
(49) Kaiser, B.; Fertig, D.; Ziegler, J.; Klett, J.; Hoch, S.; Jaegermann, W. *Chemphyschem* **2012**, *13*, 3053.
(50) Adolfsson, K.; Persson, H.; Wallentin, J.; Oredsson, S.; Samuelson, L.; Tegenfeldt, J. O.; Borgstrom, M. T.; Prinz, C. N. *Nano Lett.* **2013**.

Chapter 4

Covalent Attachment of a Iron-Based Molecular Catalyst to GaP(111)A Surfaces Through 'Click' Chemistry

I. Introduction

The search for a photocathode material for photoelectrochemical fuel production that is a good light absorber, has a defined, controllable surface chemistry, and is adaptable to a variety of sensitizing or catalytic systems is a challenge. P-type gallium phosphide (GaP) is a promising photocathode material because 1. its band gap (2.26 eV)[1,2] is well aligned for proton reduction, with the conduction band poised just negative of the H^+/H_2 redox couple,[3] 2. Bulk carrier mobilites are sufficiently fast for charge separation,[4] and 3. GaP is a technologically mature material for which commercial methods for contacting, doping and depositing are available.[5-7] One major impediment to more wide spread incorporation of GaP into photoelectrochemical systems is the susceptibility of the native, unmodified surface to chemical attack and degradation under ambient or aqueous conditions, which leads the formation of deleterious surface defects that act as sites for charge recombination.[8,9] While there have been efforts to chemically modify the surface of GaP through thiol/sulfide chemistry,[10,11] reactions with organic azides,[12] or photochemical grafting of alkenes,[11,13] very few of these strategies simultaneously impart chemical stability to the surface, while affording the capability to attach a variety of molecular sensitizers or catalysts.

We have previously demonstrated that GaP(111)A surfaces, featuring only Ga atop surface atoms, can be reacted through a two-step chlorination/Grignard reaction sequence to introduce allyl groups containing a terminal, reactable olefin.[14] The olefin

can be reacted through several well-known homogeneous organic reactions (Heck cross-coupling metathesis, hydrosilylation, and electrophilic addition of bromine) without compromising the underlying organic layer, assuming that secondary reactions are performed without exposing the surface to ambient conditions. Thus, we have created a "toolbox" of secondary reactions that can be drawn upon to design a versatile, simple reaction strategy to covalently bind a host of organic molecules.

In this chapter, I will detail a specific reaction pathway utilizing Huisgen 1,3-dipolar cycloaddition ('Click') chemistry (Reaction Scheme 1) that can be used to covalently bond any organic group containing an alkyne functionality to the functionalized surface of GaP(111)A. First, the Grignard reaction sequence was used to introduce an organic group with a terminal olefin, in this case a longer organic chain (4-pentenyl group) was used. Electrophilic addition of bromine across this olefin produces a homogeneous bromine-terminated organic layer, which is then fully converted to an azide-terminated layer through reaction with sodium azide. The copper catalyzed 'Click' reaction with azide-terminated monolayers on surfaces has been well established on many types of materials (Si,[15-17] metal oxides,[18-20] etc.). In this chapter, the 'Click' reaction is used to covalently bond a molecular Fe-based catalyst for hydrogen production. The catalyst selected is known to exhibit extremely high stability in oxygen and water (essentially limitless in the solid state) and activation for proton reduction by weakly acidic acetic acid solutions (pH > 3) in homogeneous solutions. In addition to having a highly-customizable ligand framework, these attributes make it an ideal specimen for testing 'Click' adhesion to GaP surfaces and the resulting proton reduction activity of the covalently bound catalyst. X-ray photoelectron (XP) and grazing angle attenuated total reflection (GATR) Fourier transform infrared spectroscopy was used to characterize the resulting surfaces. The cumulative data shown herein demonstrates that I have designed an adaptable reaction pathway to easily introduce complex organic molecules to the surface of GaP(111)A for the context of photoelectrochemical systems.

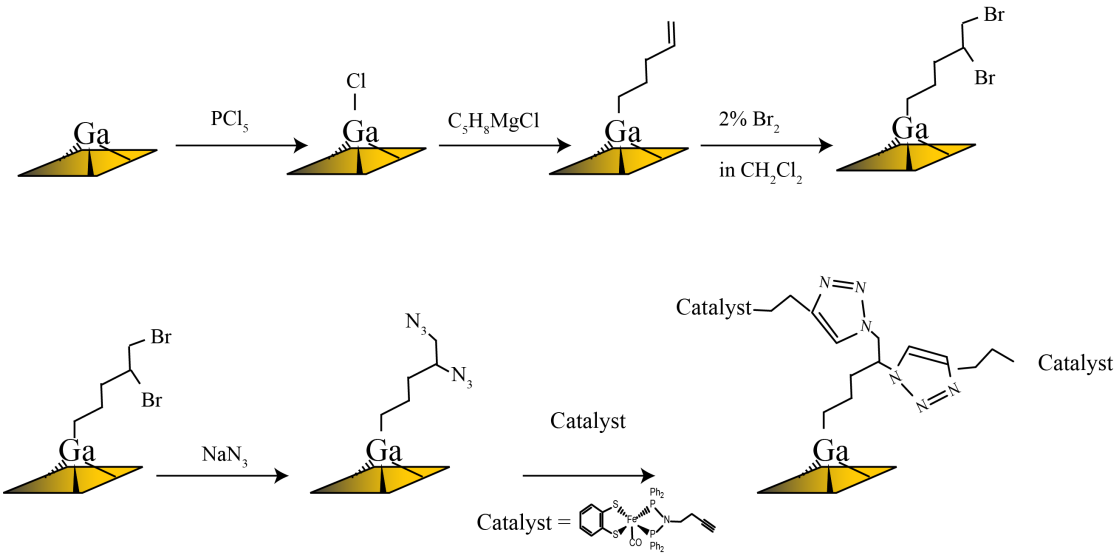

Scheme 1. A reaction scheme detailing the complete 'Click' reaction strategy to covalently bind a molecular catalyst to the Ga-rich surface of GaP(111)A.

II. Experimental

Materials and Chemicals. Unless otherwise noted, all materials and chemicals were purchased from Aldrich and were used as received. Methanol (anhydrous, 99.8% and ACS grade, BHD), acetone (HPLC-grade, Fisher), doubly distilled sulfuric acid (95-98%), chlorobenzene (anhydrous, 99.8%), phosphorus pentachloride (95%), tetrahydrofuran (anhydrous, ≥99.9%), C_5H_9MgBr (0.5 M in THF), bromine (99+%, Acros Organics), dichloromethane (anhydrous, ≥98.7%), dimethylformamide (anhydrous, 99.8%), 1,2-benzenedithiol (99%), ferrous sulfate heptahydrate (>99%), chlorodiphenylphosphine (98%), triethylamine (>99%), glacial acetic acid, 1-amino 3-butyne (95%), acetonitrile (anhydrous, 99.8%), indium metal, and spin on glass (Filmtronics). Benzoyl peroxide (≥97%, Fluka) and sodium azide (99%) were dried under a vacuum of <200 mTorr for at least 24 hours before introduction into a N_2(g) purged glovebox. Methanol, methylene chloride, and hexanes were obtained from Fischer (ACS grade), distilled over calcium hydride, degassed and placed over molecular sieves prior to use. Water with a resistivity of >18 MΩ•cm (Barnsted Nanopure system) was used throughout. Polished p-type GaP(111)A wafers doped with Zn at 2.7 x 10^{18} cm^{-3} with a thickness of 350 ± μm were purchased from ITME.

Etching. GaP(111)A samples were cut into ~ 1 cm^{-2} square pieces and then degreased through sequential sonication in water, methanol, acetone, methanol, and water (1 minute each). Samples were then immediately etched in neat sulfuric acid for 30 sec, rinsed with water, and then dried in a stream of N_2(g)

Reaction of C_5H_9MgBr with GaP(111)A. Etched GaP(111)A samples were introduced into a N_2(g) purged glovebox immediately after etching. The samples were then immersed in a saturated solution of PCl_5 in chlorobenzene containing a few grains of benzoyl peroxide for 50 minutes at 90°C. The sample was then rinsed with fresh chlorobenzene and then transferred to a pressurized reaction vessel containing C_5H_8MgCl and was heated to 100-120°C for 16-18 h. Samples were rinsed with fresh THF and methanol and then allowed to dry in the glovebox.

Reaction of Br_2 with C_5H_9-terminated GaP(111)A. Pentenyl-terminated GaP surfaces were immersed in a 2% solution of bromine in CH_2Cl_2 for 2-4 hours at room temperature. The samples were then rinsed with fresh CH_2Cl_2, CH_3OH, and C_2H_5OH and were allowed to dry in the glovebox.

Reaction of NaN_3 with $C_5H_9Br_2$-terminated GaP(111)A. Immediately after bromine reaction, dried GaP samples were immersed in a saturated solution of NaN_3 in DMF for 3 days at room temperature. Samples were rinsed with fresh DMF and then allowed to dry in the glovebox.

Preparation of $(C_6H_5)_2PN(butyne)P(C_6H_5)_2$ (PNP). Chlorodiphenylphosphine (1.08 mL, 6 mmol) was added slowly dropwise to a stirring solution of 1-amino-3-butyne (0.25 mL, 3 mmol) and triethylamine (1.4 mL, 10 mmol) in methylene chloride, causing a fine white precipitate to form. The mixture was allowed to stir overnight, after which time solvent was removed in vacuo. The solids were washed thoroughly with methanol (5x, 20 mL) and the filtered white product was dried by vacuum.

Preparation of $Fe((C_6H_5)_2PN(3\text{-}butyne)P(C_6H_5)_2)(S_2(C_6H_4))CO$ (1). In a large vial 1,2-benzenedithiol (0.07 g, 0.05 mmol) and sodium methoxide (0.055 g, 1 mmol) were dissolved in 10 mL of methanol. In a schlenk flask **PNP** (0.22, 0.5 mmol) and ferrous sulfate heptahydrate (0.140 g, 0.5 mmol) were combined in methanol (30 mL). The schlenk flask was charged with CO pressure, and the benzenedithiol solution was added dropwise via addition funnel to the mixture while stirring. Addition of this solution caused an immediate change in color to reddish-brown. The mixture was allowed to stir under CO pressure for 5 hours, after which time the solvent was removed in vacuo. The solids were washed with methylene chloride and filtered, the filtrate being collected and reduced in vacuo to a dark red-black solid.

Reaction of (1) with $C_5H_9(N_3)_2$-terminated GaP(111)A. After azide reaction, GaP(111)A samples were immersed in a 1 mmol solution of Fe catalyst (**1**) containing 20 % by mol of CuBr in acetonitrile for 3 days at room temperature. Samples were then rinsed with fresh acetonitrile and dichloromethane and allowed to dry in the glovebox.

X-ray photoelectron spectroscopy. All X-ray photoelectron (XP) spectra were acquired with a PHI 5400 analyzer using either an Al Kα (1486.6 eV) or Mg Kα (1253.6 eV) source without a monochromator. To avoid convolution with Ga auger signatures, N

1s spectra were collected with the Mg source. All other high-resolution spectra (C 1s, Br 3d, Ga 3d, P 2p, Fe 2p and S 2s) were collected with the Al source with a pass energy of 23.5 eV. Survey spectra were collected with a pass energy of 117.4 eV. All spectra were collected under a base pressure < 2.5 x 10^{-9} torr. A 6 mA emission current and 12 kV anode HT were used. The binding energy of all spectra were corrected with respect to the binding energy of adventitious carbon (284.6 eV).[21,22] Samples did not undergo any observable degradation, as evidenced by an attenuation of signal, under prolonged exposure to x-ray source.

The surface monolayer coverages after bromine and click reactions were calculated using the full two-layer overlayer model:[23]

$$\left(\frac{I_{ov}}{I_{sub}}\right) = \left(\frac{SF_{ov}}{SF_{sub}}\right)\left(\frac{\rho_{ov}}{\rho_{sub}}\right)\left(\frac{1 - e^{\frac{-d_{ov'}}{\lambda_{ov}\sin\phi}}}{e^{\frac{-d_{ov}}{\lambda_{sub}\sin\phi}}}\right) \qquad (4.1)$$

where I_{ov} and I_{sub} are the intensities of the element of interest in the overlayer and the substrate, respectively. SF_{ov} or SF_{sub} are the sensitivity factors of the overlayer or substrate for our instrument, ρ_{ov} and ρ_{sub} are the molar densities in mol/cm^2. $d_{o'}$ is the thickness of the second, top overlayer, which contains the element of interest, in nm. d_o is the thickness of the entire overlayer in nanometers. λ_{ov} and λ_{sub} are the escape depths through the substrate and overlayer, respectively. The escape depths were calculated based off of the model proposed by Laibinis,[24] which was chosen because of the length of the organic chain between the surface and element of interest (ie. Br, N, or Fe).[23,25] Long organic films introduce uncertainty in the effective scattering within the film.[26] The bond lengths were calculated using Chemdraw using the assumption that all bound organic groups are oriented perpendicular to the surface normal and possess an all trans configuration.[27] The overlayer thickness for the resulting surface groups are as follows: $C_5H_9Br_2$- : 9.5 Å, $C_5H_9(N_3)_2$: 9.8 Å, and C_5H_9(**1**)$_2$: 11.5 Å.

All high-resolution XP spectra were fit using CASAXPS version 2.313 software. All peaks were fit using a Shirley background. The monolayer coverage after the bromine reaction was calculated from both the Br 3d and C 1s high-resolution spectra. The Br 3d

peak was fit with a doublet with an area ratio of 0.667, a peak separation of 1.05 eV, a fwhm constrained between 0.6 and 1.3, and 80% Gaussian and 20% Lorentzian line shapes. An additional set of doublets was used to fit C-Br species at higher binding energies. The C 1s was fit with a singlet with the fwhm constrained between 0.8 and 2.0 using 45% Gaussian and 55% Lorentzian line shapes. Additional peaks using the same constraints were added to fit higher binding energy moieties. Monolayer coverages after click reaction were calculated from the Fe 2p and S 2s high-resolution spectra. The Fe 2p spectra was fit using a pair of doublets with an area ratio of 0.5, 80% Gaussian and 20% Lorentzian line shapes and a peak separation of 13.1 eV. No constraints on the fwhm were applied. The high-resolution S 2s was fit with a singlet with the fwhm constrained between 0.6 and 2.8, using 80% Gaussian and 20% line shapes. The presented high-resolution N 1s spectra are the difference spectra taken by subtracting the N 1s spectrum of a bromine-terminated GaP surface from the N 1s spectrum of an azide-terminated GaP surface. The N 1s spectrum after click reaction was similarly achieved. This approach was used because of Ga Auger peaks that convoluted this region.

Infrared Spectroscopy. Infrared spectra were collected using a Thermo-Fisher 6700 FTIR spectrometer with a DTGS detector. A grazing angle attenuated total reflectance (GATR) accessory with a Ge crystal was used. An average pressure of 580-600 psi was applied to the sample during acquisition. Incident light was *p*-polarized with a fixed incident angle of ~65°. All spectra were referenced to a bare Ge spectrum that was freshly cleaned with methyl ethyl ketone. The included spectra were recorded with a 4 cm^{-1} resolution and corrected with a linear background subtraction.

III. Results and Discussion

Pentenyl-Terminated GaP(111)A. Pristine single crystalline GaP(111)A surfaces were sequentially activated by chlorination with PCl_5 and then reacted with C_5H_9MgBr to covalently bind pentenyl groups with a terminal reactable olefin. The resulting surfaces were consistently more hydrophobic than etched GaP, (contact angle = 92 ± 4°) and the normalized C 1s XP data supports the introduction of an organic group containing five carbons. GATR-FTIR spectra of freshly prepared pentenyl-terminated

GaP(111)A surfaces are presented in Figure 4.1. Pentenyl-terminated GaP(111)A surfaces show the characteristic C=C and asymmetric C=C-H stretches at 1647 cm^{-1} and 3080 cm^{-1}, respectively (Figure 1a, 1b).[28] The symmetric and asymmetric CH_2- and CH_3- stretching region for freshly prepared pentenyl-terminated GaP surfaces is highlighted in Figure 4.1c. The quality of the packing of the organic groups can be qualitatively assessed by the position of the asymmetric CH_2- stretch.[28] A crystalline "well-packed" monolayer manifests the asymmetric CH_2- stretch at 2920 cm^{-1}, as the monolayer becomes more disordered or "liquid-like" this stretch shifts towards 2928 cm^{-1}.[29-31] The pristine pentenyl-terminated GaP(111)A surfaces exhibit this stretch at 2921 cm^{-1} (Table 4.1) indicating that these surfaces are at least initially well-ordered. I have previously shown that exposure of allyl-terminated GaP(111)A surfaces to ambient has a detrimental effect on the packing of the monolayer, resulting in a more disordered monolayer. This effect translated to a decrease in reactivity of the olefin. Therefore, while pentenyl-terminated GaP surfaces have shown a resistance to surface oxidation comparable to similarly sized alkyl-terminated GaP surfaces, all subsequent reaction steps were carried out without exposure to ambient to preserve full reactivity of the olefin.

Reaction of Br_2 with C_5H_9-terminated GaP(111)A. Previous efforts to react allyl-terminated GaP[14] or Si[28] surfaces with dilute Br_2 solutions resulted in incomplete monolayer coverages (approximately a half monolayer) and heterogeneous addition across the terminal olefin. In an effort to circumvent any steric challenges imparted by having the reactable functional group in close proximity to the surface, a longer pentenyl group was used for further studies. After pentenyl-terminated GaP samples were immersed in dilute Br_2 solution there was a disappearance of the C=C and asymmetric C=C-H stretches in the FTIR spectrum (Figure 1a,b). The methylene stretching region (Figure 4.1c) exhibits features that are consistent with methylene groups with only one type of Br-C bonding environment, i.e. a homogeneous monolayer. The position of the asymmetric methylene stretch shifts slightly to 2925 cm^{-1} indicating that the process of adding bromine across the olefin slightly disrupts the packing of the monolayer.

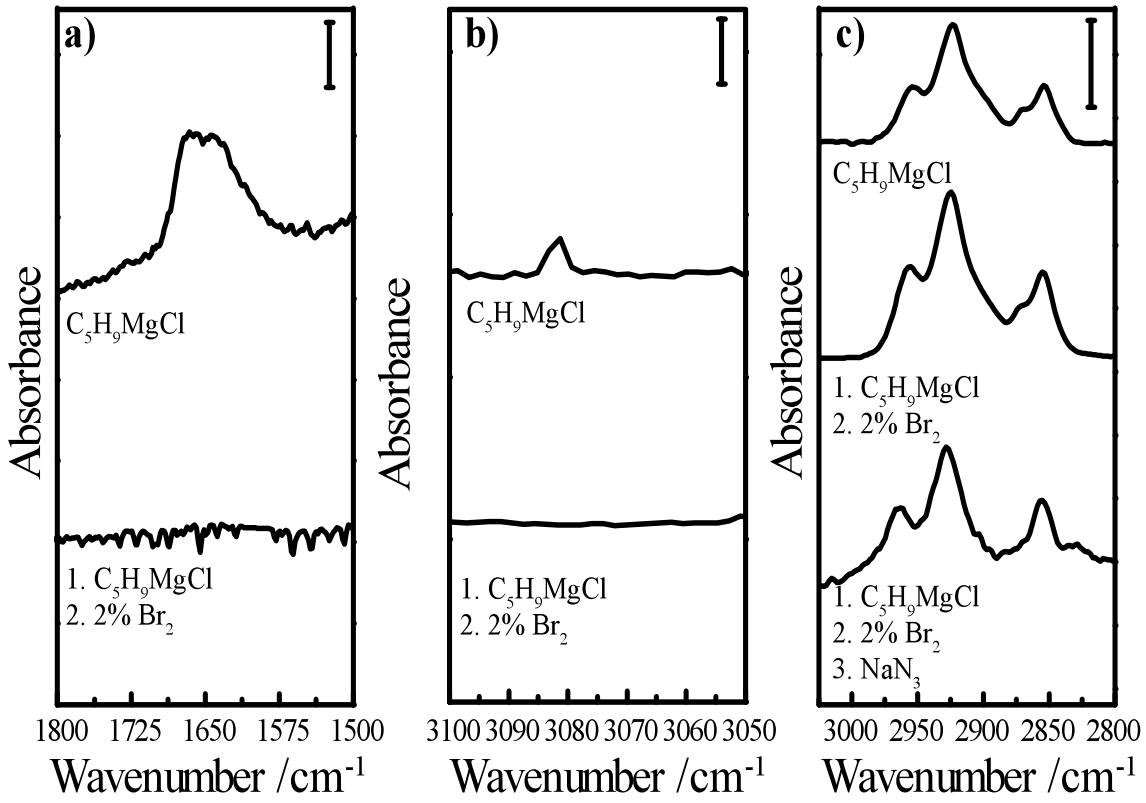

Figure 4.1. (a) GATR-FTIR spectra in the region for the C=C stretch for GaP(111)A samples that were sequentially chlorinated and then reacted with C_5H_9MgCl (top) and then immersed in a dilute bromine solution (bottom). Verticle scale bar = 0.002 absorbance units. (b) GATR-FTIR spectra in the region for the asymmetric C=C-H stretch for GaP(111)A samples that were sequentially chlorinated and then reacted with C_5H_9MgCl (top) and then immersed in a dilute bromine solution (bottom). Verticle scale bar = 2 x 10^{-5} absorbance units. (c) GATR-FTIR spectra in the region for the asymmetric and symmetric CH_2- and CH_3- stretches for GaP(111)A samples that were sequentially chlorinated and then reacted with C_5H_9MgCl (top) and then immersed in a dilute bromine solution (middle) and then NaN_3 solution. Verticle scale bar = 0.002 absorbance units. Spectra are offset for clarity.

Table 4.1 IR spectral assignments for Asymmetric CH_2- Stretching Region of Pentenyl-Terminated GaP(111)A Surfaces After Various Treatments.

Condition	$CH_{2,asym}$ /cm^{-1}
As prepared	2921
After Bromine Reaction	2925
After Azide Reaction	2927

Pentenyl-terminated GaP samples have also been characterized with XPS after immersion in Br_2 solution. High-resolution Br 3d XP spectra (Figure 4.2) exhibited two distinct bromine species, where each can be fit with a pair of doublets. One pair of doublets with the Br $3d_{5/2}$ centered at 68.5 eV is observed on all samples exposed to bromine (bare and alkyl-terminated samples, alike) and has been attributed to direct attack of Br^- onto the GaP surface.[28] The second pair of doublets with the Br $3d_{5/2}$ centered at 70.1 eV is attributed to Br bound to C.[28] Monolayer coverage calculated from the C-Br peak in the Br 3d spectra = 1.0 ± 0.2 ML.

The high-resolution C 1s spectra is shown in Figure 4.3 and compares a pentenyl-terminated GaP(111)A surface before and after immersion in Br_2 solution. Both the pentenyl and brominated spectra contain signatures characteristic of adventitious carbon (284.6 eV) and two separate carbon species at higher binding energies. These signatures are consistent with C-O (hydroxyl, epoxy) at 285.6 eV and C=O at 288.4 eV.[22] After immersion in bromine a separate peak at 286.6 eV emerges and is assigned to C-Br.[28] The monolayer coverage calculated from the C 1s peak at 287 eV is 0.85 ± 0.2 ML. Small discrepancies in the calculation of monolayer coverage likely arise when comparing the Br 3d and C 1s due to differences in fitting parameters. However, these two values are in close agreement with one another, supporting the formation of a homogeneous bromine layer. The pentenyl-terminated GaP sample separately exhibits a shoulder at 283.6 eV, which is assigned to a C-Ga bond.[32]

A homogeneous bromine-terminated monolayer is incredibly desirable because bromine is an excellent platform for nucleophillic substitution reactions, a very important class of chemical reactions in organic and inorganic chemistry.[33] Bromine is amendable to the exchange with a wide variety if nucleophiles, such as –OH, $-N_3$, -CN, etc. Bromine addition across an olefin also affords two active bromine sites for further reaction. Bromine-terminated GaP monolayers were then further reacted with NaN_3 to produce an azide-terminated layer.

Reaction of NaN_3 with $C_5H_9Br_2$-Terminated GaP(111)A. The reaction of NaN_3 with an alkyl bromide occurs *via* a SN2 nucleophilic substitution reaction. Therefore, the azide molecule has to attack from the backside of the alkyl bromide. Similar to what has been reported with densely packed alkyl bromide layers on silicon,[34] full conversion to an

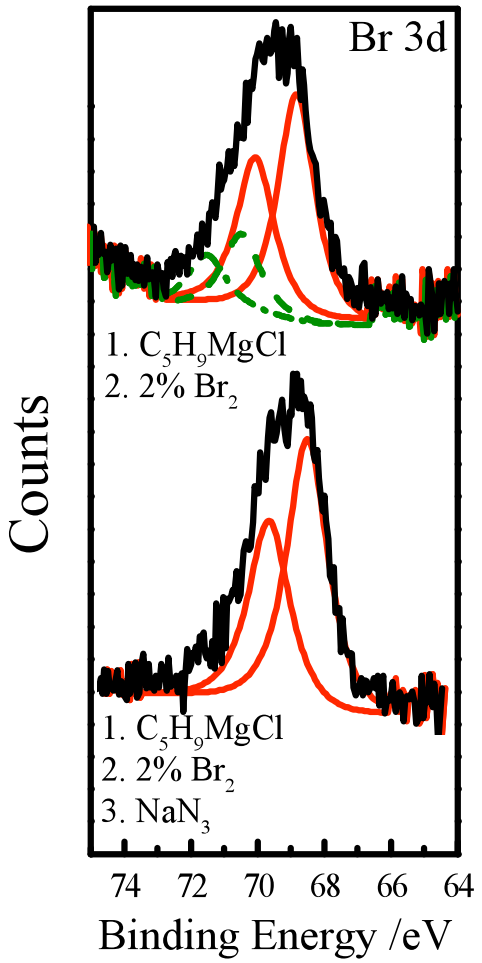

Figure 4.2. High-resolution Br 3d XP spectra of GaP(111)A samples after sequential chlorination and then reaction with C_5H_9MgCl and then immersion in dilute bromine solution (top) and then sodium azide solution (bottom). Spectra are offset for clarity.

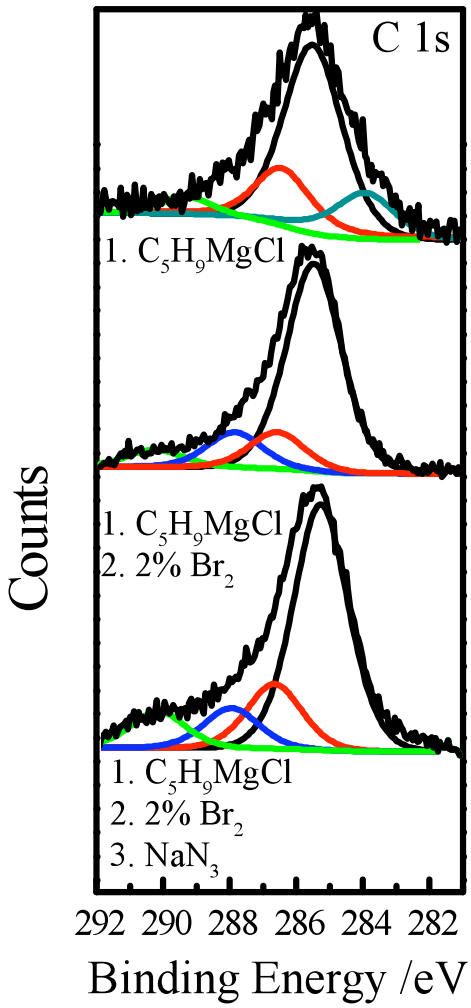

Figure 4.3. High-resolution C 1s XP spectra of GaP(111)A samples after sequential chlorination and then reaction of C_5H_9MgCl (top) and then immersion in dilute bromine solution (middle) and then immersion in sodium azide (bottom). Spectra are offset for clarity.

azide-terminated layer takes 3 days. The high-resolution Br 3d spectra (Figure 4.2) of GaP surfaces after immersion in NaN_3 solution shows a complete disappearance of the doublet at 70.1 eV, supporting full conversion from C-Br to C-N_3. Anionic bromine (peak centered at 68.5 eV) is still observed. Unfortunately, the presence of C-N (288 eV)[22] in the high-resolution C 1s spectrum (Figure 4.3) cannot be unambiguously detected because of the presence of C=O from adventitious carbon that is also found at 288 eV. However, we observe an increase in signal at 288 eV compared to a bromine-terminated GaP sample and a decrease in the peak used to fit the C-Br signature at 287 eV. However, due to the resolution of our spectrometer monolayer coverage cannot be calculated from this data.

The high-resolution N 1s (Figure 4.4) spectrum of GaP after immersion in azide solution supports the attachment of the azide group. An azide group is expected to have two separate N 1s peaks at 402 eV and 405 eV,[35] because this group contains both positively and negatively charged nitrogen atoms ($^{-}$N=N^{+}=N-R). Unfortunately the resolution of our spectrometer prohibits clear differentiation of these peaks, however the fwhm is consistent with multiple types of nitrogen present. Monolayer coverage was not calculated from the N 1s spectrum because it is a difference spectrum between the bromine-terminated and azide treated surfaces. However, complete disappearance of any C-Br signals in the Br 3d spectra indicate full conversion to an azide-terminated monolayer. Figure 4.5 presents the GATR-FTIR spectrum of GaP after immersion in sodium azide highlighting the region the azide stretch is expected. The stretch at 2107 cm^{-1} is assigned to an azide group.

An azide-terminated monolayer can be further reacted through the copper-catalyzed 'Click' reaction with an alkyne to form a triazole linkage to the desired molecule. This is an incredibly versatile reaction that is amendable to a wide variety of molecules assuming they can be functionalized with an alkyne. This is also a low-energy intensive reaction that is carried out at room temperature.

'Click' reaction between Catalyst 1 and azide-terminated GaP(111)A. After azide-terminated samples were immersed in a solution containing catalyst **1** a shift in the N 1s peak from 405-402 eV to 399 eV was observed. This is consistent with the expected binding energy of a N-C group.[22] The N 1s peak is also less broad (smaller fwhm) after

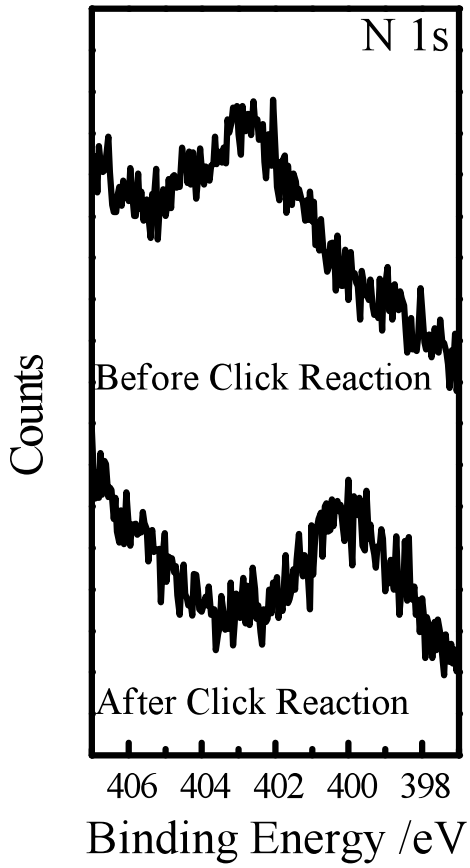

Figure 4.4. High-resolution N 1s XP spectra of azide-terminated GaP(111)A samples before (top) and after (bottom) immersion in catalyst **1** solution.

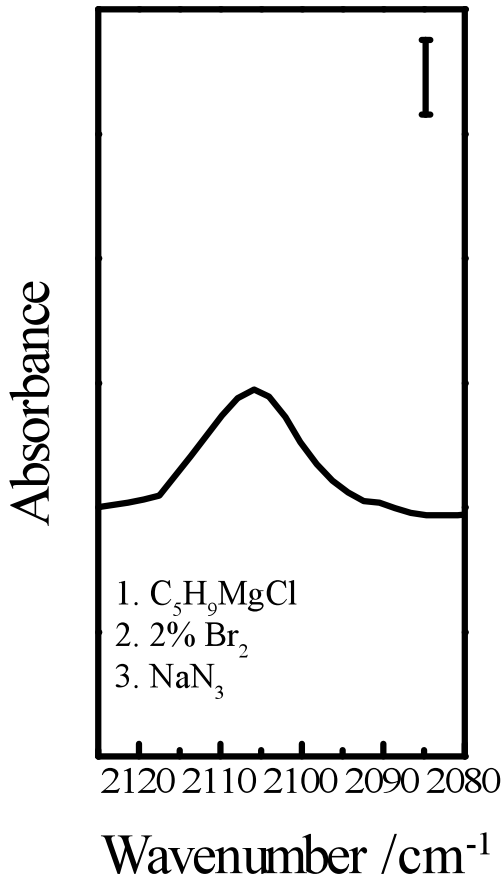

Figure 4.5. GATR-FTIR spectrum in the region of the azide vibrational stretch of a GaP(111)A sample after sequential chlorination and reaction with C_5H_9MgCl and then sequential immersion in a dilute bromine solution and then a sodium azide solution. Verticle scale 6 x 10^{-4} absorbance units.

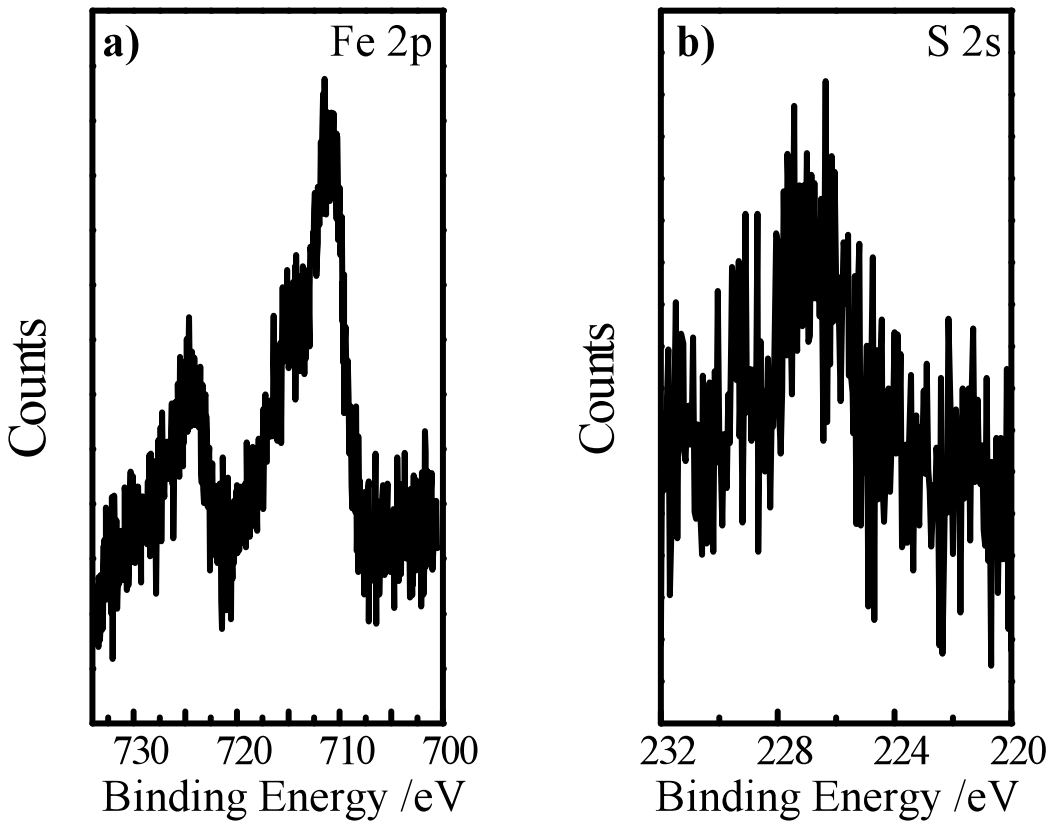

Figure 4.6. High-resolution Fe 2p (a) and S 2s (b) XP spectra of azide-terminated GaP(111)A samples immediately after immersion in catalyst **1** solution.

immersion in **1**, indicating N in a single oxidation state. Signatures in the high-resolution Fe 2p and S 2s spectra further support the attachment of **1**. The high-resolution Fe 2p spectra (Figure 4.6a) exhibit distinct features for the Fe $2p_{1/2}$ and Fe $2p_{3/2}$. There is also a shoulder at 715 eV, which can be assigned to Fe bound to either S or P.[22] Monolayer coverage calculated from the Fe 2p is 0.93 ± 0.2. These signatures remained unchanged even after exposure to ambient for 3 days. The S 2s is shown (Figure 4.6b), albeit with lower sensitivity, because the S 2p is convoluted with the Ga 3s. Monolayer coverage calculated from the S 2s is 1.04 ± 0.2. There was no observed change in the P 2p spectra, likely due to domination from the bulk P signal.

IV. Summary

In this report we have demonstrated a successful tunable, versatile reaction pathway to covalently bind a alkyne-derivatized molecules to the surface of GaP(111)A utilizing click chemistry. In additional, the functionality of the 'Clicked' catalyst has been shown, which suggests this is a viable pathway to afford a variety of functional catalyst-assisted photocathode systems such as those for hydrogen production. This is a low-energy wet chemical reaction scheme that simultaneously imparts stability to the surface of GaP while affording chemical tunability at the surface. This strategy also can be further applied to other Ga-rich III-V semiconductors such as GaAs and GaN.

V. References.

(1) Finklea, H. O. *Semiconductor Electrodes*; Elsevier: Amsterdam, 1984.
(2) Tomkiewicz, M.; Woodall, J. M. *Science* **1977**, *196*, 990.
(3) Dean, P. J.; Herbert, D. C. *J. Lumin.* **1976**, *14*, 24.
(4) Goldberry, Y. A. *Handbook Series on Semiconductor Parameters*; World Scientific: London, 1996; Vol. 1.
(5) Gerischer, H. *J. Vac. Sci. Technol.* **1978**, *15*, 1422.
(6) Gorton, H. C.; Swartz, J. M.; Peet, C. S. *Nature* **1960**, *188*, 303.
(7) Grimmeiss, H.; Rabenau, A.; Koelmans, H. *J. Appl. Phys.* **1961**, *32*, 2123.
(8) Gershenzon, M.; Mikulyak, R. M. *J. Electrochem. Soc.* **1961**, *108*, 548.
(9) Stringfellow, G. B. *J. Vac. Sci. Technol.* **1976**, *13*, 908.

(10) Flores-Perez, R.; Zernlyanov, D. Y.; Ivanisevic, A. *J. Phys. Chem. C.* **2008**, *112*, 2147.
(11) Richards, D.; Zemlyanov, D.; Ivanisevic, A. *Langmuir* **2010**, *26*, 8141.
(12) Richards, D.; Luce, P.; Zemlyanov, D.; Ivanisevic, A. *Scanning* **2012**, *34*, 332.
(13) Moore, G. F.; Sharp, I. D. *J. Phys. Chem. Lett.* **2013**, *4*, 568.
(14) Peczonczyk, S. L.; Brown, E. S.; Maldonado, S. *Langmuir* **2014**, *30*, 8.
(15) Ciampi, S.; B√∂cking, T.; Kilian, K. A.; James, M.; Harper, J. B.; Gooding, J. J. *Langmuir* **2007**, *23*, 9320.
(16) Gouget-Laemmel, A. C.; Yang, J.; Lodhi, M. A.; Siriwardena, A.; Aureau, D.; Boukherroub, R.; Chazalviel, J. N.; Ozanam, F.; Szunerits, S. *J. Phys. Chem. C.* **2012**, *117*, 368.
(17) Marrani, A. G.; Dalchiele, E. A.; Zanoni, R.; Decker, F.; Cattaruzza, F.; Bonifazi, D.; Prato, M. *Electrochim. Acta* **2008**, *53*, 3903.
(18) Benson, M. C.; Ruther, R. E.; Gerken, J. B.; Rigsby, M. L.; Bishop, L. M.; Tan, Y.; Stahl, S. S.; Hamers, R. J. *ACS Appl. Mater. Inter.* **2011**, *3*, 3110.
(19) Cardiel, A. C.; Benson, M. C.; Bishop, L. M.; Louis, K. M.; Yeager, J. C.; Tan, Y.; Hamers, R. J. *ACS Nano* **2011**, *6*, 310.
(20) Duan, T.; Fan, K.; Fu, Y.; Zhong, C.; Chen, X.; Peng, T.; Qin, J. *Dyes Pigm.* **2012**, *94*, 28.
(21) Haber, J. A.; Lewis, N. S. *J. Phys. Chem. B.* **2002**, *106*, 3639.
(22) Wagner, C. D.; Riggs, W. M.; Davis, L. E.; Moulder, J. F.; Muilenberg, G. E. *Handbook of X-ray Photoelectron Spectroscopy*; Perkin Elmer Corporation: Eden Prairie 1979.
(23) Fadley, C. S. *Solid State- and Surface-Analysis by Means of Angular-Dependent X- Ray Photoelectron Spectroscopy*; Pergamon Press, 1976.
(24) Laibinis, P. E.; Bain, C. D.; Whitesides, G. M. *J. Phys. Chem.* **1991**, *95*, 7017.
(25) Sturzenegger, M.; Prokopuk, N.; Kenyon, C. N.; Royea, W. J.; Lewis, N. S. *J. Phys. Chem. B* **1999**, *103*, 10838.
(26) Hamers, R. J. In *Annu. Rev. Anal. Chem.* 2008; Vol. 1, p 707.
(27) Allen, F. H.; Kennard, O.; Watson, D. G.; Brammer, L.; Orpen, A. G.; Taylor, R. *J. Chem. Soc., Perkin Trans. 2* **1987**, *0*, S1.
(28) Toledano, T.; Biller, A.; Bendikov, T.; Cohen, H.; Vilan, A.; Cahen, D. *J. Phys. Chem. C* **2012**, *116*, 11434.
(29) Porter, M. D.; Bright, T. B.; Allara, D. L.; Chidsey, C. E. D. *J. Am. Chem. Soc.* **1987**, *109*, 3559.
(30) Seitz, O.; Bocking, T.; Salomon, A.; Gooding, J. J.; Cahen, D. *Langmuir* **2006**, *22*, 6915.
(31) Snyder, R. G.; Strauss, H. L.; Elliger, C. A. *J. Phys. Chem.* **1982**, *86*, 5145.
(32) Mukherjee, J.; Erickson, B.; Maldonado, S. *J. Electrochem. Soc.* **2010**, *157*, H487.
(33) Fox, M. A.; Whitesell, J. K. *Organische Chemie: Grundlager Mechanismen, Bioorganische Anwendungen*; Spektrum Akademischer Verlag GmbG Heidelberg: Oxford, 1995.
(34) Fryxell, G. E.; Rieke, P. C.; Wood, L. L.; Engelhard, M. H.; Williford, R. E.; Graff, G. L.; Campbell, A. A.; Wiacek, R. J.; Lee, L.; Halverson, A. *Langmuir* **1996**, *12*, 5064.

(35) Haensch, C.; Hoeppener, S.; Schubert, U. S. *Chem. Soc. Rev.* **2010**, *39*, 2323.

Appendix I

Wet Chemical Functionalization of III-V Semiconductor Surfaces: Alkylation of Gallium Phosphide Using a Grignard Reaction Sequence

***** This chapter was adapted from a published work.
Mukherjee, J.; Peczonczyk, S.; Maldonado, S. *Langmuir,* **2010**, *26,* 10890

I. Introduction

Gallium phosphide (GaP) has a midsized optoelectronic band gap (2.26 eV at T = 300K) that is well suited for solar-powered water electrolysis.[1-3] GaP was one of the first semiconductor materials where methods for depositing, doping, and contacting[4-6] were developed and used at scale in commercial technologies. For these reasons, GaP was one of the prototypical semiconductors used during the early development of the field of photoelectrochemistry.[7,8] However, two key deficiencies in GaP were recognized by the early 1980s as serious impediments to its use as a feasible photoelectrode material and interest accordingly waned. First, GaP has an indirect bandgap, rendering thin, planar GaP films inefficient as light absorbers. The small optical absorptivities, α, of light with energies near the band gap require a GaP film thickness of at least 28 mm to capture light effectively.[9] Short carrier diffusion lengths, L_D, relative to the depth of visible light absorption (α^{-1}), are common in low-grade GaP and limit the capacity of planar GaP photoelectrodes for optical energy conversion to wavelengths ≤ 450 nm.[2] Recently, our group has demonstrated that defect-rich n-GaP that possesses poor optoelectronic properties can still function as a high quality photoelectrode material.[2] By adopting non-planar, high-aspect-ratio photoelectrode form factors, low-grade GaP can be used to

capture and convert photogenerated charge carriers from visible light with high internal quantum efficiencies and still generate large photovoltages.[2]

The chemical instability of GaP interfaces represents the second major deficiency that effectively stemmed the development of GaP-based photoelectrochemical systems.[10] The surfaces of GaP and GaP-based alloys are readily subject to chemical attack and degradation.[11] Accordingly, in the absence of deliberate surface protection layers, GaP interfaces possess large densities of surface electrical defects.[12] Although the susceptibility of GaP towards corrosion/dissolution and deleterious surface degradation is not nearly as severe as for gallium arsenide (GaAs)[13] or zinc oxide (ZnO)[14] interfaces, GaP does not possess an electrically passivating, lattice-matched native/thermal oxide.[15] There are no established etching treatments that produce chemically well-defined and rigorously durable GaP surfaces.[15] Surface modification strategies based on thiols and sulfides have previously been documented,[16,17] but the resultant GaP surfaces are neither durable[16] nor has the mode of adsorbate attachment been clearly identified.[17] Data both refuting and supporting the predominance of surficial P-S bonding, in addition to Ga-S bonding, at treated GaP surfaces have been reported.[16,18-20] Further, the effectiveness of thiol/sulfide chemical treatments diminishes with time in air and/or in water.[17] The limitations of sulfur-based wet chemical reaction sequences for improving GaP surface properties are not surprising since they were first developed for GaAs interfaces[21] and were not evolved from a specific molecular-level understanding of GaP reactivity. Recently, alternative chemical modification strategies for III-V semiconductors have emerged. Photochemical grafting of alkenes onto Ga-containing III-V semiconductors following activation with hydrogen plasma has been reported.[22] The pretreatment step is apparently necessary for good surface coverage and helps to minimize deleterious surface oxide growth during the alkylation step. Efforts to circumvent this step for GaP surfaces were recently documented and the reported data illustrated only partial surface coverage with a considerable amount of surface oxide.[17] Hence, despite interest in GaP photoelectrode materials dating back more than four decades, there are still no purely wet chemical surface passivation strategies that are effective for improving and controlling GaP interfaces.

In this appendix, the initial findings on wet chemical reactions between GaP(111)A surfaces and Grignard reagents are detailed. Specifically, the presented results demonstrate that such wet chemical treatments introduce stable, protective alkyl surface groups that begin to address the long-standing issues associated with GaP interfacial chemistry. This approach is based upon a synthetic axiom in the preparation of organogallium compounds, i.e. the formation of Ga-C bonds *via* the reaction between $GaCl_3$ and Grignard reagents.[23] Scheme 1 outlines the heterogeneous analog for this reaction sequence at GaP(111)A surfaces which feature uncoordinated, atop Ga atoms. The two-step process is based on using surficial Ga-Cl bonds as reaction intermediates for the preparation of high-quality alkyl monolayers. Analogous wet chemical reaction sequences have been previously documented for substrates composed of Group IV elements (Si,[24,25] Ge,[26-28] and C[29]) but as of yet there has been no demonstration of this chemistry applied to III-V semiconductor surfaces, despite the compelling precedence set forth in organogallium reaction chemistry. X-ray photoelectron spectra are presented here that indicate this surface reaction sequence results in GaP interfaces that are substantially more resistant to surface oxidation in air. Further, data are highlighted that show this chemical approach can be used to modulate the physicochemical and electrical properties of GaP interfaces.

II. Experimental

Materials and Chemicals All chemicals were purchased from Aldrich, unless otherwise specified. Methanol (low water, JT Baker), acetone (HPLC grade, Fisher), tetrahydrofuran (THF, anhydrous, Acros), CH_3MgCl (3 M solution in THF), $C_{18}H_{37}MgCl$ (0.5 M solution in THF), dichloromethane (HPLC grade), chlorobenzene (anhydrous 99.8%), PCl_5 (95%) and doubly distilled H_2SO_4(aq) (95-98%) were used as received. Benzoyl peroxide (≥ 97%) was purchased from Fluka and dried under vacuum of < 200 mTorr for 24 h. Water with a resistivity > 18 MΩ.cm (Barnsted Nanopure sytem) was used throughout. N-type GaP(111)A wafers (miscut ≤ 0.5º, MTI Inc.) had a thickness of 550 ± 25 μm and were intrinsically doped at 7 x 10^{16} cm^{-3}. N-type GaP(111)B wafers (miscut ≤ 0.5º, ITME) were doped with S at 5 x 10^{17} cm^{-3} and had a thickness of 400 ± 25 μm.

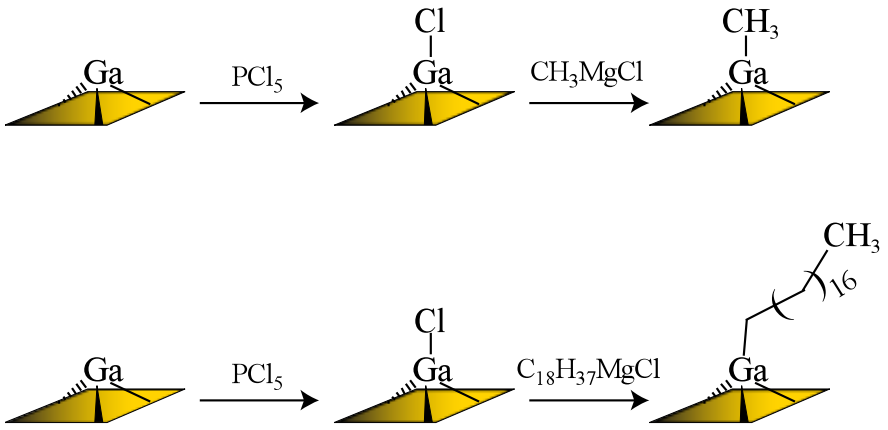

Scheme 1. Reaction scheme of wet chemical attachment of short and long-chain alkyl groups on GaP(111)A surfaces using a Cl-activation step followed by reaction with a Grignard reagent.

Etching Prior to use, n-GaP(111)A crystals were cut into ~ 0.5 cm^2 sections and degreased by sequential sonication in a series of organic solvents: acetone (1 min), methanol (1 min), dichloromethane (30 s), methanol (1 min) and water (1 min). The samples were rinsed with a copious amount of water and either used immediately or stored in water. For etching, samples were immersed in concentrated H_2SO_4(aq) for 30 s, followed by a water rinse and dried with a stream of N_2(g).

X-ray Photoelectron Spectroscopy All X-ray photoelectron (XP) spectra were acquired with a PHI 5400 analyzer using either Al Kα (1486.6 eV) or Mg Kα (1253.6 eV) source without a monochromator. To avoid overlap with Ga Auger signals, the Al Kα source was used to acquire high-resolution C 1s spectra for analysis, albeit with a lowered spectral resolution. The Al Kα source was also used for determination of Cl coverage for similar reasons. For collection of high-resolution P 2p and Ga 3d spectra, the Mg Kα source was used. Spectra were recorded without charge neutralization at a base pressure of < 2.5 x 10^{-9} torr. A 6 mA emission current and 10 kV anode HT were used. Survey scans were acquired between 0 - 1150 eV (Mg source) and 0 - 1350 eV (Al source) at a pass energy of 117.40 eV. High-resolution C 1s and P 2p spectra were recorded at a pass energy of 23.5 eV. The binding energy (BE) of all spectra were corrected using the expected BE for adventitious carbon (284.6 eV).[30] Typical acquisition times for high-resolution spectra ranged from 30 - 45 minutes. The samples did not undergo any observable degradation upon exposure to the X-ray source.

Spectra were fit and analyzed using CASAXPS Version 2.313 software. A Shirley background correction was applied to all spectra. The C 1s signatures were peak fit using a 45% Gaussian and 55% Lorentzian line shape for a singlet with the full width at half maximum (fwhm) constrained between 2.08 - 2.15 eV. The bulk P 2p spectra were fit with a doublet possessing an area ratio of 0.5, a peak separation of 0.85 eV, and values of the fwhm constrained within 0.8 - 1.0 eV. The fractional monolayer coverage of surface oxide on GaP surfaces was calculated using the simplified substrate-overlayer model (equation I.1),[31]

$$d = \lambda_{ov} \ln\left(1 + \frac{I_{overlayer}}{I_{substrate}} \frac{I^0_{substrate}}{I^0_{overlayer}}\right) \sin\phi \qquad \text{(I.1)}$$

where d is the thickness of the oxide overlayer in nm, λ_{ov} is escape depth of the emitted electrons through the oxide overlayer, f is the take-off angle (54º) between the sample surface and the detector, $I_{substrate}$ is the integrated area of the bulk signal, $I_{overlayer}$ is the integrated area of the oxide signals, $I^0_{substrate}$ is the integrated area of the bulk signal obtained from a GaP sample freshly etched with NH_4F(aq) for 30 s. $I^0_{overlayer}$ is the integrated signal for a thick (>>500 nm) thermal oxide on GaP. The escape depths for P 2p, Ga 3d, Cl 2s, and C 1s electrons were estimated with Equation I.2,

$$\lambda = 0.41A^{3/2}E^{1/2} \tag{I.2}$$

where A is the mean diameter of one unit in the overlayer in nm and E is the kinetic energy of the ejected core electron in eV.[31] For C 1s and Ga 3d electrons ejected through an overlayer of CH_3- groups measured with the Al Kα source, the escape depths were calculated to be 1.49 nm and 1.63 nm, respectively. For Cl 2s and Ga 3d electrons ejected through a Cl monolayer measured with the Mg Kα source, the escape depths were 2.45 and 2.69 nm, respectively. The escape depths of P 2p electrons and Ga 3d electrons measured with the Mg Kα source through both a surface oxide layer and the bulk were 1.55 and 1.63 nm, respectively. These latter values for λ assume a surface oxide density comparable to $GaPO_4$[32] (3.56 g cm^{-3})[33,34]

The surface coverages of Cl-terminated and CH_3-terminated GaP(111)A were calculated using the full substrate-overlayer model (equation I.3),[31]

$$\left(\frac{I_{ov}}{I_{sub}}\right) = \left(\frac{SF_{ov}}{SF_{sub}}\right)\left(\frac{\rho_{ov}}{\rho_{sub}}\right)\left(\frac{1-e^{\frac{-d_{ov}}{\lambda_{ov}\sin\phi}}}{e^{\frac{-d_{ov}}{\lambda_{sub}\sin\phi}}}\right) \tag{I.3}$$

where SF_{sub} is the instrument sensitivity factor for the element of interest in the substrate, SF_{ov} is the instrument sensitivity factor for the element of study in the overlayer, ρ_{sub} is the molar density of the element of interest in the substrate (mol cm^{-3}), ρ_{ov} is the density of the element of interest in the overlayer (mol cm^{-3}), and the other symbols are as

defined above. The molar density of solid methane (0.0258 mol cm^{-3})[35] was used as an estimate for ρ_{CH_3}. The thickness of a monolayer of CH_3- groups on GaP(111)A was approximated as the distance between Ga and the plane defined by the H atoms in the methyl groups in trimethylgallium (0.236 nm) determined from literature values of the Ga-C and C-H bond lengths and angles.[36] The molar density of elemental Cl (0.057 mol cm^{-3})[30] was used to determine a value of 0.308 nm for A_{Cl}.

Chlorine Activation and Grignard Reaction Before chemical functionalization, the degreased sample was etched in H_2SO_4(aq) and immediately introduced into a N_2(g)-purged glove box. The residual O_2 and H_2O contents in the glove box were checked using diethyl zinc and an exposed tungsten filament.[37,38] An open vessel of diethyl zinc in the glove box did not combust, substantially fume, or visibly decompose. Similarly, an exposed tungsten filament remained lit when powered inside the glovebox, indicating that O_2 and H_2O levels were at the 100 ppm level or lower after purging with N_2(g).[37,38] For activation of the surface with surficial Cl, the sample was immersed in a saturated solution of PCl_5 in chlorobenzene containing a few grains of benzoyl peroxide and heated at 95-98 ˚C for 50 minutes, similar to conditions previously described for Cl-activation of Si surfaces.[24] The sample was then removed from the reaction mixture, thoroughly rinsed with chlorobenzene, and allowed to dry in the glove box. Alkylation of the Cl-terminated samples was performed using short and long chain length alkyl Grignard reagents. Chlorine-terminated GaP samples were immersed in CH_3MgCl and reacted for a short time (3 h) at various temperatures (65-70 ˚C and 145-150 ˚C) and also at longer times (13 h at 65-70 ˚C). At the end of the reaction, the samples were removed from the reaction solution and rinsed with THF followed by a generous rinse with anhydrous methanol. For reactions at 145-150 ˚C, the samples were reacted in a closed pressurized reaction vial to prevent solvent evaporation. After reaction completion, the samples were allowed to dry in the glove box and then used for further studies.

Static Sessile Contact Angle Measurements The contact angle formed between a droplet of distilled water and GaP interfaces were recorded using a CAM 100 optical contact angle meter (KSV instrument, Helsinki, Finland). A ~ 2.2 μL water droplet was carefully dispensed onto the polished side of the crystal. Images of the contacts between water and GaP were acquired and analyzed using the KSV software analysis package.

Time Dependent Oxide Growth on GaP(111)A Immediately after preparation, each sample was introduced into the XPS chamber (within 30 seconds of first exposure to ambient air) for analysis and this measurement corresponded to t = 0. Subsequent measurements were taken by exposing the sample to laboratory ambient air for a designated period of time in the spectrometer load-lock and then re-inserting back into the XPS chamber. The vacuum pressure of the UHV chamber was sufficiently low to minimize oxidation of the surface while in the chamber.

Preparation of Ohmic Contact for GaP(111)A Ohmic contacts to n-GaP(111)A were prepared before surface functionalization. The unpolished edge of a GaP(111)A wafer section was gently scratched and coated with a thin layer of In solder. The sample was purged in a tube furnace with Ar for 50 minutes and then annealed at 400°C for 10 minutes in a stream of Ar(g) and forming gas (5:95 H_2(g):N_2(g), v/v). The sample was then slowly cooled to room temperature in Ar(g). Spot contacts separated by 2-3 mm prepared in this fashion exhibited resistances less than 10 ohms. The front face of the GaP section was partially etched with H_2SO_4(aq), and care was taken to protect the annealed solder contact. The crystal was then immediately inserted into the glovebox. Functionalization was performed by carefully exposing only the non-soldered part of the crystal to the reagents so that the ohmic contact remained uncompromised. The GaP substrate was chlorinated at 95 °C for 50 minutes in a saturated solution of PCl_5 containing a few grains of benzoyl peroxide. Reaction with $C_{18}H_{37}MgCl$ was performed at 70 °C for two hours. Care was taken to continuously replenish evaporating THF. Static sessile contact angles with water were obtained to ensure that the surface had been sufficiently functionalized prior to any electrical measurement.

n-GaP(111)A/Hg Contact Formation and Measurement Schottky contacts using Hg as the metal top contact were prepared by first placing contacted n-GaP(111)A sections on top of a stainless steel support. An o-ring was placed on the etched/functionalized surface and filled with Hg (junction area = 0.063 cm^2). A Pt wire was used to contact the Hg droplet. Current-voltage responses were measured in the dark using a CH Instruments 440 potentiostat at a scan rate of 20 mV s^{-1}.

Atomic Force Microscopy Atomic force microscopy (AFM) images were obtained with a Veeco Multimode Nanoscope IIIA and an E scanner. AFM imaging was

conducted in tapping mode at a scan rates between 1-1.5 Hz with SSS-NCHR-10 tips (Nanosensors, radius < 2 nm).

Fourier Transform Infrared Spectroscopy Infrared spectra were acquired using a Thermo-Fisher 6700 FT-IR spectrometer equipped with a grazing angle attenuated total reflectance (GATR) accessory. A Ge hemisphere was used with *p*-polarized light at an incidence angle of 65°. Ge crystal was cleaned with methyl ethyl ketone prior to each data collection. All spectra were referenced to a bare freshly cleaned Ge crystal spectrum.

III. Results

Chlorination of GaP(111) Surfaces GaP(111)A surfaces were first etched with concentrated H_2SO_4(aq) to remove any native oxide. The physicochemical properties of GaP(111) after an initial wet etch with concentrated H_2SO_4(aq) have been previously described.[15] These surfaces were then reacted with PCl_5 in chlorobenzene in an attempt to deliberately functionalize the surface with chlorine groups. Representative results from XP spectroscopic analyses for reaction between PCl_5 and GaP(111) are shown in Figure I.1. The Cl 2p and Cl 2s signatures were consistently observed for GaP(111)A surfaces that had been reacted with PCl_5.[39] Using the Cl 2s signal, we determined the Cl surface coverages of 1.2 ± 0.1 monolayers (ML) from the X-ray photoelectron spectra. Coverages in excess of a single monolayer likely reflect the surface roughness (> 0.2 nm) of GaP(111)A interfaces after wet etching. For GaP(111)A, the root mean square (rms) surface roughness after treatment with PCl_5 was determined to be 1.5 ± 0.4 nm (Figure I.2a). In contrast to the results for GaP(111)A, GaP(111)B (P-rich) surfaces could not be reproducibly functionalized with surficial Cl (Figure I.1). These surfaces instead were macroscopically roughened with visible and irregular etch pits after exposure to PCl_5 solutions, obfuscating precise measurements of the rms surface roughness (Figure I.2b). The Cl content was typically below the limit of detection of the spectrometer, indicating GaP(111)B was also reactive towards PCl_5 but the product was not a well defined, stable surface-bound chlorine species. The inability to controllably functionalize GaP(111)B with PCl_5 is broadly consistent with a prior report of selective surface chlorination of GaP(111)A, but not GaP(111)B, surfaces after etching in HCl(aq).[15] Reaction with PCl_5

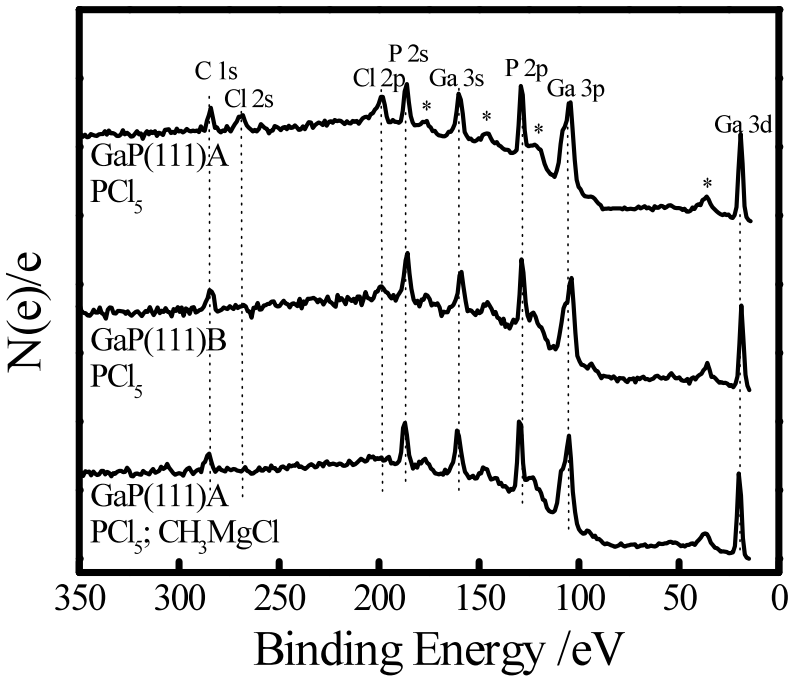

Figure I.1. Comparison of the survey scans obtained with (top) GaP(111)A and (middle) GaP(111)B surfaces after treatment with PCl_5 in chlorobenzene. The survey scan for (bottom) GaP(111)A surfaces after reaction with PCl_5 and then CH_3MgCl is also shown.

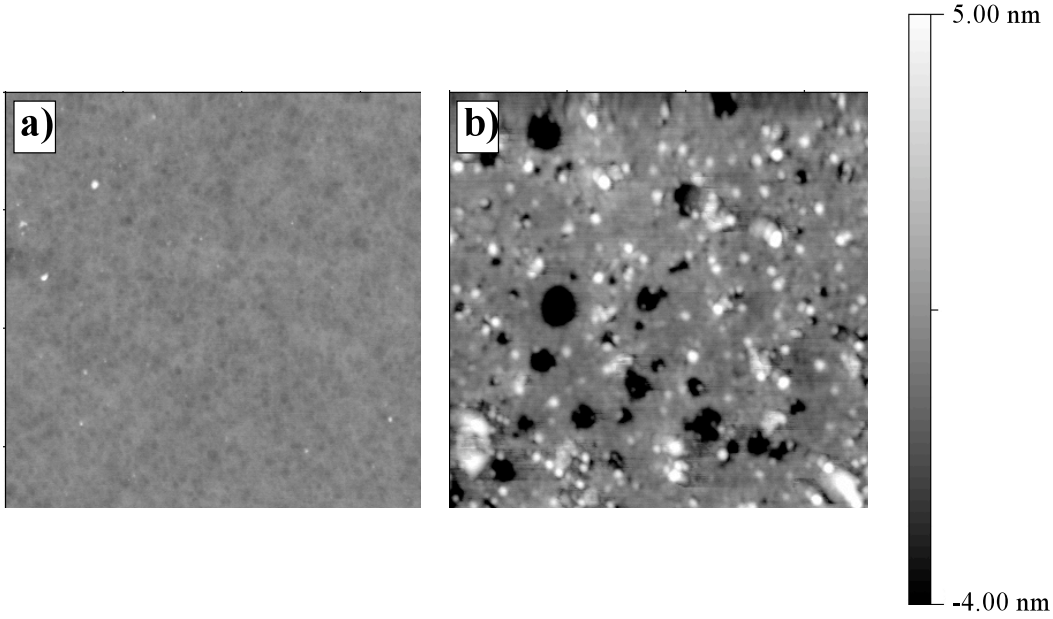

Figure I.2. Atomic force micrographs of GaP(111)A (a) before and (b) after treatment with PCl_5 in chlorobenzene. Both images are 3.5 μm x 3.5 μm, with the z-axis spanning 9 nm (white indicates ≥ +5 nm and black indicates ≤ -4 nm)

in chlorobenzene gave more reproducible levels of surficial Cl as compared to etching in HCl(aq). The latter treatment unavoidably resulted in residual surface oxides that obfuscated subsequent attempts at surface alkylation. For this reason, we concluded that PCl_5 was a more reliable chlorine-activation agent.

Functionalization of GaP(111)A *via* Reaction with Alkyl Grignard Reagents

Following chlorine-activation with PCl_5, exposure of GaP(111)A surfaces to solutions containing Grignard reagents resulted in marked changes in their physicochemical properties. Figure I.3 illustrates the change in wetting character of GaP(111)A towards water after reaction with Grignard reagents. Freshly etched GaP was strongly hydrophilic with wetting contact angles, θ_c, $\leq 20^o$. However, after treatment with CH_3MgCl, the hydrophobicity of GaP(111)A increased significantly. Control experiments with GaP(111)A immersed in THF in the absence of any Grignard reagents but subject to the same heating and temporal conditions also rendered GaP(111)A less hydrophilic, suggesting the possibility of solvent attack by THF on GaP(111)A interfaces. Similar observations have been noted for group IV semiconductors immersed in hot THF.[40] However, the values of θ_c for these control GaP(111)A surfaces were not reproducible and were always $\leq 40^o$, indicating that adventitious solvent binding did not impart high quality interfaces. For GaP(111)A surfaces reacted with CH_3MgCl, $\theta_c = 67 \pm 4^o$. GaP(111)A surfaces reacted with $C_{18}H_{37}MgCl$ were noticeably more hydrophobic, with $\theta_c = 119 \pm 6^o$. Such values are consistent with surfaces modified with a tightly-packed monolayer of long chain alkanes with terminal methyl groups.[41] The standard deviation noted in the contact angle measurements suggested some degree of disorder was present in surfaces treated with alkyl Grignard reagents. Grazing-angle attenuated total reflectance Fourier transform infrared (GATR-FTIR) spectra were collected (Figure I.4) for these surfaces that were consistent with a shallow angle of alignment of the $C_{18}H_{37}$-groups with respect to the surface plane.[42]

The wetting contact angle values of GaP(111)A surfaces remained unchanged and strongly hydrophobic after repeated wetting contact angle measurements, indicating that direct contact with water did not destroy the integrity of the surface layer. The values of θ_c for GaP(111)A surfaces reacted with $C_{18}H_{37}MgCl$ remained high ($\theta_c \geq 100^o$) after 42 days of continuous exposure to the ambient air. To determine whether the time-invariant

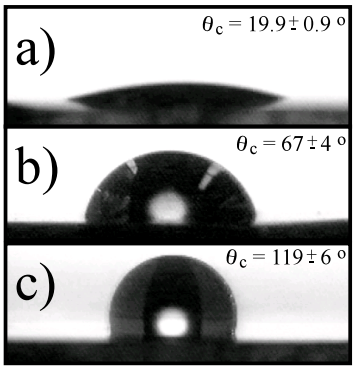

Figure I.3. Optical photographs of contacts between a H_2O droplet and (a) freshly etched GaP(111)A, (b) GaP(111)A after sequential reaction with PCl_5 in chlorobenzene and then CH_3MgCl in THF, and (c) GaP(111)A after sequential reaction with PCl_5 in chlorobenzene and then $C_{18}H_{37}MgCl$ in THF.

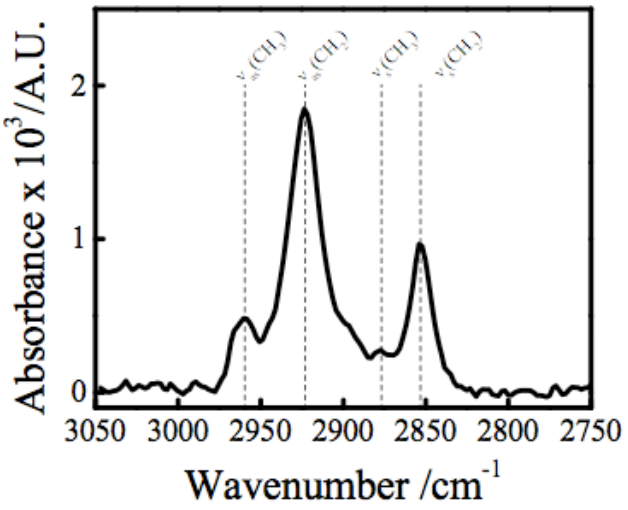

Figure I.4. GATR-FTIR spectra for GaP(111)A surfaces following sequential reaction with PCl_5 in chlorobenzene and then $C_{18}H_{37}MgCl$ in THF. The dashed lines denote the symmetric and asymmetric modes for the $–CH_2$ and $–CH_3$ modes, respectively.

nature of GaP(111)A surfaces treated with alkyl Grignard reagents corresponded to a strong covalent interaction between the alkyl group and underlying GaP(111)A substrate, high-resolution C 1s spectra were collected. Controls consisting of GaP(111)A treated in just THF exhibited the same adventitious carbon signatures (C-C and C-O)[43] that were evident in etched GaP(111)A samples handled in air, with no detectable peaks at binding energies lower than 284.6 eV. In contrast, high-resolution C 1s XP spectra for GaP(111)A exposed to CH_3MgCl indicated that a fraction of the carbon at these surfaces was distinct from adventitious carbon, denoted by a shoulder at lower binding energies in the C 1s spectrum in Figure I.5. Although independent reference XP spectra of separate materials featuring covalent Ga-C bonding were not collected, we note that similar low binding energy shoulders have been observed in general for materials with carbon bonded to a less electronegative element[44] and specifically for trimethylgallium adsorbed onto clean GaAs(100).[45] These data thus support the contention that chemical bonding between atop Ga atoms and alkyl groups occurs as a result of reaction with alkyl Grignards. The integrated intensity of the shoulder at lower binding energies in the C 1s XP spectra, relative to the integrated intensity of the Ga 3d signal, for GaP(111)A treated with CH_3MgCl corresponded to a CH_3- surface coverage of 0.9 ± 0.1 ML. The approximate values used for ρ_{CH_3} and d_{CH_3} limit the accuracy of this measurement. Still, this value suggests a high efficiency for surface coverage for atop Ga atoms with CH_3-groups, similar to CH_3-terminated Si(111) prepared *via* reaction with CH_3MgCl.[46] A concomitant decrease in the surficial chlorine coverage apparent in the XP spectra was observed after treatment with Grignard solutions in THF. Control samples treated in neat THF did not show significantly lower Cl surface contents. However, after reaction with Grignard reagents, residual Cl (< 0.5 ML) and Mg were initially apparent in XP spectra for GaP(111)A surfaces (Figure I.6). These signatures were completely removed after additional sonication in CH_3OH for 2 minutes (Figure I.1). This sonication step did not alter the appearance or magnitude of the low binding energy shoulder in the high-resolution C 1s XP spectra or perturb the observable wetting properties.

Oxidation Resistance of Modified GaP(111)A Surfaces The resistance of the alkyl-terminated GaP(111)A surfaces against chemical attack was also assessed from XP spectral data. High-resolution P 2p XP spectra of chemically treated GaP(111)A were

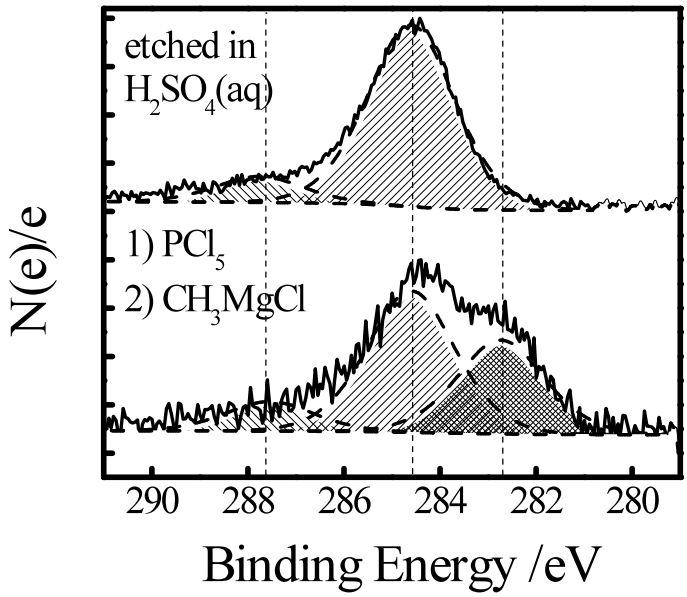

Figure I.5. Comparison of the high-resolution C 1s XP spectra obtained with (top) GaP(111)A after etch with H_2SO_4(aq) and (bottom) GaP(111)A after sequential reaction with PCl_5 in chlorobenzene and then CH_3MgCl in THF. The vertical dashed lines indicate the peak position used to fit each component.

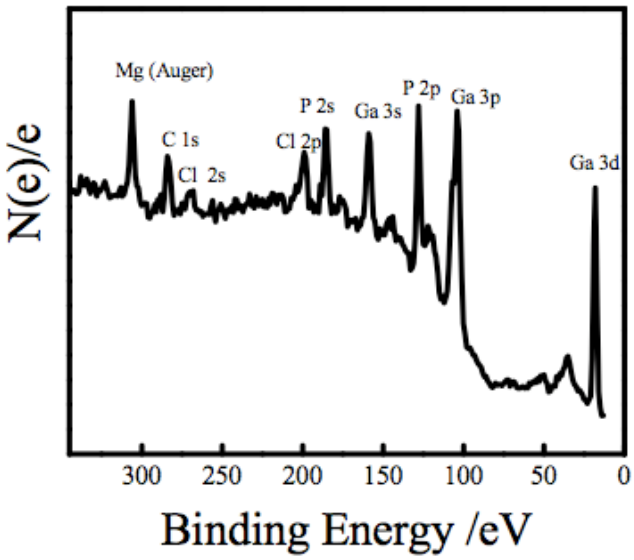

Figure I.6. Survey XP spectra of GaP(111)A after sequential reaction with PCl_5 in chlorobenzene and then CH_3MgCl in THF without post work up sonication in CH_3OH.

collected and highlighted a marked difference in the susceptibility of GaP(111)A surfaces towards oxidation (Figure I.7). In the P 2p spectra, the P 2p doublet (not resolvable with our spectrometer) corresponding to the bulk P atoms occurs at binding energies between 129 and 131 eV. The values of fwhm for the bulk P 2p spectral signatures in Figure I.7 did not statistically vary across the three investigated GaP(111)A surface types. Signals observed at binding energies between 132 and 136 eV were indicative of surface PO_x for these GaP(111)A interfaces.[15] Signals in the latter range were used to track the rate of surface oxidation resulting from exposure of the GaP(111)A surfaces to laboratory ambient air. Freshly etched GaP(111)A surfaces exposed to laboratory air showed rapid formation of oxide on the time scale of minutes. GaP(111)A surfaces treated with CH_3MgCl exhibited a lower rate of oxide formation, with an estimated oxide layer thickness less than one third that observed at the native surface after 1 h. GaP(111)A surfaces reacted with $C_{18}H_{37}MgCl$ demonstrated even greater resistance against oxide formation. These samples showed oxide inhibition on the timescale of weeks, exhibiting less than 0.01 ± 0.04 nm of surficial PO_x after more than 7 weeks of storage under ambient conditions. The precision of analogous measurements of surface oxide content using the Ga 3d spectra (Figures I.8 and I.9) was limited by the resolution of our spectrometer for differentiating the small shift associated with GaO_x[15] but the series of spectra gave nominally equivalent trends to those shown in Figure I.7.

Current-Voltage Response of Hg/GaP(111)A Schottky Junctions The electrical properties of semiconductor heterojunctions are sensitive to the nature of the interface and can be used as a diagnostic measure of the condition of the semiconductor surface[47,48] Hg is a particularly attractive Schottky top contact due to its non-destructive nature and facile preparation of the junction.[47,48] Figure I.10 shows the current-voltage (*J-V*) responses of heterojunctions between n-GaP(111)A and Hg drops. Contacts between freshly etched n-GaP(111)A and Hg exhibited strongly rectifying behavior, with an applied forward bias of +0.67 V needed to pass 1 mA cm^{-2}. The apparent exchange current density for etched n-GaP(111)A/Hg heterojunctions at room temperature was approximately 1 x 10^{-12} mA cm^{-2}. Incorporation of $C_{18}H_{37}$-groups onto GaP(111)A prior to contacting with Hg resulted in heterojunctions with markedly altered properties. Following surface modification, the observable exchange current densities were several

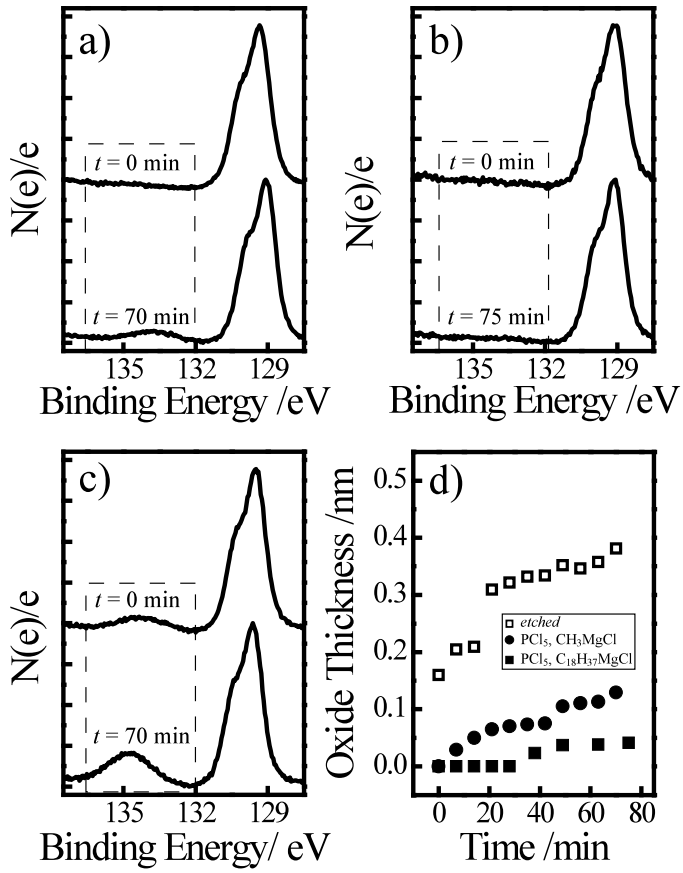

Figure I.7. High-resolution P 2p XP spectra of GaP(111)A surfaces after exposure to air for various times. The dashed boxes highlight the range of binding energies where signatures for PO_x are expected. (a) A comparison of the spectra for GaP(111)A sequentially reacted with PCl_5 in chlorobenzene and then CH_3MgCl in THF just after reaction and after 70 min of exposure to laboratory air. (b) A comparison of the spectra for GaP(111)A sequentially reacted with PCl_5 in chlorobenzene and then $C_{18}H_{37}MgCl$ in THF just after reaction and after 75 min of exposure to laboratory air. (c) A comparison of the spectra for GaP(111)A immediately after etching with H_2SO_4(aq) and after 70 min of exposure to laboratory air. (d) Oxide thicknesses on GaP(111)A surfaces that was (open squares) etched with H_2SO_4(aq), or sequentially reacted with PCl_5 in chlorobenzene and then (solid circle) CH_3MgCl in THF or (solid square) $C_{18}H_{37}MgCl$ in THF. Oxide thickness calculated from high-resolution P 2p spectra.

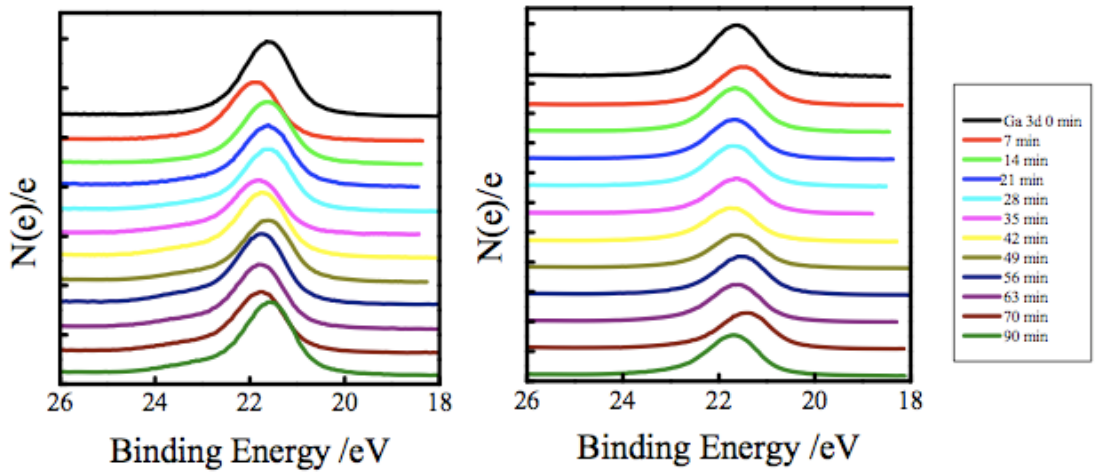

Figure I.8. High-resolution Ga 3d XP spectra for GaP(111)A surfaces that was (left) freshly etched with H_2SO_4(aq) and (right) sequentially reacted with PCl_5 in chlorobenzene and then CH_3MgCl. The shoulder at higher binding energies is diagnostic of GaO_x.

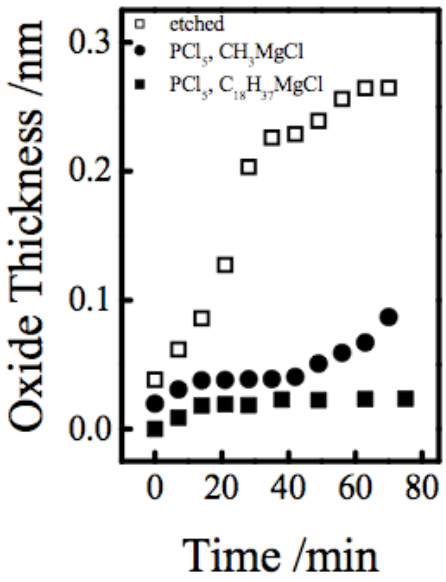

Figure I.9. Comparison of oxide thickness of GaP(111)A that was (open squares) etched with H_2SO_4(aq), or sequentially reacted with PCl_5 in chlorobenze and then (solid circle) CH_3MgCl in THF or (solid square) $C_{18}H_{37}MgCl$ in THF. Oxide thickness calculated from high-resolution Ga 3d spectra.

orders of magnitude lower (4 x 10^{-16} mA cm^{-2}). For GaP(111)A surfaces modified with $C_{18}H_{37}$- groups, a total applied bias of +1.12 V was needed to drive the same 1 mA cm^{-2} forward bias current density. The additional 0.45 V in the applied bias was a direct consequence of the grafted covalent groups. The suppression of current flow across these interfaces was not due to artifacts associated with the back ohmic contact, as control samples did not yield suppressed interfacial current flow and the electrical responses were consistent across three separately prepared substrates that allowed several contact measurements each. The responses of the alkyl-terminated samples were insensitive to aging and exposure to air, unlike that of the freshly etched GaP(111)A interfaces. The modified n-GaP(111)A/Hg diodes exhibited a diode quality factor of 1.3 ± 0.2 across three separately prepared substrates, indicating a deviation from pure thermionic emission as the dominant mode of heterogeneous charge transfer at these heterojunctions. The responses shown in Figure I.10 were consistent with the $C_{18}H_{37}$- groups acting as an insulating layer, resulting in a metal-insulator-semiconductor (MIS)[49] junction based on a purely organic interfacial barrier.

IV. Discussion

Reactivity of GaP(111) The two related crystallographic planes, GaP(111)A and GaP(111)B, highlight the distinct chemical reactivities of uncoordinated atop Ga and P atoms, respectively. The results presented herein indicate that this form of chlorine-activation is not a viable chemical strategy for introducing organic moieties bound at surfaces that feature predominantly atop P atoms. The presented experimental observations, coupled with previous reports for etching with HCl(aq),[15] suggest that GaP(111)B is very reactive towards chlorination agents but the product is not a surface that features stable surficial Cl. In solution at elevated temperatures, PCl_5 is in equilibrium with Cl_2.[50]

$$PCl_5 \rightleftarrows PCl_3 + Cl_2 \qquad (I.4)$$

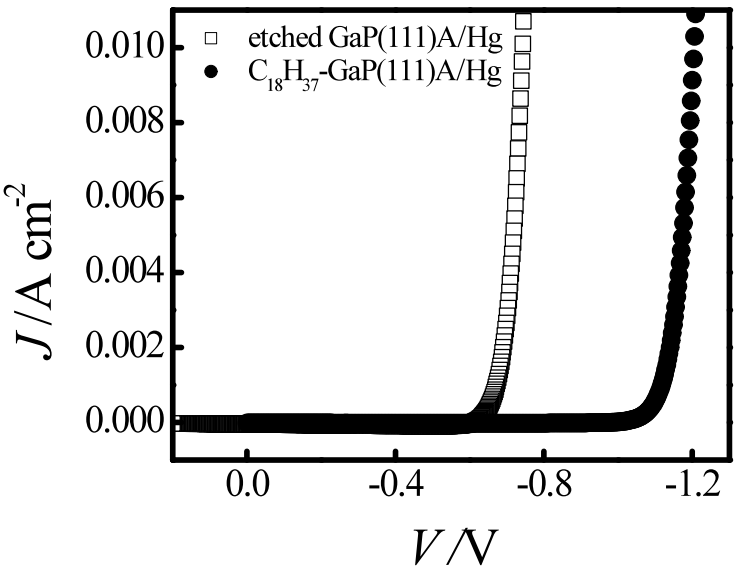

Figure I.10. Dark current-voltage responses for heterojunctions between n-GaP(111)A surfaces (open squares) freshly etched with H_2SO_4(aq) or (solid circles) after sequential reaction with PCl_5 in chlorobenzene and then $C_{18}H_{37}MgCl$ in THF and Hg. $T = 298 \pm 3$ K.

The reverse direction of this reaction indicates that dissolved Cl_2 is reactive towards P-containing species with available lone pairs of electrons. Presuming a similar equilibrium exists between Cl_2 and atop P atoms at an etched GaP(111)B surface, the additional strain introduced by chemisorbed Cl_2 would likely favor dissolution from the surface and facilitate bulk etching. This hypothesis is in accord with the marked instability of GaP(111)B in the investigated chlorine-activation solutions. In contrast, the data highlight the more mild reactivity of GaP(111)A surfaces towards a chlorinating agent such as PCl_5. This treatment successfully produced GaP(111)A surfaces which then could be modified according to reaction pathways originally developed in homogeneous organogallium chemistry.

An important validation of Scheme 1 is the determination and unambiguous identification of the prevailing binding mode for the grafted alkyl groups. The XP spectroscopic data suggest that GaP(111)A surfaces reacted through Scheme 1 feature unusually stable alkyl adsorbates, most likely through Ga-C bonds. The observation of a shoulder at lower binding energies is consistent with the occurrence of covalent Ga-C bonds. Detailed analyses of high-resolution Ga 3d spectra that corroborated the C 1s spectra were difficult due to the resolution capabilities of the XP spectrometer in this study. Further high-resolution spectroscopic analyses that could more clearly identify covalent surface Ga-C bonds directly would greatly aid in the understanding of this particular surface reaction strategy. Specifically, the prevalence and stability of potential surficial Ga-C bonds is interesting since compounds like triethylgallium ($Ga(C_2H_5)_3$) are highly unstable in air. In fact, the propensity of alkylgallium compounds towards decomposition makes them useful for chemical vapor deposition processes. Based on these facts, the initial findings that the grafted alkyl groups are stable in air for prolonged periods of time appears surprising. However, an air-stable Ga-C bond is not without precedent in organogallium chemistry. Ga-C bonds in Ga complexes formed with N-heterocyclic carbenes are unusually stable and unreactive in air.[51] The observed stability of alkyl groups grafted onto GaP(111)A surfaces through the demonstrated Grignard reactions may thus indicate a strong difference in the nature/strength of Ga-C bonds in simple alkylgallium compounds as compared to the apparent surface Ga-C linkage. Further investigations are warranted to more fully assess the specific binding

strength of the grafted alkyl groups. Elucidation of the covalent/ionic bond character will undoubtedly enable the development of better protection strategies for this and related semiconductor surfaces. Further experiments on the mechanism of surface grafting on GaP(111)A are also warranted since the data presented here do not provide microscopic insight on this process. However, the similarity in reaction conditions employed in this work and those previously described for group IV semiconductors suggest that reaction pathways may be comparable. One point of difference, though, may involve intermediate surficial H- groups. For Si, hydrogen termination of atop Si atoms has been identified as the bonding condition for sites that are not covalently attached to an organic group following reaction with Grignard reagents.[52] Surficial Ga-H bonding has not been previously observed at treated GaP(111)A interfaces[15] and it is unclear if such a motif would be stable. Experiments are underway to determine this point and will be reported separately.

The specific mechanism of degradation for pristine GaP surfaces in air or aqueous solutions is also not well known. Whether the key condition for extending the lifetime of the GaP(111)A surfaces involves blocking molecular water, O_2, or both from reaching the underlying substrate remains unclear. However, the presented data are in accord with the hypothesis that prolonged stability of the alkyl-modified GaP(111)A interfaces is at least partially due to a kinetic effect, i.e. slowing the rate transport of deleterious reaction species to atop Ga atoms. The observation that GaP(111)A surfaces reacted with $C_{18}H_{37}MgCl$ show enhanced oxidation resistance relative to GaP(111)A surfaces reacted with CH_3MgCl suggests the improved durability of the former surfaces arises from steric blocking of oxidative species by the packing of long alkyl chains. However, as in the case of Si(111),[53] long chain alkyl groups with footprints larger than CH_3- groups cannot yield monolayers that are in perfect registry with every available underlying atop Ga atom due to steric crowding. More data is needed to determine whether oxide inhibition can further be improved by increasing the fraction of atop Ga atoms coordinated to organic groups.

Since GaP surfaces have not been studied at the same level of detail as other technologically relevant semiconductors, there are presently no data on the chemical nature of defect sites at GaP interfaces. Specifically, little is known whether there is a correlation between the density of deleterious electronic trap sites at GaP interfaces and

the chemistry of atop Ga atoms. The reaction sequence presented here, in conjunction with non-destructive methods for measuring surface recombination events, allows for systematic investigation of the hypothesis that GaP(111)A surfaces featuring predominantly coordinated atop Ga atoms correspond to surfaces with significantly lower rates of carrier recombination. This information would greatly aid the further design of microelectronics, chemical sensing, and energy conversion technologies that utilize GaP and related Ga-based III-V semiconductors.

Controlling Heterogeneous Charge-Transfer for Optical Energy Conversion/Storage An advantage that GaP has over small bandgap semiconductors such as Si or Ge for photoelectrochemical/photovoltaic applications is the capacity for large photovoltages under illumination.[1] The photovoltage represents the electromotive force generated by light absorption that can be used to drive electrochemical reactions.[11] For an ideal GaP heterojunction (with L_d = 100 nm) under solar insolation, the maximum attainable photovoltage dictated by bulk recombination processes is ~ 1.6 V.[54] There are two ways to achieve high photovoltages with GaP photoelectrodes: either increase the equilibrium barrier height of the contact and/or specifically increase the steady-state injection ratio between the minority-carrier to majority-carrier fluxes across the 'front' contact.[49,54] A covalently grafted alkyl layer will likely affect the surface band edge energetics of GaP and accordingly alter the value of the equilibrium barrier height for a given heterojunction. Such an effect has been well documented for both Si[47] and Ge[55] following modification with alkyl groups. Comparison between 'native' GaP surfaces and alkyl-terminated surfaces here is complicated by the fact that the apparent surface energetics of pristine GaP are strongly sensitive to the etching procedure used to prepare 'native' GaP surfaces.[15] Still, introducing stable surface groups *via* Grignard reagents may be a route to define stable surface energetics for GaP, which will accordingly aid in the design of GaP photoelectrochemical cells. The data presented here do demonstrate the possibility of GaP-based MIS heterojunctions. In MIS contacts, the injection ratio between the minority- and majority-carriers is increased because the insulating layer decouples electronic communication between the majority-carrier band and the metal. The data shown here illustrates that this low-temperature, wet chemical methodology yields a compact organic barrier layer on GaP interfaces that can be used to substantially

suppress majority carrier flow across a heterojunction contact. GaP MIS heterojunctions are unique because traditional MIS devices involve an oxide layer as the interfacial barrier material;[49] and, as stated above, controllable and high-quality oxides are not tenable with GaP. Similar buffer organic layers have proven useful for dramatically improving the photoresponses of Si heterojunctions[56,57] but to date have not been successfully demonstrated for GaP photoelectrodes in photoelectrochemical applications. The data shown here thus suggest that alkyl-groups introduced *via* surface Grignard reactions are durable enough to explore as a means to further increase the photoresponse of GaP photoelectrodes.

V. Conclusions

In the context of the surface chemistry of III-V semiconductors, this appendix highlights an untapped chemical methodology for gaining molecular control over the physicochemical and electrochemical properties of GaP interfaces. GaP(111)A interfaces have been terminated with short and long chain alkyl groups through a chlorine-activation and Grignard alkylation reaction sequence. The data show that GaP surfaces that specifically feature atop Ga atoms can be chemically protected by surface alkylation from oxidation in ambient air on the time scale of at least weeks. Further, the alkyl groups form a compact layer that substantially alters the observable wetting and electrical properties. Coupled with separate efforts addressing the optical absorptivity/carrier-collection length scale mismatch, the data presented here suggests the two distinct deficiencies that have historically limited the use of GaP in photoelectrochemical systems are solvable. Work is ongoing to explore and develop this chemical strategy to augment the surface properties of GaP for such applications.

VI. References

(1) Finklea, H. O. *Semiconductor Electrodes*; Elsevier: Amsterdam, 1984.
(2) Price, M. J.; Maldonado, S. *J. Phys. Chem. C* **2009**, *113*, 11988.
(3) Tomkiewicz, M.; Woodall, J. M. *Science* **1977**, *196*, 990.

(4) Gershenzon, M.; Mikulyak, R. M. *J. Electrochem. Soc.* **1961**, *108*, 548.
(5) Gorton, H. C.; Swartz, J. M.; Peet, C. S. *Nature* **1960**, *188*, 303.
(6) Grimmeiss, H.; Rabenau, A.; Koelmans, H. *J. Appl. Phys.* **1961**, *32*, 2123.
(7) Gerischer, H. *J. Electroanal. Chem.* **1975**, *58*, 263.
(8) Tributsch, H.; Gerischer, H. *Berich Bunsen Gesell* **1969**, *73*, 251.
(9) Aspnes, D. E.; Studna, A. A. *Phys. Rev. B* **1983**, *27*, 985.
(10) Gerischer, H. *J. Vac. Sci. Technol.* **1978**, *15*, 1422.
(11) Khaselev, O.; Turner, J. *J. Electrochem. Soc.* **1998**, *145*, 3335.
(12) Stringfellow, G. B. *J. Vac. Sci. Technol.* **1976**, *13*, 908.
(13) Lunt, S. R.; Ryba, G. N.; Santangelo, P. G.; Lewis, N. S. *J. Appl. Phys.* **1991**, *70*, 7449.
(14) Valtiner, M.; Borodin, S.; Grundmeier, G. *Langmuir* **2008**, *24*, 5350.
(15) Mukherjee, J.; Erickson, B.; Maldonado, S. *J. Electrochem. Soc.* **2010**, *157*, H487.
(16) Flores-Perez, R.; Zernlyanov, D. Y.; Ivanisevic, A. *J. Phys. Chem. C.* **2008**, *112*, 2147.
(17) Richards, D.; Zemlyanov, D.; Ivanisevic, A. *Langmuir* **2010**, *26*, 8141.
(18) Hammond, C.; Back, A.; Lawrence, M.; Nebesny, K.; Lee, P.; Schlaf, R.; Armstrong, N. R. *J. Vac. Sci. Technol.* **1995**, *13*, 1768.
(19) Suzuki, Y.; Sanada, N.; Shimomura, A.; Fukuda, Y. *Appl. Surf. Sci.* **2004**, *235*, 260.
(20) Yuan, Z. L.; Ding, X. M.; Lai, B.; Hou, X. Y.; Lu, E. D.; Xu, P. S.; Zhang, X. Y. *Appl. Phys. Lett.* **1998**, *73*, 2977.
(21) Yablonovitch, E.; Bhat, R.; Harbison, J. P.; Logan, R. A. *Appl. Phys. Lett.* **1987**, *50*, 1197.
(22) Kim, H.; Colavita, P. E.; Metz, K. M.; Nichols, B. M.; Sun, B.; Uhlrich, J.; Wang, X.; Kuech, T. F.; Hamers, R. J. *Langmuir* **2006**, *22*, 8121.
(23) Green, M. L. H.; Mountford, P.; Smout, G. J.; Speel, S. R. *Polyhedron* **1990**, *9*, 2763.
(24) Bansal, A.; Li, X.; Lauermann, I.; Lewis, N. S.; Yi, S. I.; Weinberg, W. H. *J. Am. Chem. Soc.* **1996**, *118*, 7225.
(25) Yu, H. Z.; Morin, S.; Wayner, D. D. M.; Allongue, P.; de Villeneuve, C. H. *J. Phys. Chem. B* **2000**, *104*, 11157.
(26) Amick, J. A.; Cullen, G. W.; Gerlich, D. *J. Electrochem. Soc.* **1962**, *109*, 127.
(27) Cullen, G. W.; Amick, J. A.; Gerlich, D. *J. Electrochem. Soc.* **1962**, *109*, 124.
(28) Gerlich, D.; Cullen, G. W.; Amick, J. A. *J. Electrochem. Soc.* **1962**, *109*, 133.
(29) Lockett, M. R.; Smith, L. M. *Langmuir* **2009**, *25*, 3340.
(30) Haber, J. A.; Lewis, N. S. *J. Phys. Chem. B.* **2002**, *106*, 3639.
(31) Briggs, D.; Seah, M. P. *Practical Surface Analysis by Auger and X-ray Photoelectron Spectroscopy*; John Wiley & Sons: New York 1984.
(32) Morota, H.; Adachi, S. *J. Appl. Phys.* **2006**, *100*.
(33) Pies, W.; Weiss, A. *Crystal Structure Data of Inorganic Compounds*; Springer-Verlag: Berlin, 1979; Vol. 7.

(34) ka
(35) McLennan, J. C.; Plummer, W. G. *Nature* **1928**, *122*, 571.
(36) Bock, C. W.; Trachtman, M. *J. Phys. Chem.* **1994**, *98*, 95.
(37) Mao, O.; Altounian, Z.; StromOlsen, J. O. *Rev. Sci. Instrum.* **1997**, *68*, 2438.
(38) Shriver, D. F.; Drezdzon, M. A. *The Manipulation of Air-Sensitive Compounds*; Wiley: New York, 1986.
(39) Radde, A.; Kolditz, L. *Zeitschrift Fur Chemie* **1983**, *23*, 436.
(40) Amy, S. R.; Michalak, D. J.; Chabal, Y. J.; Wielunski, L.; Hurley, P. T.; Lewis, N. S. *J. Phys. Chem. C* **2007**, *111*, 13053.
(41) Bain, C. D.; Evall, J.; Whitesides, G. M. *J. Am. Chem. Soc.* **1989**, *111*, 7155.
(42) Lummerstorfer, T.; Kattner, J.; Hoffmann, H. *Anal Bioanal Chem* **2007**, *56*, 55.
(43) Barr, T. L.; Seal, S. *J. Vac. Sci. Technol. A* **1995**, *13*, 1239.
(44) Mizokawa, Y.; Geib, K. M.; Wilmsen, C. W. *J. Vac. Sci. Technol. A.* **1986**, *4*, 1696.
(45) McCaulley, J. A.; McCrary, V. R.; Donnelly, V. M. *J. Phys. Chem.* **1989**, *93*, 1148.
(46) Webb, L. J.; Nemanick, E. J.; Biteen, J. S.; Knapp, D. W.; Michalak, D. J.; Traub, M. C.; Chan, A. S. Y.; Brunschwig, B. S.; Lewis, N. S. *J. Phys. Chem. B* **2005**, *109*, 3930.
(47) Maldonado, S.; Plass, K. E.; Knapp, D.; Lewis, N. S. *J. Phys. Chem. C.* **2007**, *111*, 17690.
(48) Pressman, L. D.; Forrest, S. R.; Bonner, W. A.; Vanuitert, L. G. *Appl. Phys. Lett.* **1982**, *41*, 969.
(49) Pulfrey, D. L. *IEEE Trans. Electron Devices* **1978**, *25*, 1308.
(50) Wyman, D. P.; Freeman, W. R.; Wang, J. Y. C. *J. Org. Chem.* **1963**, *28*, 3173.
(51) Marion, N.; Escudero-Adan, E. C.; Benet-Buchholz, J.; Stevens, E. D.; Fensterbank, L.; Malacria, M.; Nolan, S. P. *Organometallics* **2007**, *26*, 3256.
(52) Johansson, E.; Hurley, P. T.; Brunschwig, B. S.; Lewis, N. S. *J. Phys. Chem. C.* **2009**, *113*, 15239.
(53) Yu, H. B.; Webb, L. J.; Ries, R. S.; Solares, S. D.; Goddard, W. A.; Heath, J. R.; Lewis, N. S. *J. Phys. Chem. B* **2005**, *109*, 671.
(54) Fonash, S. *Solar Cell Device Physics*; Academic Press: New York, 1982.
(55) Sharp, I. D.; Schoell, S. J.; Hoeb, M.; Brandt, M. S.; Stutzmann, M. *Appl. Phys. Lett.* **2008**, *92*.
(56) Har-Lavan, R.; Ron, I.; Thieblemont, F.; Cahen, D. *Appl. Phys. Lett.* **2009**, *94*.
(57) Maldonado, S.; Knapp, D.; Lewis, N. S. *J. Am. Chem. Soc.* **2008**, *130*, 3300.